

**DEVELOPMENT OF THE UPRM EARTHQUAKE SIMULATOR FACILITY FOR  
DYNAMIC MODEL ANALYSIS**

by

María D. Cortés Delgado

A thesis submitted in partial fulfillment of the  
requirements for the degree of

MASTER OF SCIENCE  
in  
CIVIL ENGINEERING

UNIVERSITY OF PUERTO RICO  
MAYAGÜEZ CAMPUS  
2005

Approved by:

\_\_\_\_\_  
Ricardo López, Ph.D.  
Member, Graduate Committee

\_\_\_\_\_  
Date

\_\_\_\_\_  
Luis Suárez, Ph.D.  
Member, Graduate Committee

\_\_\_\_\_  
Date

\_\_\_\_\_  
Daniel Wendichansky, Ph.D.  
President, Graduate Committee

\_\_\_\_\_  
Date

\_\_\_\_\_  
Genock Portela Gauthier, Ph.D.  
Representative of Graduate Studies

\_\_\_\_\_  
Date

\_\_\_\_\_  
Ismael Pagán Trinidad, M.S.  
Chairperson of the Department

\_\_\_\_\_  
Date

# **DEVELOPMENT OF THE UPRM EARTHQUAKE SIMULATOR FACILITY FOR DYNAMIC MODEL ANALYSIS**

## **Abstract**

The University of Puerto Rico at Mayagüez has recently added an earthquake simulator to its facilities in the Structural Laboratory. The small-uni-directional-electro-hydraulic shaking table has been designed to investigate the behavior of small-scaled model structures under dynamic loading. The shaking table consists of a rigid platform sliding over a near frictionless linear bearing system and driven by an actuator attached to a reaction mass connected to the floor. A 1:4 model scale building has also been constructed for testing its behavior under dynamic loading. The components of the shaking table system were designed and sized for 1:4 model structures and to reproduce five historical earthquakes. The dynamic characteristics of the reaction frame, simulator platform and oil column were examined along with the possible interaction effects with a test structure. An initial determination of the quality of shake table reproduction has been obtained by carrying out preliminary experimental tests and analyzing the data. These tests were periodic in motion, although the table is also capable of applying random motion.

## **DESARROLLO DEL SIMULADOR DE TERREMOTOS DE LA UPRM PARA ANÁLISIS DE MODELOS DINÁMICOS**

### **Resumen**

Recientemente, la Universidad de Puerto Rico en Mayagüez (RUM) ha añadido a sus instalaciones del Laboratorio de Estructuras un simulador de terremotos. La mesa vibradora se puede clasificar como pequeña, uni-direccional y electro-hidráulica. La mesa vibradora fue diseñada para hacer investigaciones en el área de modelos a escala bajo carga dinámica. Consiste de una plataforma rígida deslizándose en unos “bearings” lineales sin fricción movidos por un gato hidráulico que está conectado a un pórtico de reacción. El pórtico de reacción está conectado a la losa del laboratorio. Los componentes del sistema de la mesa vibradora fueron diseñados y dimensionados para probar modelos a escala de 1:4 y para reproducir cinco terremotos históricos. Las características dinámicas de la plataforma, del pórtico de reacción y de la columna de aceite fueron estudiados, como así también sus posibles interacciones con un estructura en la mesa vibradora. A través de unos experimentos preliminares, se obtuvo una determinación inicial de la calidad de reproducción de comando de desplazamientos de la mesa vibradora. Los ensayos consistieron en movimientos periódicos, aunque la mesa puede aplicar movimientos aleatorios.

## DEDICATION

I would like to dedicate this investigation to my family for their continued support, understanding, love and respect throughout this project.

“Small kindnesses, small courtesies, small considerations, habitually practiced in our social intercourse, give a greater charm to the character than the display of great talent and accomplishments”.

Kelty

I would also like to dedicate this project to GOD, who has been my inspiration and my rock, where I can stand up when there is a sea of problems and preoccupations. Thanks GOD for always been there for me!

“I press on toward the goal for the prize of the upward call of God in Christ Jesus”

Philippians 3:14

## ACKNOWLEDGMENTS

I would like to thank Dr. Daniel Wendichansky for the opportunity to work on this investigation and for his support and guidance throughout its duration. I would also like to thank my graduate committee composed of Dr. Ricardo López and Dr. Luis Suárez for their help and assistance during this investigation.

I would like to acknowledge the Structural Laboratory's technicians for their help in the construction of the shaking table, especially to Mr. Elvis Ramos.

Many thanks to the MTS technicians for their continued assistance during this project. Special thanks to Mr. Brad Schroenghamer and Mr. Steve Carlsen who always were available to answer questions regarding the shaking table and the hydraulic equipment.

I am grateful to Mr. Mark Pitman, of the University of Buffalo, for his help and guidance on shaking table dynamics.

Special thanks to all the Civil Engineering Department Staff (all the secretaries and personnel) for their continued support during this investigation.

In addition, many thanks to all the graduate students who were involved in this investigation.

Many thanks to all of you!

# TABLE OF CONTENTS

<b>ABSTRACT .....</b>	<b>ii</b>
<b>RESUMEN .....</b>	<b>iii</b>
<b>DEDICATION .....</b>	<b>iv</b>
<b>ACKNOWLEDGMENTS .....</b>	<b>v</b>
<b>TABLE OF CONTENTS .....</b>	<b>vi</b>
<b>LIST OF TABLES .....</b>	<b>x</b>
<b>LIST OF FIGURES .....</b>	<b>xi</b>
<b>LIST OF APPENDICES .....</b>	<b>xv</b>
<b>CHAPTER 1 INTRODUCTION.....</b>	<b>1</b>
1.1 BACKGROUND .....	1
1.2 JUSTIFICATION OF PROPOSED RESEARCH .....	2
1.3 RESEARCH POTENTIAL OF THE EARTHQUAKE SIMULATOR .....	4
1.4 RESEARCH OBJECTIVES .....	5
1.5 METHODOLOGY FOR DEVELOPMENT OF RESEARCH .....	6
1.5.1 DEVELOPMENT OF SHAKING TABLE FACILITY .....	6
1.5.2 DETERMINATION OF SHAKING TABLE PERFORMANCE AND CALIBRATION .....	7
<b>CHAPTER 2 LITERATURE REVIEW.....</b>	<b>9</b>
2.1 SHAKING TABLES .....	9
2.2 MODEL TESTS ON EARTHQUAKE SIMULATORS .....	11
2.3 DESIGN PARAMETERS FOR SHAKING TABLE SYSTEMS .....	13
2.3.1 SIMULATOR PLATFORM (SLIP TABLE) .....	13
2.3.2 SUPPORT SYSTEM .....	13
2.3.3 REACTION MASS (FOUNDATION) .....	14
2.3.4 SIMILITUDE REQUIREMENTS .....	15
2.4 DYNAMICS OF SHAKING TABLES .....	15
<b>CHAPTER 3 DESCRIPTION OF SHAKING TABLE COMPONENTS .....</b>	<b>17</b>

3.1	INTRODUCTION .....	17
3.2	DESIGN CONCEPT .....	17
3.3	SHAKING TABLE COMPONENTS .....	18
3.3.1	HYDRAULIC POWER SYSTEM .....	20
3.3.2	SERVOVALVE .....	22
3.3.3	LINEAR ACTUATOR .....	22
3.3.4	SIMULATOR PLATFORM .....	24
3.3.5	LINEAR BEARING SYSTEM .....	25
3.3.6	REACTION MASS .....	27
3.3.7	SERVO-CONTROLLER .....	28
3.3.8	CONTROL AND DATA ACQUISITION .....	29
3.3.9	INSTRUMENTATION FOR MEASUREMENTS .....	30
<b>CHAPTER 4</b>	<b>DYNAMIC MODELING THEORY .....</b>	<b>31</b>
4.1	INTRODUCTION .....	31
4.2	MODELING THEORY .....	31
4.3	DIMENSIONAL ANALYSIS .....	31
4.4	SIMILITUDE RELATIONSHIPS AND TYPES OF MODELS .....	33
4.5	PHYSICAL MODELS FOR SHAKE TABLE STUDIES .....	35
4.5.1	TRUE REPLICA MODELS .....	35
4.5.2	ADEQUATE MODELS .....	37
<b>CHAPTER 5</b>	<b>DESIGN OF SHAKING TABLE COMPONENTS .....</b>	<b>41</b>
5.1	INTRODUCTION .....	41
5.2	TYPICAL EARTHQUAKE RECORDS SELECTION .....	41
5.3	SCALING OF PROTOTYPE GROUND MOTIONS .....	41
5.3.1	SIMILITUDE SCALING .....	41
5.3.2	MAGNITUDE SCALING .....	43
5.4	REACTION MASS .....	44
5.5	SIMULATOR PLATFORM (SLIP TABLE) .....	46
5.6	LINEAR ROLLER BEARINGS .....	46

5.7 PAYLOAD .....	51
5.8 HYDRAULIC ACTUATOR .....	51
5.9 SERVO- HYDRAULIC SYSTEM .....	53
5.10 CONTROLLER SPECIFICATIONS .....	54
5.11 DATA ACQUISITION SYSTEM SPECIFICATIONS .....	55
<b>CHAPTER 6 SERVO-HYDRAULIC SYSTEM .....</b>	<b>57</b>
6.1 INTRODUCTION .....	57
6.2 HYDRAULIC POWER SUPPLY .....	57
6.3 HYDRAULIC SERVICE MANIFOLD .....	58
6.4 SERVOVALVE .....	63
6.5 LINEAR ACTUATOR .....	67
6.6 PERFORMANCE ENVELOPES .....	69
6.6.1 FLOW LIMITS FOR HARMONIC AND RANDOM ACTUATOR MOTION .....	69
6.6.2 SPAN AND FORCE LIMITS .....	71
<b>CHAPTER 7 DYNAMIC MODELS OF SEISMIC SIMULATOR .....</b>	<b>75</b>
7.1 COMPONENTS OF SEISMIC SIMULATOR .....	75
7.1.1 SIMULATOR PLATFORM (SLIP TABLE) .....	75
7.1.2 REACTION FRAME .....	79
7.1.3 HYDRAULIC ACTUATOR DYNAMICS .....	83
<b>CHAPTER 8 SHAKING TABLE CONSTRUCTION .....</b>	<b>88</b>
8.1 INTRODUCTION .....	88
8.2 ASSEMBLY OF REACTION FRAME .....	88
8.3 ASSEMBLY OF SIMULATOR PLATFORM .....	88
8.4 CONNECTION OF REACTION FRAME TO FLOOR .....	90
8.5 MOUNTING OF LINEAR BEARING SYSTEM .....	90
8.6 LEVELING AND ALIGNMENT OF LINEAR BEARING SYSTEM .....	91
8.7 MOUNTING OF SIMULATOR PLATFORM .....	95
8.8 CONNECTION OF HYDRAULIC ACTUATOR .....	96

<b>CHAPTER 9</b>	<b>MEASURES OF SHAKING TABLE PERFORMANCE .....</b>	<b>97</b>
9.1	INTRODUCTION .....	97
9.2	EXPERIMENTAL TESTS FOR DETERMINATION OF SHAKING TABLE PERFORMANCE .....	97
9.3	CALIBRATION PARAMETERS .....	98
9.3.1	PROPORTIONAL GAIN (P) .....	99
9.3.2	INTEGRAL GAIN (I) .....	99
9.3.3	DERIVATIVE GAIN .....	100
9.3.4	FEED FORWARD GAIN (F) .....	100
9.3.5	TUNING PROGRAM .....	101
9.4	SQUARE WAVE .....	101
9.5	SINUSOIDAL WAVE .....	105
9.5.1	COMPARISON OF INPUT/RESPONSE AMPLITUDE .....	105
9.5.2	CHECKING FOR ROTATIONAL MODES OF VIBRATION .....	113
9.5.3	COMPARISON IN THE FREQUENCY DOMAIN .....	129
<b>CHAPTER 10</b>	<b>CONCLUSIONS .....</b>	<b>137</b>
<b>REFERENCES</b> .....		<b>141</b>
<b>APPENDIX A: CHARACTERISTICS OF THE MODEL TEST STRUCTURE .....</b>		<b>144</b>

## LIST OF TABLES

TABLE	TITLE	PAGE
Table 1.1	Damage estimates of the most significant earthquakes from 1994 to 2001 .....	1
Table 1.2	The most significant earthquakes registered in Puerto Rico from 1670 to 1918 .....	2
Table 2.1	Classification of Shaking Tables .....	9
Table 2.2	Methods for Supporting Tables .....	14
Table 4.1	Dimensionless Products .....	34
Table 4.2	Similitude Relationships for Artificial Mass Simulation Method .....	40
Table 5.1	Historical Earthquake Records Used in Analysis and Design of System Components .....	42
Table 5.2	Technical Specifications of Linear Bearing System .....	50
Table 6.1	MTS Model 506.61 HPS Specifications .....	60
Table 6.2	MTS Model 293.11A HSM Specifications .....	62
Table 6.3	MTS Model 252.25 Servovalves Specifications .....	65
Table 6.4	Components of the Servo-Hydraulic System .....	71
Table 7.1	Physical and Dynamic Properties of the UPRM Servo-Hydraulic System .....	87

## LIST OF FIGURES

FIGURE	TITLE	PAGE
Figure 3.1	Plan and Elevation Views of the Earthquake Simulator .....	17
Figure 3.2	UPRM Earthquake Simulator .....	18
Figure 3.3	Block Diagram of Seismic Simulator .....	19
Figure 3.4	Hydraulic Power Unit .....	20
Figure 3.5	Hydraulic Service Manifold .....	21
Figure 3.6	Dual Servovalves Mounted on the Actuator .....	22
Figure 3.7	Linear Actuator and Components .....	23
Figure 3.8	Basic Cylinder Components .....	24
Figure 3.9	Simulator Platform mounted to the Reaction Mass .....	25
Figure 3.10	Linear Bearing System .....	26
Figure 3.11	Reaction Mass fixed to the Laboratory Strong Floor .....	27
Figure 3.12	Servo-Controller .....	28
Figure 3.13	MTS TestStar IIs AP Control Computer and Data Acquisition Computer .....	29
Figure 3.14	Piezoresistive Accelerometer .....	30
Figure 5.1	Connection to Structural Lab Strong Floor .....	45
Figure 5.2	Simulator Platform Components .....	47
Figure 5.3	Plan View of Simulator Platform showing Locations of Sliding Bearings .....	48
Figure 5.4	Dimensions of a Crossed Roller Slide Table NBT-6310 .....	49
Figure 5.5	Permissible Moment Load Ratings .....	50
Figure 5.6	Maximum Actuator force for Five Representative Earthquake Records .....	52
Figure 6.1	Block Diagram for MTS Model 506.61 Hydraulic Power Supply .....	59
Figure 6.2	MTS Model 293.11A HSM Parts .....	61
Figure 6.3	Functional Diagram of a Single Servovalve and Manifold Mounted to the Actuator .....	63
Figure 6.4	Cross-Section of Dual Servovalves Mounted to Servovalve's Manifold .....	64

Figure 6.5	MTS Theoretical Performance Curves for the Series 252 Servovalves .....	66
Figure 6.6	Force Transducer .....	67
Figure 6.7	Displacement vs. Frequency Performance Envelope .....	73
Figure 6.8	Velocity vs. Frequency Performance Envelope .....	73
Figure 6.9	Acceleration vs. Frequency Performance Envelope .....	74
Figure 7.1	Simulator Platform Model .....	76
Figure 7.2	First Three Modes of Simulator Platform .....	78
Figure 7.3	Reaction Frame Model .....	80
Figure 7.4	First Three Modes of Reaction Frame .....	82
Figure 7.5	Equivalent SDOF of Actuator and Oil System .....	83
Figure 7.6	Schematic of Hydraulic Actuator .....	84
Figure 8.1	Lateral Bracing of Reaction Frame .....	89
Figure 8.2	New Beam Welded to Simulator Frame .....	89
Figure 8.3	Linear Bearing System #1 Mounted to the Reaction Frame .....	90
Figure 8.4	Top Flange's Surface Initial Leveling .....	91
Figure 8.5	Next Leveling of 4-LBS .....	92
Figure 8.6	Last Leveling of 4-LBS .....	93
Figure 8.7	Elevations Layout .....	93
Figure 8.8	Elevation Profiles of the Two Lines of Bearings .....	94
Figure 8.9	Simulator Platform Bolted to the Top Plate of the 4-LBS .....	95
Figure 8.10	Steel Plates Attached to Simulator Frame .....	95
Figure 8.11	Attachment of Actuator to Simulator Platform .....	96
Figure 9.1	Definitions of Error and Phase Lag .....	98
Figure 9.2	Effects of Proportional Gain on Sensor Feedback .....	99
Figure 9.3	Effects of Integral Gain on Sensor Feedback .....	100
Figure 9.4	Effects of Derivative Gain on Sensor Feedback .....	100
Figure 9.5	Effects of Feed Forward Gain on Sensor Feedback .....	101
Figure 9.6	Effects of Sensitivity on a Square Waveform .....	102
Figure 9.7	P-Gain ( $K_p$ ) Tuning for a Square Wave .....	103
Figure 9.8	Close-Up of Oscillations at $K_p = 2.5$ .....	104

Figure 9.9	Scope Graphics for $K_P = 2.1$ to $2.4$ .....	104
Figure 9.10	Effect of $K_I$ on the Waveform .....	105
Figure 9.11	Command Error (peak) vs. P-gain ( $K_P$ ) Tuning for 1.0 to 10.0 Hz .....	106
Figure 9.12	Command Error (valley) vs. P-gain ( $K_P$ ) Tuning for 1.0 to 10.0 Hz .....	107
Figure 9.13	Command Error (peak) vs. P-gain ( $K_P$ ) Tuning for 11.0 to 18.0 Hz .....	108
Figure 9.14	Command Error (valley) vs. P-gain ( $K_P$ ) Tuning for 11.0 to 18.0 Hz .....	109
Figure 9.15	Effect of $K_P$ on 1.0 Hz Sinusoidal Waveform .....	110
Figure 9.16	Effect of $K_P$ on 5.0 Hz Sinusoidal Waveform .....	111
Figure 9.17	Effect of $K_P$ on 10.0 Hz Sinusoidal Waveform .....	112
Figure 9.18	Effect of $K_P$ on 15.0 Hz Sinusoidal Waveform .....	112
Figure 9.19	Effect of $K_P$ on 18.0 Hz Sinusoidal Waveform .....	113
Figure 9.20	Shake Table Rotational Modes .....	113
Figure 9.21	Accelerometers Layout .....	114
Figure 9.22	Effect of $K_P$ on RFN-RFS for 11.0 Hz .....	116
Figure 9.23	RFN-RFS for 15.0 Hz Sine Wave - $K_P = 3.5$ .....	117
Figure 9.24	RFN-RFS for 17.0 Hz Sine Wave - $K_P = 3.5$ .....	117
Figure 9.25	Effect of $K_P$ on SPN-SPS for 11.0 Hz .....	120
Figure 9.26	SPN-SPS for 15.0 Hz Sine Wave - $K_P = 3.5$ .....	121
Figure 9.27	SPN-SPS for 17.0 Hz Sine Wave - $K_P = 3.5$ .....	121
Figure 9.28	Close-Up of 11.0 Hz Sine Wave Acceleration for SPN, SPS and Zero-SPW .....	122
Figure 9.29	Close-Up of 15.0 Hz Sine Wave Acceleration for SPN, SPS and Zero-SPW .....	122
Figure 9.30	Close-Up of 17.0 Hz Sine Wave Acceleration for SPN, SPS and Zero-SPW .....	123
Figure 9.31	Rigid Mass with Translation and Rotation .....	124
Figure 9.32	(SPN-Zero)-11.0 Hz Sine Wave - $K_P = 3.5$ .....	126
Figure 9.33	(SPN-Zero)-15.0 Hz Sine Wave - $K_P = 3.5$ .....	126
Figure 9.34	(SPN-Zero)-17.0 Hz Sine Wave - $K_P = 3.5$ .....	127

Figure 9.35	(SPS-Zero)-11.0 Hz Sine Wave – $K_p = 3.5$ .....	127
Figure 9.36	(SPS-Zero)-15.0 Hz Sine Wave – $K_p = 3.5$ .....	128
Figure 9.37	(SPS-Zero)-17.0 Hz Sine Wave – $K_p = 3.5$ .....	128
Figure 9.38	Sine Wave Performance .....	129
Figure 9.39	7.0 Hz Sine Wave Performance .....	130
Figure 9.40	8.0 Hz Sine Wave Performance .....	132
Figure 9.41	9.0 Hz Sine Wave Performance .....	133
Figure 9.42	11.0 Hz Sine Wave Performance .....	134
Figure 9.43	17.0 Hz Sine Wave Performance .....	136

## LIST OF APPENDICES

APPENDIX	TITLE	PAGE
Appendix A	Characteristics of the Model Test Structure .....	144

## 1. INTRODUCTION

### 1.1. BACKGROUND

The word "earthquake" is synonymous with loss of life and property. Damage estimates of the world's most significant earthquakes from 1989 to 2001 are illustrated in Table 1.1. These destructive earthquakes, with magnitudes (Richter's scale) ranging from 6.5 to 8.4, resulted in hundreds of casualties and hundreds of millions of dollars in property damages.

Puerto Rico is located in a zone of high seismicity between the edges of the North American and Caribbean tectonic plates. Table 1.2 shows the most significant earthquakes registered in Puerto Rico. From this table, it can be seen that four strong earthquakes with magnitudes of 7.5 and 8.0 have affected Puerto Rico. Methods for predicting the occurrence of seismic events give us an indication that there is a significant probability for the future occurrence of a destructive earthquake in Puerto Rico and that we should prepare for it.

Table 1.1. Damage estimates of the most significant earthquakes from 1994 to 2001. <sup>1</sup>

Date	Location	Magnitude	Casualties <sup>2</sup>	Property Damages
January 26, 2001	India	7.7	D-18,602 I-166,836 H-600,000	Damage estimates are of \$1.3 billion US dollars; 751,000 houses damaged and 332,000 destroyed.
August 17, 1999	Turkey	7.4	D-17,127 I-43,953 H-250,000	Damage estimates range from \$3 to \$6.5 billion US dollars; 214,000 houses and 30,500 business units where lightly to heavily damage; more than 20,000 reinforced concrete buildings collapsed.
January 17, 1995	Kobe, Japan	7.2	D-5,500 I-35,000 H-300,000	Damage is estimated at over \$147 billion US dollars; 180,000 buildings were badly damaged or destroyed.
January 17, 1994	Northridge, California	6.9	D-57 I-9,000 H-20,000	Damage estimates range from \$20 to 40 billion US dollars; more than 1,600 buildings were tagged "unsafe"; damages to more than 170 freeway bridges; fractured steel frames in more than 100 seismic-resistant buildings; some reinforced concrete columns were crushed.

Notes: 1. Modified from [1].

2. D = deaths; I = injured; H = homeless (displaced people).

Table 1.2. The most significant earthquakes registered in Puerto Rico from 1670 to 1918. <sup>1</sup>

Date	Location	Magnitude/ Intensity <sup>2</sup>	Damages
August 15, 1670	Not Available	Not Determined	Damages in San Juan and San German.
May 2, 1787	Puerto Rico Trench (Estimated)	M = 8.0 (Estimated)	Felt strongly all across the island; demolished the Arecibo church, El Rosario and La Concepción monasteries; damages to the churches at Bayamón, Toa Baja, and Mayagüez; considerable damaged the castles of San Felipe del Morro and San Cristóbal braking cisterns, walls and guard houses.
November 18, 1867	Anegada Passage, Virgin Islands (between PR and St. Croix)	M = 7.5 VIII all PR	Felt strong in all PR, but the most severe effects were in the eastern part; a tsunami ran inland almost 150 m (490 ft) in the coast of Yabucoa; 70 of the 80 chimneys of the talents of sugar collapsed in Ponce; more than 500 retorts felt during a period of six to seven months after earthquake.
October 11, 1918	Mona Canyon	M = 7.5 VIII-IX in western part of PR V- VI in Guayanilla	116 deaths; damages estimated at more than \$4 million US dollars; accompanied by a tsunami that got up to 6 meters (19.5 ft); continued retorts of this earthquake were felt for several months.

Notes: 1. Modified from [2].  
2. The intensity scale is MM (Modified Mercalli).

## 1.2. JUSTIFICATION OF PROPOSED RESEARCH

As seen from Table 1.1, property losses can amount to hundreds of millions in the event of a major earthquake. The structures most affected by a destructive earthquake are fixed structural systems such as buildings, bridges and dams. Therefore, it is necessary to develop analytical tools for the design of earthquake-resistant structures. Analytical models can be developed for the prediction of the dynamic elastic-inelastic response of structures during earthquake loading. However, these analytical models involve the idealization and assumption of the structure's behavior based on current theoretical

knowledge. Experimental research provides an alternate means of analysis and of extending the limits of theoretical knowledge [3]. In addition, the capabilities of these analytical models can only be validated by experimental work.

Experimental research can be accomplished through the development of an adequate dynamic testing facility. The Civil Engineering Department at the University of Puerto Rico at Mayagüez understands the importance and necessity of an adequate testing facility for conducting experimental research in the area of earthquake engineering in Puerto Rico. The Structural Laboratory at the Civil Engineering Department has facilities for material and component testing. These facilities allow for testing of materials, individual elements and structural assemblies. However, the Structural Laboratory lacked the facilities for testing of complete structures under simulated environmental loads, such as those produced by wind and earthquakes. For this purpose, a proposal was submitted and accepted for the development of an earthquake simulator by means of a shaking table. Shaking tables provide the most versatile resource for exciting the dynamic response of a test structure [3]. Although it is physically impossible to completely duplicate the ground motion produced by an earthquake, shake tables possess the capability to generate earthquake-like motion. Thus, they can apply forces to the test structure in the same way the ground motion applies forces to an actual structure during an earthquake.

The addition of a shaking table completes the dynamic testing facilities at the Structural Laboratory at the Civil Engineering Department. Furthermore, the shaking table facility at the Civil Engineering Department at the University of Puerto Rico at Mayagüez is the first of its kind in Puerto Rico.

### **1.3. RESEARCH POTENTIAL OF THE EARTHQUAKE SIMULATOR FACILITY**

The dynamic testing facilities at the Structural Research Laboratory, with the addition of the earthquake simulator facility, by means of a shaking table, could be used to test a variety of systems such as individual elements, assemblages of elements, and complete structures. Small-scale model testing can be used as complement for and/or an alternative to analytical investigations [4]. Furthermore, it can be used for comparative studies or for controlled parameter variations. Replica model testing would enable the investigation of earthquake related phenomena such as [4]:

1. Rate of loading effects
2. Dynamic response characteristics under realistic seismic excitation (from low amplitude vibrations to excitation producing inelastic response and failure)
3. Failure mechanisms
4. Effects of mass and stiffness irregularities
5. Torsional and overturning effects
6. Dynamic instability
7. Idealized soil structure interaction effects

It will be also possible the demonstration of the integrity and safety of designed structures under various levels of earthquake inputs.

Examples of testing of full-scale assemblages of components under realistic earthquake conditions include [4]:

1. Frames with different combinations of geometry, beams, columns, and joints
2. Frames infilled with shear walls
3. Lateral bracing systems for frames

4. Core elements such as stairs wells and elevator shafts
5. Wall and roof diaphragms
6. Architectural elements

The addition of the shaking table system, consisting of high-performance mechanical and electrical equipment, creates a multi-disciplinary environment for research in the fields of civil, mechanical and electrical engineering [5]. More important, the shaking table facility provides the engineering teachers with a tool for illustrating the principles of structural dynamics.

#### **1.4. RESEARCH OBJECTIVES**

This research project has two main objectives:

1. The first main objective is the development and construction of an earthquake simulator facility by means of a shaking table. The primary purpose of the shaking table will be to simulate earthquake ground motion to study their effects on reduced scale structural models of complete structures. The proposed working concept for the shaking table facility consists of a small-size uni-directional electro-hydraulic shaking table.

The reproduction through shaking tables of commanded dynamic signals (target ground motion) is imperfect [7].

2. Therefore, the second main objective of this investigation is to gain an understanding of the dynamic behavior of the shaking table built at the Civil Engineering Department of the University of Puerto Rico at Mayagüez and to show that it can be used effectively for structural

dynamic testing. In order to achieve this objective, both the shaking table performance and the calibration parameters will be determined experimentally. The calibration parameters will consist of the values of the control gain parameters that give an *acceptable* response of the table. An *acceptable* response of the shaking table means having a feedback displacement not too different from the target command displacement and a stable response.

## **1.5. METHODOLOGY FOR DEVELOPMENT OF RESEARCH**

The methodology for the development of this investigation can be divided in two parts:

1. The first part involves the development and construction of the shaking table facility.
2. The second part involves experimentally measuring shaking table performance and determining calibration parameters for the constructed shaking table.

### **1.5.1. DEVELOPMENT OF SHAKING TABLE FACILITY**

The methodology for the development of the earthquake simulator was concentrated in the construction of a small-size uni-directional electro-hydraulic shaking table.

## **I. DESIGN OF SHAKING TABLE COMPONENTS**

The following chapter will discuss the criteria for the design of the shaking table components. This criteria was based on the review of literature of existing earthquake simulators.

## **II. CONSTRUCTION OF SHAKING TABLE FACILITY**

The shaking table components, after being properly designed and selected, were assembled at the indoor facility of the Structural Laboratory at the Civil Engineering Department of the UPRM. The hydraulic power equipment and electronic control system was acquired from the MTS Corporation.

### **1.5.2. DETERMINATION OF SHAKE TABLE PERFORMANCE AND CALIBRATION**

The shaking table performance and calibration parameters were determined experimentally, as described in the following sections.

#### **I. SHAKING TABLE PERFORMANCE**

##### *Preliminary Experimental Tests [3]*

An initial subjective determination of the quality of shake table reproduction was obtained by carrying out preliminary experimental tests. The preliminary tests involved the following input motions:

1. Square wave - provided information on the bare (unloaded) shaking table stability and rate of response.
2. Sinusoidal wave - provided the amplitude spectra envelope of the shaking table response and the frequency performance limitations.

## II. CALIBRATION PARAMETERS [3, 9]

The set of gain parameters for an *acceptable* table response was obtained for the bare table condition. An *acceptable* response of the shaking table means having a feedback displacement not too different from the target command displacement and a stable response. With this tuning or calibrating procedure, we assure that the shaking table is able to reproduce the commanded time histories with the degree of precision desired.

## 2. LITERATURE REVIEW

### 2.1. SHAKING TABLES

Recorded attempts at earthquake simulation in the laboratory for structural testing have been made as early as the turn of the nineteenth century [10]. But it was only after the late 1960's that experimental earthquake simulation was revolutionized as a result of advances in electrohydraulic servo-controls, analog and digital computer hardware and dynamic instrumentation. Several servo-hydraulic shaking tables were first constructed in the United States during the late 1960's and the 1970's. Table 2.1 shows different examples of existing shaking tables and their classification. The majority of the shaking tables in the U.S. can be classified as small tables, 3.05 m x 3.05 m (10 ft x 10 ft) and smaller, although a small number of medium, 3.05 m to 9.14 m square (10 ft to 30 ft) size tables exist [3].

Table 2.1. Classification of Shaking Tables. <sup>1</sup>

Example of Shaking Table Facilities	Dimensions m (ft)	Payload Limit kN (lb)	$A_{max}, g^2$		$D_{max}, \pm cm (\pm in)$		$F_{max},$ Hz
			Hor.	Vert.	Hor.	Vert.	
<b>SMALL (&lt; 10 ft)</b>							
Stanford University	1.5 x 1.5 (5 x 5)	22.2 (5,000)	5.0	-	6.35 (2.5)	-	50.0
Rice University	1.5 x 1.5 (5 x 5)	6.67 (1,500)	6.0	-	7.62 (3.0)	-	70.0
University of Calgary	1.4 x 1.4 (4.5 x 4.5)	8.9 (2,000)	20.0	-	7.62 (3.0)	-	-
<b>MEDIUM (10-30 ft)</b>							
University of California at Berkeley	6.1 x 6.1 (20 x 20)	444.8 (100,000)	1.5	1.0	12.7 (5.0)	5.08 (2.0)	15.0
University of Illinois	3.65 x 3.65 (12 x 12)	44.48 (10,000)	7.0	-	10.16 (4.0)	-	100
Us Corps of Engineers	3.65 x 3.65 (12 x 12)	53.38 (12,000)	34	60	5.59 (2.2)	4.57 (1.8)	200
State University of New York at Buffalo	3.65 x 3.65 (12 x 12)	195.7 (44, 000)	4.2	8.7	15.24 (6.0)	7.62 (3.0)	60.0
<b>LARGE (&gt; 30 ft)</b>							
National Research Center, Japan	15.24 x 15.24 (50 x 50)	4,448.2 (1,000,000)	0.6	1.0	3.048 (1.2)	-	16.0
Berkeley - Proposed	30.5 x 30.5 (100 x 100)	17,792.9 (4,000,000)	0.6	0.2	15.24 (6.0)	7.62 (3.0)	-

Note: 1. Modified from [3].  
2. Capacity for the unloaded or bare table condition.

Large shaking tables provide valuable tools for gaining understanding of structural behavior through testing of full-scale prototypes or large models [3]. Small rolled sections can be used for models of steel structures, and prototype material (reinforcing bars and concrete) can be used for reinforced concrete models [4]. However, large shaking tables involve significant development and high operating expenses as well as problems meeting similitude requirements. Smaller-sized tables are better suited for small-scale model analysis, not only on the basis of size requirements, but also on the basis of their ability to satisfy similitude laws for scaling of input displacement, acceleration, and frequency [3].

Real earthquakes have no restrictions on the direction of the ground motion. To completely reproduce the ground motion, an earthquake simulator would have to be capable of movement in three reference directions, two horizontal and one vertical, assuming that ground motion is homogenous over the base of the structure and that rotational modes of ground motion can be neglected [3]. Multi-component earthquake simulators involve high development and operating costs and also require specialized and experienced knowledge for the developers and operators of the facility. Uni-directional earthquake simulators have often been used in the past as stepping-stones in the direction of multi-directional earthquake simulators.

From the preceding discussion of shaking tables, the design process will be focused on cost-effective, state of the art small-size uni-directional shaking table facilities.

## 2.2. MODEL TESTS ON EARTHQUAKE SIMULATORS

Testing of complete structures on shaking tables will be generally limited to small-scale models of complete structures, due to size constraints. For this reason, most of the earlier shaking tables were used only for demonstration purposes, qualitative studies, or component testing. They were not utilized for replica modeling of actual structures, due to the lack of information available on the possibilities and limitations of small-scale replica modeling [4].

Various research studies were conducted in order to address this problem. One of the most important of such research studies was a four-year NSF sponsored program at Stanford University where the feasibility and limitations of small-scale model testing in earthquake engineering was investigated. The first part of this study, conducted by Mills [3], concentrated on shake table performance and on data acquisition systems needed for small-scale model testing. The second part conducted by Moncarz [4], investigated the general aspects of dynamic modeling theory, model material behavior and the accuracy of prototype response prediction through small-scale model tests. Some of the most important conclusions of this four-year study were:

1. The dynamic response of structural buildings systems could be simulated accurately at model scales.
2. The quality of response prediction was dependent on the accuracy of:
  - a. Material simulation
  - b. Reproducibility of dynamic input of the earthquake simulator

This research investigation is concentrated on the reproducibility of dynamic input of the earthquake simulator.

Numerous tests have been conducted at the dynamic testing facilities at the University of California at Berkeley [11]. The first significant structure tested at the shaking table facility was a three-story single-bay moment-resistant steel frame in 1975 [12]. The main objectives of this study were to gain experience with the earthquake simulator facility and to observe the linear and non-linear behavior of the structure under earthquake type motion. Furthermore, a mathematical model was developed from the test results, which could be used to predict adequately the seismic behavior of the structure. Since then many structures have been tested including reinforced concrete structures [6, 7, and 13].

At the State University of New York at Buffalo, extensive research has also been conducted in their shaking table facility [14]. In reference [15], the dynamic characteristics of a full-size five-story steel prototype structure and a 2/5-scale laboratory model were compared and correlated. In addition, different bracing and configuration systems were investigated. Another important research study conducted at this facility was related to the investigation of energy dissipation devices, in particular on fluid viscous dampers [16].

Shaking table facilities have also been used in the investigation on models of dams and bridges. In addition, tests have been conducted on buildings of unusual design like shell-type structures and towers, and on mechanical and electrical equipment. Mills [3] and Moncarz [4] present an extensive compilation of these references.

### **2.3. DESIGN PARAMETERS FOR SHAKING TABLE SYSTEMS**

Looking at the existing seismic simulators revealed helpful design criteria for the design and construction of the UPRM seismic simulator. A summary of these criteria is presented in the following paragraphs.

#### **2.3.1. SIMULATOR PLATFORM (SLIP TABLE)**

The simulator platform acts as the moving base for the model structures fixed to its surface [5]. Its movement is controlled by the movement of an actuator fixed to one end of the reaction mass or foundation. The simulator platform requires considerable rigidity, both in-plane and out of plane and should possess adequate mass to help minimize feedback interface effects from a vibrating model on the table [3, 6, 7, 17 and 18].

The simulator platform must satisfy three constraints [5]:

1. The platform natural frequency must be at least three to four times the maximum operating frequency to be tested.
2. The platform mass should be as light as possible to reduce inertia forces, thus requiring smaller actuator forces to drive the platform. In addition, the maximum acceleration capacity of the simulator increases as the platform mass is reduced [19].
3. The platform must be stiff enough to prevent excessive rotation of the sliding bearings [19].

#### **2.3.2. SUPPORT SYSTEM**

The support system provides the sliding surface for the simulator platform. A properly designed table should have a support system characterized by the following [3, 17 and 18]:

1. Low friction: necessary to minimize distortion of the desired table response.
2. Rigidity: prevents adverse table motion such as rotation.
3. Large load capacity: necessary even for small-scale replica model studies.

Some of the methods for supporting shaking tables are: air pressure and vertical actuators, oil film, flexural support and roller bearings. Table 2.2 illustrates existing shaking tables with their choice of support system. The most common support system method for small-sized shaking tables is the use of roller bearings.

Table 2.2 Methods for Supporting Tables<sup>1</sup>

Example of Shaking Table Facility	Support Method	Payload Capacity kN (lb)	Size m (ft)
U.C. Berkeley	Air pressure and vertical actuators <sup>2</sup>	444.8 (100,000)	6.1 x 6.1 (20 x 20)
ISMES	Oil film	1.33 (300)	3.05 x 1.98 (10 x 6.5)
University of Illinois	Flexural supports	44.82 (10,000)	3.65 x 3.65 (12 x 12)
Stanford University	Roller bearings	22.24 (5,000)	1.5 x 1.5 (5 x 5)
Rice University	Roller bearings	6.67 (1,500)	1.5 x 1.5 (5 x 5)
State of New York at Buffalo	Vertical and horizontal actuators	195.7 (44,000)	3.65 x 3.65 (12 x 12)
Washington State University	Roller Bearings	32.02 (7,200)	2.28 x 1.52 (7.5 x 5)

Note: 1. Modified from [3].  
2. Enables vertical motion.

### 2.3.3. REACTION MASS (FOUNDATION)

The entire shaking table system (simulator platform, support system, actuator, and servovalve) is fixed or supported by a reaction mass [5]. One of the purposes of the reaction mass is to provide a firm base for the actuator's force. It is recommended the use of large reaction mass, about 30 to 50 times the mass of the simulator/structure system, to prevent motion of the reaction mass caused by the motion of the simulator platform and test structure [3, 6, 7, 17, 18 and 19].

#### **2.3.4. SIMILITUDE REQUIREMENTS**

Several general design goals for shake table performance capabilities can be derived from the requirements of similitude laws for scaling of length, acceleration and time for small-scale dynamic models [3].

1. Actuator with considerable displacement sensitivity:

Displacements in models are decreased by scaling of prototype lengths, requiring simulator systems to accurately reproduce displacements of small magnitudes.

2. Relatively powerful force actuator:

Accelerations on the table will generally be equal or greater than the accelerations of the prototype time history, requiring a high shaking table acceleration capacity.

3. High frequency capability:

This is specified by the inverse of the time scale. These displacement and acceleration requirements will lead to compaction of the time scale, thus the shake table motion will occur at a much faster rate than for the prototype.

4. Capability to test structures of at least 1:4 scales.

#### **2.4. DYNAMICS OF SHAKING TABLES**

The dynamic behavior of small-size uni-directional shaking tables has been discussed previously by a few researchers such as Rea [6], Rinawi [7] and Trombetti [9].

Rea et.al [6] determined experimentally the frequency response of a 8.9 kN (2,000 lb) and 444.82 kN (100,000 lb) shaking tables. They studied the effects of a resonant structure on the lighter table, and the effects of foundation compliance on the heavier

table. Mathematical models were also developed for the two conditions. A detailed analysis of the simulators is presented in which the dynamics of the servovalve/actuator, simulator platform and test structure are included.

Rinawi et.al [7] tested the 6.1 m x 6.1 m (20 x 20 ft) shaking table at UC-Berkeley for interaction effects. The tests included three loading conditions: the bare table, a rigid mass and a flexible SDOF structure. Mathematical models are derived for analyzing the table-structure system.

Trombetti [9] presented an experimental/analytical approach to modeling and calibrating shaking tables for structural dynamic applications. This approach was successfully applied at the shaking table facility at Rice University. The dynamics of the actuator-foundation-specimen system is modeled and analyzed combining linear control theory and linear structural dynamics. This mathematical model accounts for numerous variables such as: actuator oil compressibility, oil leakage in the actuator, time delay, foundation flexibility and dynamic characteristics of MDOF specimens. Also, in order to study the actual dynamic behavior of the shaking table, the transfer function between target and actual table accelerations were identified using experimental results and spectral estimation techniques.

### 3. DESCRIPTION OF SHAKING TABLE SYSTEM COMPONENTS

#### 3.1. INTRODUCTION

The earthquake simulator is a system that consists of several components which must be designed to effectively work together. Each component was designed with the needs of the entire system in mind.

#### 3.2. DESIGN CONCEPT

The design concept of the UPRM Earthquake Simulator was the design of a small uni-directional electro-hydraulic shaking table facility. The initial design concept consisted of a rigid platform sliding over a near frictionless linear bearing system and driven by an actuator attached to a reaction mass. Figure 3.1 illustrates the final design of the uni-directional electro-hydraulic shaking table.

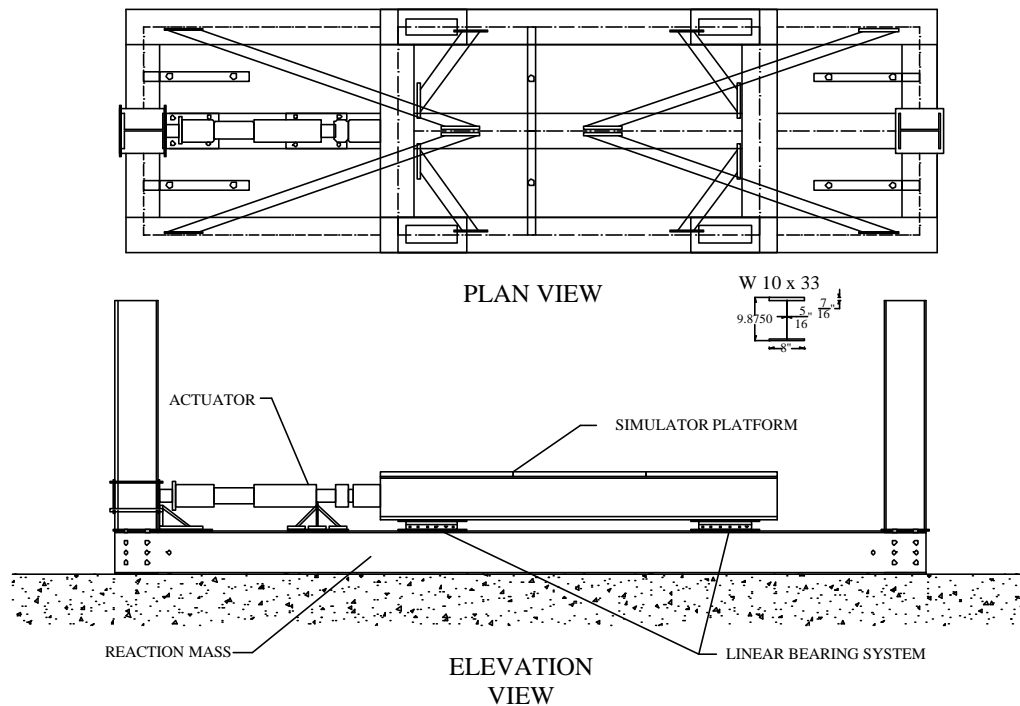


Figure 3.1 Plan and Elevation Views of the Earthquake Simulator.

### 3.3. SHAKING TABLE COMPONENTS

The components of the UPRM Shaking Table facility can be summarized in the following:

1. Reaction Mass
2. Simulator Rigid Platform
3. Linear Roller Bearings
4. Hydraulic Power Unit
5. Servovalve and Actuator
6. Servo-Controller
7. Control & Data Acquisition
8. Instrumentation for Measurements

Figure 3.2 shows the UPRM earthquake simulator.



a) West Side View.



b) East Side View.

Figure 3.2 UPRM Earthquake Simulator.

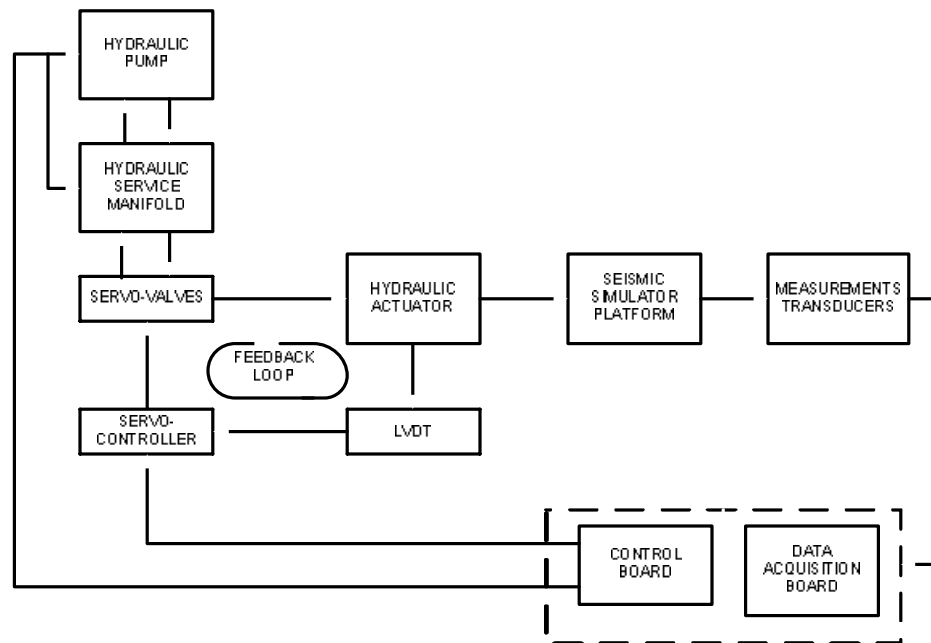


Figure 3.3 Block Diagram of Seismic Simulator [19].

Figure 3.3 illustrates how these components work together. The process is initiated by a signal from the Control Computer to activate the Hydraulic Pump Unit (HPU) and the Hydraulic Service Manifold (HSM). The HPU delivers constant flow of hydraulic fluid. The HSM distributes this hydraulic fluid to the different actuator channels. The HSM houses a pressure accumulator and return accumulator. This helps the system during peak flow demands. The same Control Computer sends a displacement command signal to the Servo-Controller that controls the displacement of the actuator and of the simulator platform. The Servo-Controller uses a closed-loop system that provides continuous correction signals for control of the simulator platform displacement. The closed loop servo-system uses a linear variable differential transformer (LVDT), which is located within the actuator, to make these corrections by comparing the command signal with the LVDT signal. This generates an error signal that is sent to the servo-valves,

which controls the amount and direction of the pressurized hydraulic fluid port to the actuator chambers from the HSM, and thus controls the direction of the actuator movement. The measurement transducers measure the motion of the platform and send the measured signals to the Data Acquisition System to be stored.

In the following sections a brief description of the components is provided to give an overview of the function of each component.

### 3.3.1. HYDRAULIC POWER SYSTEM

Hydraulic power systems typically consist of an arrangement of hydraulic power supplies, remote service manifolds, and accessory equipment. These components integrate into a hydraulic power distribution network to provide hydraulic fluid power to servo-controlled actuators. Figure 3.4 shows the HPU which creates the hydraulic power to move the simulator platform.



a) HPU front view.



b) HPU back view.

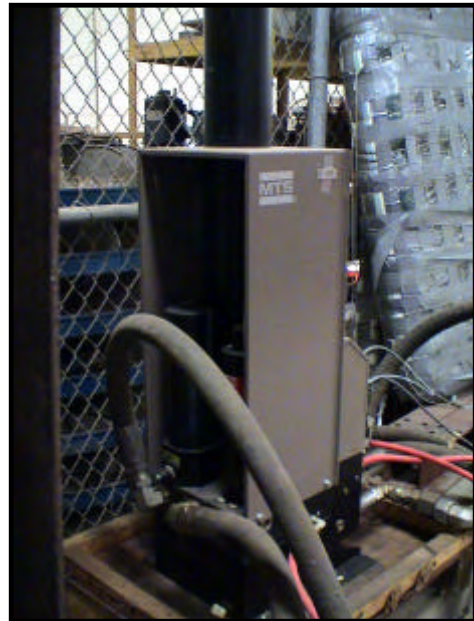
Figure 3.4 Hydraulic Power Unit.

The hydraulic power unit provides the distribution system with constant-pressure, high filtered hydraulic fluid power.

Service Manifolds provide hydraulic accumulation and filtering functions for individual actuators in a system. Hydraulic hoses provide connection of components within the hydraulic power distribution on system. Figure 3.5 shows the HSM which distributes the hydraulic fluid from the HPU to the actuator.



a) HSM front view.



b) HSM back view.

Figure 3.5 Hydraulic Service Manifold.

### 3.3.2. SERVOVALVE

The servovalve shown in Figure 3.6 provides the final control element in a closed-loop servo-hydraulic system. The servovalve ports the fluid, provided by the hydraulic power system, into the appropriate side of the actuator's chambers. This causes the actuator's piston to move the actuator's arm in the desired direction [5].

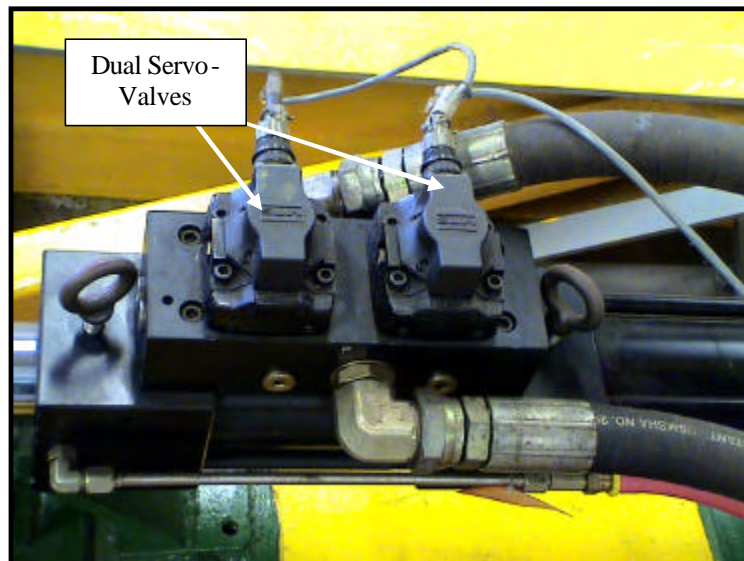


Figure 3.6 Dual Servovalves Mounted on the Actuator

### 3.3.3. LINEAR ACTUATOR

The linear actuator consists of a cylinder that contains a piston. The LVDT, which measures displacement, is inside the piston rod. The linear actuator system also consists of a load cell transducer, which measures force. Figure 3.7 shows the linear actuator with its components.

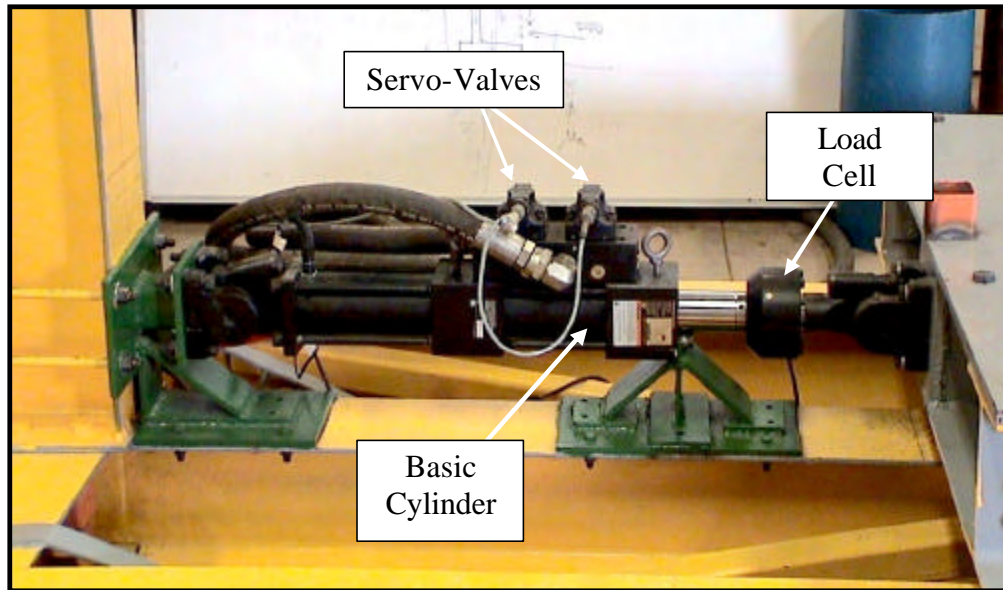


Figure 3.7 Linear Actuator and Components.

Figure 3.8 shows the actuator's cylinder with the LVDT transducer inside. As previously discussed, the movement of the actuator piston rod is accomplished by supplying high pressure hydraulic fluid to one side of the actuator piston (actuator's chamber) and opening the other side to the return line. The force rating of a linear actuator is equal to the effective piston area times the actuating pressure. The maximum flow rate available also determines the maximum simulator platform velocity [5]. The load cell is connected at the end of the actuator's piston rod and in turn to a swivel mounting head. The swivel head connects the actuator-load cell system to the simulator platform, as illustrated in Figure 3.7.

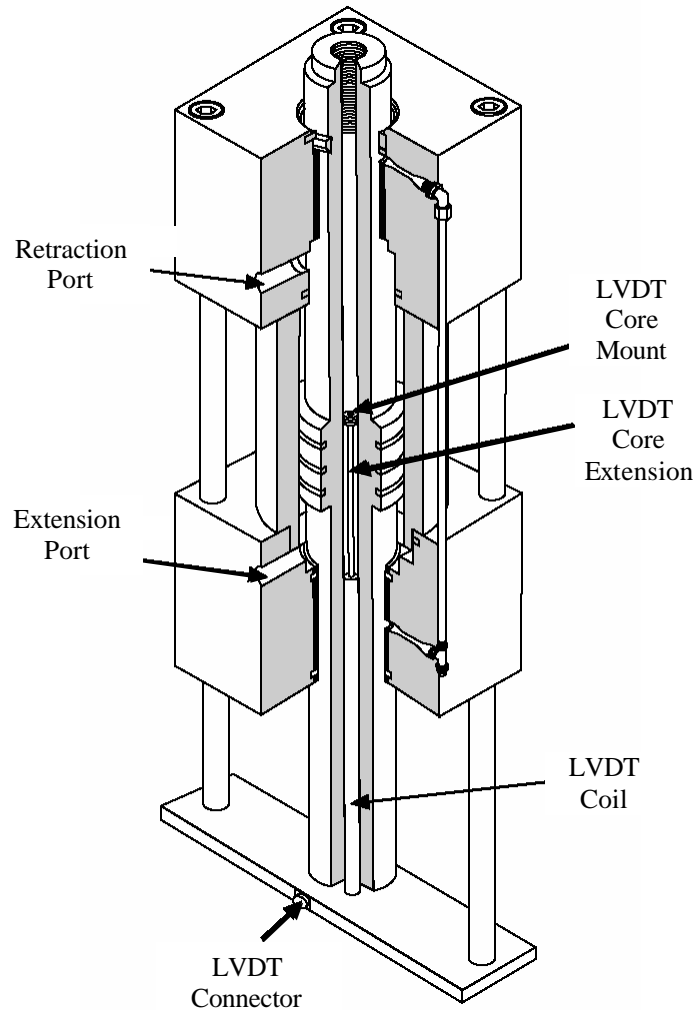


Figure 3.8 Basic Cylinder Components [20].

#### 3.3.4. SIMULATOR PLATFORM

The simulator platform attached to the actuator system is shown in Figure 3.9. The simulator platform provides the surface for model attachment. It is mounted through a system of linear bearings to the reaction mass and its motion is controlled by the movement of the actuator.

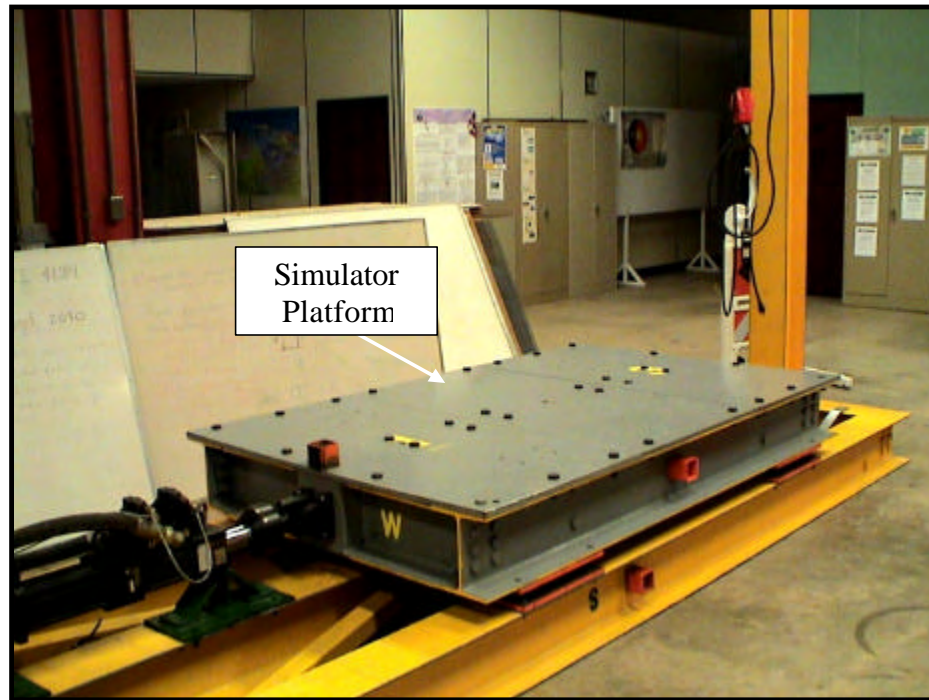
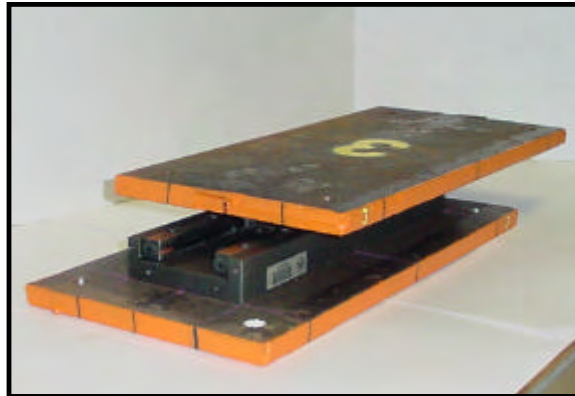


Figure 3.9 Simulator Platform mounted to the Reaction Mass.

### 3.3.5. LINEAR BEARING SYSTEM

The linear bearing system, shown in Figure 3.10, provides the sliding surface for the simulator platform to move with low friction [5]. Figure 3.10 (a) shows an individual Crossed Roller Table and Figure 3.10 (b) show the Linear Bearing System consisting of four individual Crossed Roller Tables acting as a group. This was accomplished with an efficient leveling procedure.



a) Individual Crossed Roller Table



b) Linear Bearing System mounted on Reaction Mass.

Figure 3.10 Linear Bearing System.

### 3.3.6. REACTION MASS

For structural or vibration testing, the actuator should be secured to a reaction mass using a swivel or pedestal base. The entire simulator platform system (platform, linear bearing system, actuator and servovalve) are fixed to the reaction mass [5]. The reaction mass provides a place for the actuator's force to react. Figure 3.11, illustrates the reaction mass. The reaction frame is at the same time fixed to the Structural Laboratory's strong floor.



Figure 3.11 Reaction Mass fixed to the Laboratory Strong Floor.

### 3.3.7. SERVO-CONTROLLER

The MTS Model 493.01 Servo-Controller is the bridge between the command signal sent by the Control computer and the porting of fluid to the actuator's chambers by the servo-valves. Figure 3.12 shows the Servo-Controller. The Servo-Controller utilizes two levels of control to regulate the displacement of the actuator [21]. The first level of control is called the "inner loop" and it regulates the porting of fluid by the servo-valves. This is the lowest level of control. The second level of control, called the "outer loop", utilizes the displacement signal of the LVDT mounted on the actuator and compares it to the command signal sent by the Control computer. The error signal is sent back to the "inner loop" which corrects the error by using the correct valve opening. The "outer loop" is the highest level of control of the Servo-Controller. The controller employs a **Proportional-Integral-Derivative-Feed-Forward (PIDF)** control algorithm to regulate and monitor the state of the system[5].



a) Front view.



b) Back view.

Figure 3.12 Servo-Controller

### 3.3.8. CONTROL AND DATA ACQUISITION

The control of the Servo-Controller is provided by the MTS TestStar IIs AP software in a Compaq personal computer provided by MTS for this purpose. Figure 3.13 shows the MTS TestStar IIs AP Control Computer and the Data Acquisition Computer. The Data Acquisition Computer stores the data of the transducers mounted on the simulator platform and reaction mass. This computer is equipped with an Iotech signal processing board and DasyLab software.

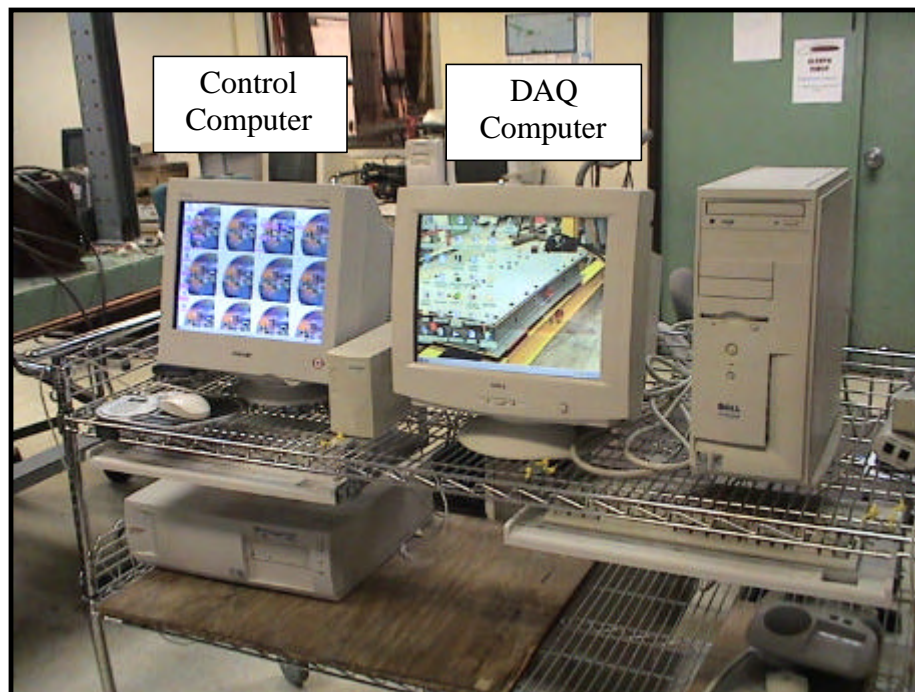


Figure 3.13 MTS TestStar IIs AP Control Computer and Data Acquisition Computer.

### 3.3.9. INSTRUMENTATION FOR MEASUREMENTS

Piezoresistive accelerometers were mounted to the reaction mass and simulator platform to measure acceleration. The accelerometers are firmly attached to their locations with screws. Figure 3.14, shows one accelerometer used for measurement of acceleration. The LVDT within the actuator is used to measure the displacement of the actuator piston head and simulator platform displacement. The load cell attached to the end of the actuator utilizes a strain gage to measure force in the actuator.



Figure 3.14 Piezoresistive Accelerometer.

## **4. DYNAMIC MODELING THEORY**

### **4.1. INTRODUCTION**

One of the main objectives of the development of the earthquake simulator facility is testing and analysis of small-scale dynamic models. The purpose of model analysis in earthquake engineering is the prediction of the dynamic response of prototype structures from laboratory tests on physical models [4]. Prior to the discussion of the design of the shaking table components it is necessary a brief discussion of *Dynamic Modeling Theory*, given that many design concepts depend on or are related to its theory. This brief discussion of *Dynamic Modeling Theory* is based on the work titled “Theory and Application of Experimental Model Analysis in Earthquake Engineering” by Moncarz [4] and on of the work titled “Analytical Modeling and Experimental Identification of a Uniaxial Seismic Simulator” by Twitchell [19].

### **4.2. MODELING THEORY**

*Modeling Theory* establishes how the properties of the model and the properties of the prototype are related. Some of these properties include geometry, material properties, initial conditions, boundary conditions and loading. To obtain a set of correlation or scaling laws for the model-prototype correspondence it is necessary to use *Similitude Theory* which can be developed by *Dimensional Analysis*.

### **4.3. DIMENSIONAL ANALYSIS**

Almost all physical phenomena can be described through mathematical expressions or equations. Dimensional analysis is developed from considering these expressions and paying attention to the significant quantities involved in them and the dimensions that

describe these quantities. This analytical tool starts from the premise that every physical phenomenon can be expressed by a dimensionally homogenous equation of the type [4]:

$$q_1 = F(q_2, q_3, \dots, q_n) \quad (4.1)$$

where  $n$  is the total number of physical quantities involved in the expression describing the phenomena,  $q_1$  is a dependent quantity and  $q_2$  to  $q_n$  are the variables and parameters on which  $q_1$  depends [4]. According to Buckingham's Pi Theorem [4]:

“a dimensionally homogenous equation can be reduced to a functional relationship between a complete set of independent dimensionless products ( $\pi$ -factors).”

Therefore Equation 4.1 can be written in the form [4]:

$$p_1 = f(p_2, p_3, \dots, p_{n-N}) \quad (4.2)$$

where  $\pi_1$  to  $\pi_{n-N}$  are dimensionless products of powers of the physical quantities  $q_1$  to  $q_n$ .

The number  $N$  is the rank of the dimensional matrix which is usually equal to the number of basic units needed to describe the physical quantities [4]. In engineering, the most common set of basic quantities are those of mass (M), length (L), time (T), and temperature ( $\theta$ ) or force (F), L, T and  $\theta$ .

Since Equations 4.1 and 4.2 are the same, they describe the same physical phenomenon and, because the dimensionless form of Equation 4.2, it must be equal in the prototype and model if complete similitude is to be attained. Therefore, for complete similitude [4]:

$$\left( p_1 \right)_p = \left( p_1 \right)_m \quad (4.3)$$

and

$$\begin{aligned} \left( p_2 \right)_p &= \left( p_2 \right)_m \\ &\vdots \end{aligned}$$

$$\left(\mathbf{p}_{n-N}\right)_p = \left(\mathbf{p}_{n-N}\right)_m \quad (4.4)$$

Equation 4.3 is the prediction equation and Equations 4.4 constitute the design conditions for the model. Methods for deriving the dimensionless products are discussed at depth by Moncarz [4]. It is important to know, though, that the number of  $N$  independent dimensionless products is equal to the total number  $n$  of physical quantities involved minus the number  $N$  of fundamental quantities needed to describe the dimensions of all physical quantities [4]. Some of the dimensionless products that are most frequently used in engineering and are commonly used in defining physical problems are shown in Table 4.1. The physical variables in the table are:  $\rho$  = mass density,  $v$  = velocity,  $L$  = length,  $\nu$  = Poisson's ratio,  $E$  = modulus of elasticity,  $\sigma$  = stress,  $P$  = pressure,  $d$  = displacement,  $t$  = time and  $g$  = acceleration of gravity.

#### 4.4. SIMILITUDE RELATIONSHIPS AND TYPES OF MODELS

Following Moncarz [4], the procedure to find the necessary conditions for complete similitude between model and prototype can be summarized in the following procedure:

1. Write down all physical quantities on which the solution of the physical phenomena under study depends significantly.
2. Develop a complete set of independent dimensionless products from these physical quantities (Eq. 4.2).
3. Establish equality between prototype and model for each of the independent dimensionless products (Eq's. 4.2 and 4.4).

This last step establishes the scaling laws for all physical quantities or products of physical quantities for the physical phenomena. These scaling laws are expressed as

ratios of the numbers of units needed to describe identical quantities in model versus prototype. For example, the length scale factor is defined as follows:

$$I_L = \frac{L_p}{L_m} = \frac{\text{Length of Prototype}}{\text{Length of Model}} \quad (4.5)$$

Table 4.1 Dimensionless Products.<sup>1</sup>

Named Dimensionless Product	Formula
Cauchy Number	$\frac{rv^2}{E}$
Froude Number	$\frac{v^2}{Lg}$
Reynolds Number	$\frac{Lv}{u}$
Dimensionless Products Commonly Encountered in Structural Engineering Problems	
$\frac{rv^2}{E}, \frac{v^2}{Lg}, \frac{sL^2}{P}, \frac{EL^2}{P}, t\sqrt{\frac{a}{L}}, aT$	
$\frac{raL^3}{P}, \frac{t}{L}\sqrt{\frac{E}{P}}, \frac{rgL}{E}, \frac{s}{E}, \frac{d}{L}, \frac{a}{g}$	

Note: 1. Modified from [4].

A model that fulfills all similitude requirements is called a “true replica model”. In many practical situations the fulfillment of all design conditions will be an impossible task. These kinds of models can be classified as “adequate” or “distorted models”.

“Adequate models” are those where the prediction equation is not affected and the design condition may be violated when insight into physical problem reveals that the results will not depend significantly on the violated design condition [4].

Distorted models are those where the distortion in one dimensionless product either leads to a distortion of the prediction equation or is accounted for by introducing compensating distortions in other dimensionless products [4].

#### 4.5. PHYSICAL MODELS FOR SHAKE TABLE STUDIES

##### 4.5.1. TRUE REPLICA MODELS

As stated earlier, true replica models must satisfy all similitude requirements. Let us assume that we want to reproduce at model scale the time history of stress components  $\mathbf{s}_{ij}(\bar{r}, t)$  in a replica model subjected to an acceleration time history vector  $a(t)$ . Since the distributions of stress and of material in the prototype and model must be the same, *Dimensional Analysis* can be applied [4]. Let's call  $\sigma$  a typical stress,  $\rho$  a typical density, and  $E$  a representative stiffness property of the material. The typical stress can be expressed through a functional relationship of the form [4]:

$$\mathbf{s} = F(\bar{r}, t, \mathbf{r}, E, a, g, L, \mathbf{s}_o, \bar{r}_o) \quad (4.6)$$

where  $\sigma_o$  and  $\bar{r}_o$  refer to initial conditions. In this expression it is assumed a similarity of material between prototype and model.

Following *Dimensional Analysis*, a complete set of dimensionless products is generated from the dimensional matrix of the quantities in Equation 4.6 [4].

$$\frac{\mathbf{s}}{E} = f\left(\frac{\bar{r}}{L}, \frac{t}{L} \sqrt{\frac{E}{\mathbf{r}}}, \frac{a}{g}, \frac{gL\mathbf{r}}{E}, \frac{\mathbf{s}_o}{E}, \frac{\bar{r}_o}{L}\right) \quad (4.7)$$

Since the gravitational acceleration can not be changed between model and prototype, the value of  $\lambda_g$  must be taken equal to one. Therefore, from the dimensionless product  $a/g$  (Froude's Number, usually written as  $v^2/Lg$ ) it follows that [4]:

$$\lambda_a = \lambda_g = 1 \quad (4.8)$$

The ratio of the modulus of elasticity,  $E$ , to the specific weight,  $\gamma$ , is called the specific stiffness of the material. This ratio is taken from the dimensionless product  $(gL\rho/E)_r$ , where  $\rho g = \gamma$  [4]. For a true replica model, the specific stiffness scale factor,  $\lambda_{E/\gamma}$ , must be satisfied. Using *Dimensional Analysis*, the specific stiffness scale factor may be determined as follows [19]:

$$\lambda_{\frac{E}{\gamma}} = \frac{\left(\frac{E}{\gamma}\right)_p}{\left(\frac{E}{\gamma}\right)_m} = \frac{\left(\frac{F}{L^2}\right)_p}{\left(\frac{F}{L^2}\right)_m} = \frac{\left(\frac{F}{L^3}\right)_p}{\left(\frac{F}{L^3}\right)_m} = \frac{L_p}{L_m} = \lambda_L \quad (4.9)$$

where  $F$  is force,  $L$  is length, and  $p$  and  $m$  distinguishes parameters of the prototype and model, respectively. From Equation 4.9, it can be seen that since  $\lambda_L$  must be greater than unity the specific stiffness of the model must be less than the specific stiffness of the prototype. This scaling law places a severe limitation on the choice of suitable model materials.

It is often desirable to construct the model of the same material as the prototype. In this case, the modulus of elasticity scale factor,  $\lambda_E$ , will be equal to unity and Equation 4.9 reduces to [19]:

$$l_{\frac{E}{g}} = \frac{\left(\frac{E}{g}\right)_p}{\left(\frac{E}{g}\right)_m} = \frac{l_E}{l_g} = \frac{1}{l_g} = l_g^{-1} = l_L \quad (4.10)$$

From Equation 4.10, the specific weight at model scale can be written as [19]:

$$g_m = l_L g_p \quad (4.11)$$

this shows that the model's material must have a larger specific weight than the prototype to comply with the true replica model similitude requirements [19]. True replica models are extremely difficult to realize because of problems in material simulation. But it is possible to deal with this problem through artificial mass simulation.

#### 4.5.2. ADEQUATE MODELS

Adequate models are physical models that although violate one dimensionless product the distortion does not affect other dimensionless products or the prediction equation. The need for such models is based on the desire to use the same materials as in prototypes [4].

##### I. MODEL TESTS WITH “ARTIFICIAL” MASS SIMULATION [19]

As it has been shown above, if both the prototype and model are constructed of the same material, the specific weight of the model material must be larger than the specific weight of the prototype material [19]. But, since the same material is being used for both the prototype and the model ( $\lambda_p = 1$ ), and the prototype and the model are subjected to

the same gravitational acceleration ( $\lambda_g = 1$ ), the specific weight scale factor will be unity (i.e.,  $\lambda_\gamma = 1$ ). The solution to this problem lies in augmenting, the specific weight of the structurally effective material with additional material which is structurally not effective [4]. An example on how to determine the required amount of additional mass necessary to meet the specific weight similitude requirement is described below [19].

Let's consider a reduced-scale model which is constructed of the same material as the prototype and is subjected to the same gravitational accelerations (i.e.,  $\lambda_g = \lambda_p = \lambda_\gamma = \lambda_E = 1$ ) [19]. The mass scale factor provided in this case is:

$$I_M^{prov} = \frac{M_p}{M_m^{prov}} = I_r I_L^3 = 1 \cdot I_L^3 = I_L^3 \quad (4.12)$$

The required mass scale factor for true replica model is:

$$I_M^{reqd} = \frac{M_p}{M_m^{reqd}} = \frac{I_g}{I_g} I_L^3 = \frac{I_L^{-1}}{1} I_L^3 = I_L^2 \quad (4.13)$$

Equation 4.10 was used to reduce  $\lambda_\gamma$  with  $\lambda_L^{-1}$ . It can be seen from Equation 4.12 and 4.13 that the provided mass of the model,  $M_m^{prov}$ , is less than the required mass of the model,  $M_m^{reqd}$ . Therefore, additional mass must be added to the model structure to meet the specific stiffness requirement. The required additional mass  $\Delta M$  is determined as follows [19]:

$$I_M^{prov} = \frac{M_p}{M_m^{prov}} \quad (4.14)$$

$$M_m^{prov} = M_p \left( I_M^{prov} \right)^{-1} = M_p I_L^{-3} \quad (4.15)$$

$$I_M^{reqd} = \frac{M_p}{M_m^{reqd}} \quad (4.16)$$

$$M_m^{reqd} = M_p \left( I_M^{reqd} \right)^{-1} = M_p I_L^{-2} \quad (4.17)$$

$$\Delta M = M_m^{reqd} - M_m^{prov} = M_p \left( I_L^{-2} - I_L^{-3} \right) \quad (4.18)$$

Equation 4.18 gives the required additional mass in terms of the mass of the prototype structure [19].

The artificial mass simulation method involves the addition of structurally not effective mass to augment the specific weight of the model structure. The method is particularly well-suited to lumped-mass models such as shear-type buildings, where the mass may be easily concentrated at discrete locations (e.g., at the floor levels) [4, 19].

Utilizing the method described above, the design of the model structure begins with the selection of values for  $N$  scale factors [19]. This scale factors are taken from Table 4.2. For seismic testing, the basic dimensions may be taken as force, length, and time, and thus  $N = 3$ . In the artificial mass simulation method in which the same materials are used in the model and prototype,  $\lambda_g = \lambda_E = 1$ . The designer must select the last scale factor which is usually the value of  $\lambda_L$ . All other quantities can be expressed in terms of these three scale factors, as shown in Table 4.2 [19].

Table 4.2 Similitude Relationships for Artificial Mass Simulation Method.<sup>1</sup>

Parameter	Units <sup>2</sup>	Any Material	Same Material as Prototype
Length	L	$I_L$	$I_L$
Time	T	$I_L^{1/2}$	$I_L^{1/2}$
Frequency	$\frac{1}{T}$	$I_L^{-1/2}$	$I_L^{-1/2}$
Velocity	$\frac{L}{T}$	$I_L^{1/2}$	$I_L^{1/2}$
Displacement	L	$I_L$	$I_L$
Gravitational Acceleration	$\frac{L}{T^2}$	1	1
Acceleration	$\frac{L}{T^2}$	1	1
Force	F	$I_E I_L^2$	$I_L^2$
Mass	$\frac{F \cdot T^2}{L}$	$I_E I_L^2$	$I_L^2$
Specific Stiffness	L	$I_L$	$I_L$
Strain	$\frac{L}{L}$	1	1
Stress	$\frac{F}{L^2}$	$I_E$	1
Modulus of Elasticity	$\frac{F}{L^2}$	$I_E$	1
Energy	FL	$I_E I_L^3$	$I_L^3$

Notes:

1. From [19].
2. L = Length, T = Time, F = Force and E = Modulus of Elasticity.

## 5. DESIGN OF SHAKING TABLE SYSTEM COMPONENTS

### 5.1. INTRODUCTION

The method used for the design of the shaking table system components is similar to those described by Muhlenkamp [5] and Twitchell [19]. First, typical earthquake records were analyzed and chosen. Then, the hydraulic system components were chosen, based on the available sizes, their compatibility with each other and their compatibility with the Structural Laboratory hydraulic system. Furthermore, it was determined prior to construction that the structures that would be tested would typically be 1/4<sup>th</sup> scaled models of actual structures.

### 5.2. TYPICAL EARTHQUAKE RECORDS SELECTION

Five earthquake records were selected for the design and analysis of the shaking table components. These were selected based on their frequency content, magnitude and soil conditions. Table 5.1 shows the characteristics of the earthquakes selected.

### 5.3. SCALING OF PROTOTYPE GROUND MOTIONS

Two types of scaling are applied to the actual earthquake ground motion time histories used for experiments on scaled test structures [5].

#### 5.3.1. SIMILITUDE SCALING

In this type of scaling the actual acceleration, velocity and displacement time histories applied to the actual structure (prototype) are scaled by a geometric scaling factor,  $\lambda_L$ , obtaining an equivalent acceleration, velocity and displacement time histories to be applied to the model structure. The geometric scaling factor was defined in Chapter 4 as,

$$I_L = \frac{L_{Prototype}}{L_{Model}} \quad (5.1)$$

Table 5.1 Historical Earthquake Records Used in Analysis and Design of System Components.

Earthquake	Station	Epicentral Distance (km)	Site Geology	Magnitude	Predominant Freq. Range (Hz)	Peak Accel. (g)	Peak Veloc. (cm/s)	Peak Displ. (cm)
Imperial Valley May 18, 1940	El Centro Comp S00E	12	Alluvium	6.7	0.5 - 2.8	0.34	33.45	10.87
Kern County July 21, 1952	Taft Lincoln School Tunnel Comp. S69E	41	Alluvium (40 ft) Over Sandstone	7.2	0.5 – 3.3	0.18	15.72	6.71
Michoacan Sept 19, 1985	SCCT (Mexico City) Comp. N90W	373	Soft Clay	8.1	0.3 – 0.6	0.16	60.50	21.20
San Salvador Oct. 10, 1986	CIG (Floor 1) Comp. 90°	-	-	5.6	-	0.69	80.04	11.90
Northridge Jan. 17, 1994	Castaic – Old Ridge Route Comp. 360°	16	Alluvium	6.8	0.5 – 2.5	0.51	76.94	15.22

where L indicates a geometric length. Therefore,  $\lambda_L = 4$  indicates that the model is 1/4<sup>th</sup> the size of the prototype structure. In the *Dynamic Modeling Theory* of an Adequate Model utilizing Artificial Mass Simulation (AMS) discussed in Chapter 4, the scaling factor for the time dimension is:

$$I_T = \sqrt{I_L} = \sqrt{4} = 2 \quad (5.2)$$

Therefore, the scaling factors for the acceleration and velocity are:

$$I_A = \frac{I_L}{(I_T)^2} = \frac{4}{(2)^2} = 1 \quad (5.3)$$

$$I_V = \frac{I_L}{I_T} = \frac{4}{2} = 2 \quad (5.4)$$

### 5.3.2. MAGNITUDE SCALING

The second type of scaling is an amplitude adjustment of the given time histories without a change in the time axis [5]. This scaling factor, K, is applied to the base acceleration, velocity and displacement records. This type of scaling will be referred to as *magnitude scaling*.

Both scaling factors, similitude and magnitude, can be applied to an earthquake ground motion to produce a model ground motion. For example, consider a 1/4<sup>th</sup> scale model ( $\lambda_L = 4$ ) of a structure to be tested on the shaking table. The ground motion time histories are scaled for similitude, by leaving the acceleration magnitude the same (since  $\lambda_A = 1$ ), decreasing the velocity magnitude by a factor of two (since  $\lambda_V = 2$ ), decreasing the displacement magnitude by a factor of 4 (since  $\lambda_D = \lambda_L = 4$ ) and compressing the time axis by a factor of 2 (since  $\lambda_T = 2$ ). In addition, the time histories can be scaled by a

magnitude scaling factor to simulate different levels of magnitude of the same seismic motions. In summary, for this particular case, the model base acceleration, velocity and displacement time histories would be given by [5]:

$$\begin{aligned}
 A_{\text{model}}(t_{\text{model}}) &= K * A_{\text{prototype}}(t_{\text{prototype}} / \lambda_L^{0.5}) \\
 V_{\text{model}}(t_{\text{model}}) &= (K / \lambda_L^{0.5}) * V_{\text{prototype}}(t_{\text{prototype}} / \lambda_L^{0.5}) \\
 D_{\text{model}}(t_{\text{model}}) &= (K / \lambda_L) * D_{\text{prototype}}(t_{\text{prototype}} / \lambda_L^{0.5})
 \end{aligned}
 \tag{5.5}$$

#### 5.4. REACTION MASS

A large reaction mass is required to minimize global simulator movement induced by the motion of the simulator platform and test structure [19]. To accomplish this, the reaction frame is rigidly connected to the strong floor at the Structural Laboratory at the UPRM Civil Engineering Department, as illustrated in Figures 5.1 (a) and (b).

The strong floor in the lab is constructed of reinforced concrete having a thickness of 12.7 cm (5.0 in). The total weight of the strong floor was calculated using the dimensions of the reaction frame connected to the floor plus 152.4 cm (5.0 ft) around the frame for a total weight of 70.54 kN (15,859 lb). Adding the reaction frame weight of 17.79 kN (4,000 lb), the total weight comes about 88.34 kN (19,859 lb). The weight of the simulator platform is 9.79 kN (2,200 lb) and the weight of the test structure (with added weight for AMS) is 9.79 kN (2,200 lb). The weight of the simulator/structure system is 19.57 kN (4,400 lb). Therefore, the weight of the reaction frame is 4.5 times the weight of the simulator/structure system. It is recommended the use of large reaction mass, about 30 to 50 times the mass of the simulator/structure system, to prevent motion of the reaction mass caused by the motion of the simulator platform and test structure [3,

6, 7, 17, 18 and 19]. Thus, it is important to measure the reaction frame's motion during tests.



(a) Middle Connection to Strong Floor.



(b) West-East Side Connection to Strong Floor.

Figure 5.1 Connection to Structural Lab Strong Floor

### **5.5. SIMULATOR PLATFORM (SLIP TABLE)**

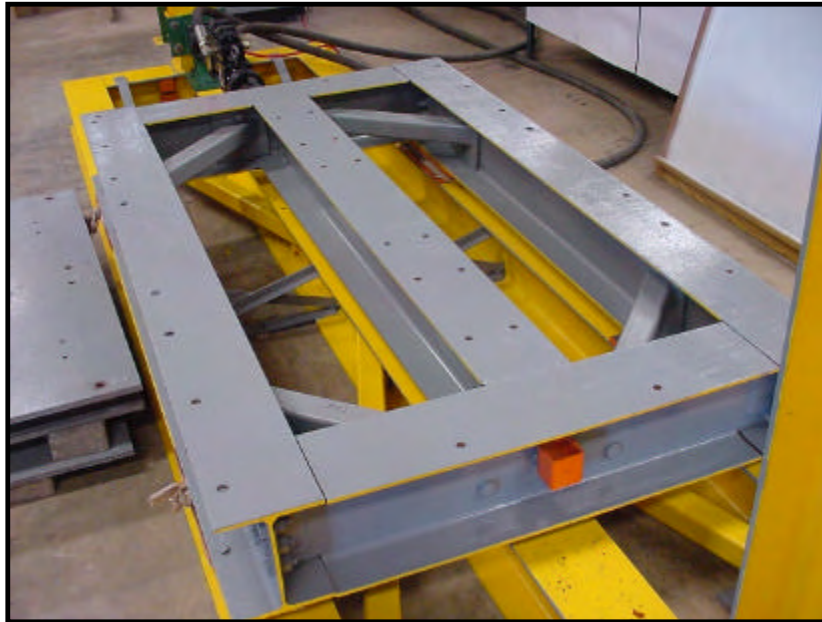
For the most part, uniaxial seismic simulator platforms are rectangular in shape and have the transverse dimension smaller than the longitudinal direction. The transverse dimension is arbitrary and it is only necessary for both stability and anchorage of test specimens [19].

The plan dimensions of the platform were selected as 228.6 cm (7.5 ft) by 137.2 cm (4.5 ft) with the longer dimension in the translating direction. These dimensions are more than sufficient to accommodate the 137.2 cm (4.5 ft) by 91.44 cm (3.0 ft) plan dimensions of the 1:4 scale test structure.

The simulator platform weighs approximately 9.79 kN (2,200 lb) and consists of a bolted steel frame built with three longitudinal wide flange beams, W10x33, four diagonal tube section beams at the corners, ST 3x3x0.25, and three 1.91 cm (0.75 in) thick steel plates at the top. Figure 5.2 (a) and (b) show the simulator platform with and without the steel top plates. The top plate has 32 attachments points consisting of 2.06 cm (0.8125 in) diameter holes for bolts with 1.91 cm (0.75 in) diameter and 5.08 cm (2.0 in) length.

### **5.6. LINEAR ROLLER BEARINGS**

The support method utilized to provide the sliding surface for the simulator platform is supplied by four-high accuracy, high-load capacity, preloaded and low-friction Crossed Roller Slide Tables (Steel) (see Figure 3.1 and Figure 5.3). Model NBT-6310 Crossed Roller Slide Tables were chosen due to its long travel, high-load capacity and low-friction coefficient of 0.003 [22]. The slide tables are mounted to the underside of the simulator platform. Each positioning table consists of a base, a carriage and a pair of



(a) Simulator Platform Welded Steel Frame.



(b) Simulator Platform with Top Steel Plate on.

Figure 5.2 Simulator Platform Components.

linear bearings. The bearings are factory preloaded to eliminate side play. In order to minimize the frictional forces developed at the bearing/rail interface, the slides tables were positioned with special care considering height deviation and parallelism. Figure 5.4 (a) and (b) illustrates the dimensions of the Crossed Roller Slide Table - NBT-6310. The technical specifications of a NBT-6310 are given in Table 5.2. Also, Table 5.2 shows the accuracy specifications. The permissible moments are [22]:

1.  $M_1 = 23,798 \text{ N-cm}$  (2,106.3 lb-inch)
2.  $M_2 = 98,587.3 \text{ N-cm}$  (8,725.7 lb-inch)
3.  $M_3 = 103,516.7 \text{ N-cm}$  (9,162.0 lb-inch)

Figure 5.5 defines the permissible moments.

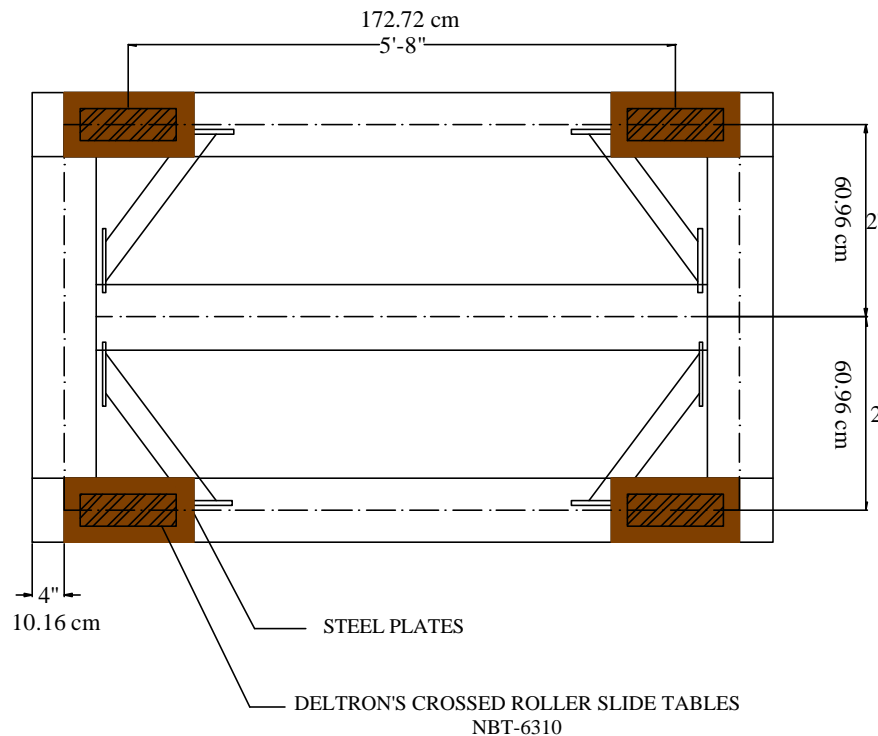
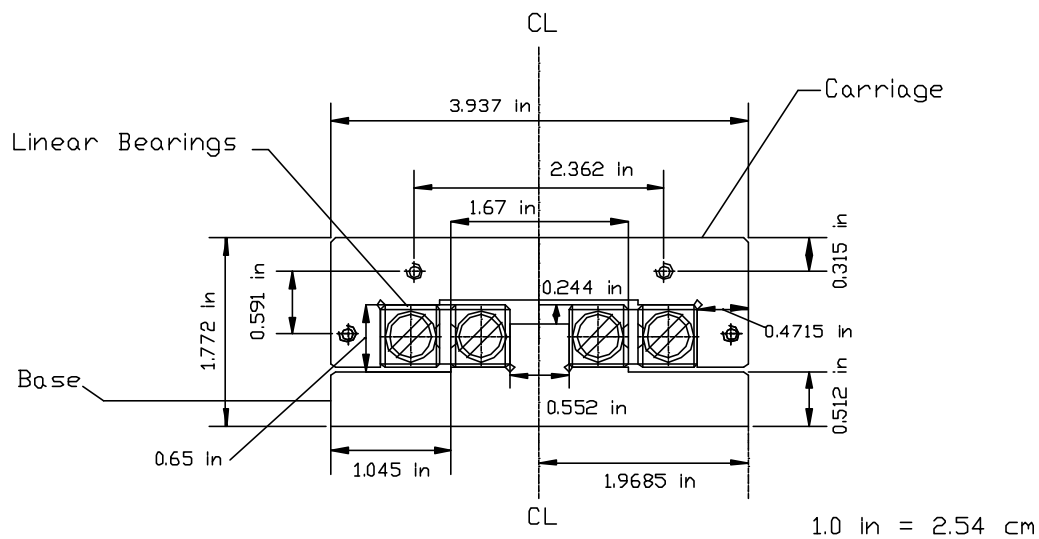
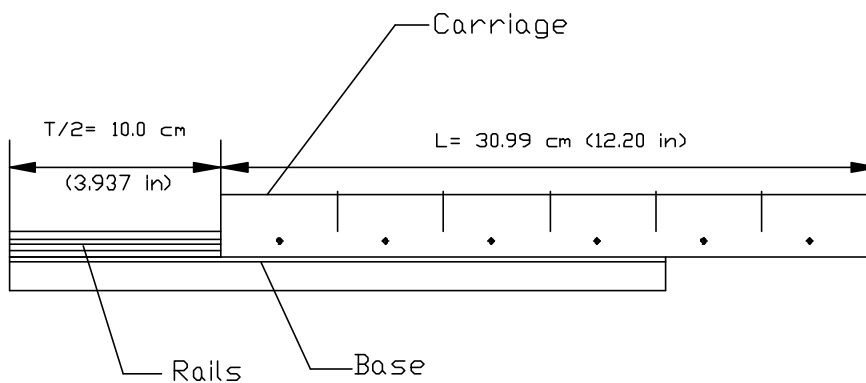


Figure 5.3 Plan View of Simulator Platform showing Locations of Sliding Bearings.



(a) Cross - Section of NBT-6310.



(b) Travel and Length Specifications.

Figure 5.4 Dimensions of a Crossed Roller Slide Table NBT-6310 [22].

Table 5.2 Technical Specifications of Linear Bearing System<sup>1</sup>

Dimensions Linear Bearing System	Distance (in)
Total height, cm	7.041 (2.772)
Width, cm	20.32 (8.0)
Length, cm	40.64 (16.0)
Horizontal centerline distance, cm	121.92 (48.0)
Longitudinal centerline spacing, cm	172.72 (68.0)
Crossed Roller Slide Tables	
Height, cm	4.50 (1.772)
Width, cm	10.0 (3.937)
Length, cm	30.99 (12.200)
Travel, cm	19.99 (7.87)
Load Capacity, N	11,743.3 (2,640 lb)
Horizontal centerline distance, cm	5.0 (1.9685)
Longitudinal centerline spacing, cm	15.494 (6.100)
Lateral height deviation accuracy, mm	0.006096 (0.00024)
Longitudinal height deviation accuracy, mm	0.003048 (0.00012)
Crossed Roller Rail Set	
Height, cm	1.501 (0.591)
Width (set), cm	3.101 (1.221)
Length, cm	30.254 (11.911)
Horizontal centerline distance between Slide Table and Rail Set, cm	$\pm 2.250 (\pm 0.886)$

Note: 1. Modified from [22].

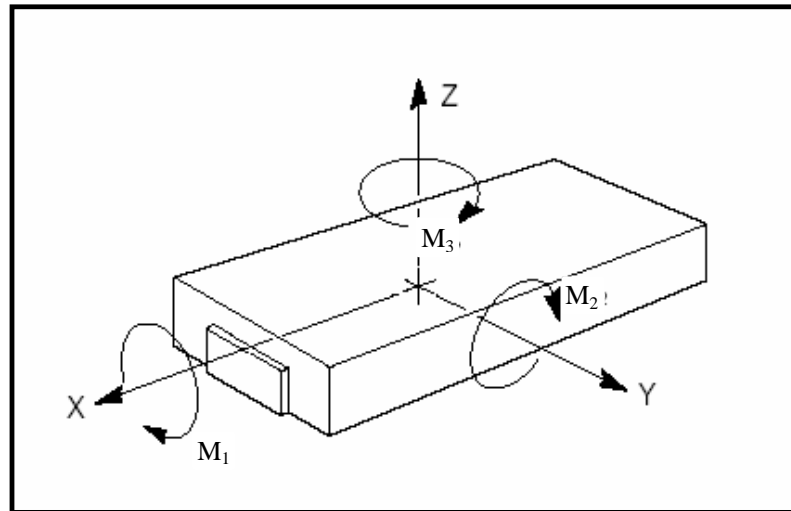


Figure 5.5 Permissible Moment Load Ratings [22].

### 5.7. PAYLOAD

For the particular case of the UPRM shaking table the maximum design payload capacity of the shaking table will depend on three factors [5]:

1. Desired maximum base acceleration,  $A_{\max}$
2. The force that can be applied by the actuator,  $F_{\max}$
3. The load bearing capacity of the Linear Bearing System

The maximum weight of the test structure plus the slip table,  $W_{\max}$  is:

$$W_{\max} = \frac{F_{\max}}{A_{\max}} g \quad (5.6)$$

in which  $g$  denotes the acceleration of gravity.

### 5.8. HYDRAULIC ACTUATOR

The maximum force required by the actuator to reproduce the five historical earthquakes chosen was determined by an analysis on the response of a three-story scale-model test structure. The test structure was modeled as a shear type structure with lumped masses at each floor level. The weight of the lumped masses varied from 0.0 N (0 lb) to 3,558.6 N (800 lb). For the analysis, each earthquake record was magnitude scaled to a peak ground acceleration of 1.0  $g$  and compressed in time by a factor of two to account for similitude requirements. The results are shown in Figure 5.6. Based on the results shown on Figure 5.6, for a story weight of 2,224.1 N (500 lb) and with a factor of safety of 1.5, a 48.93 kN (11.0 kip) actuator will give the necessary force to reproduce the five representatives historical earthquakes. For story weights greater than 2,224.1 N (500 lb) and smaller than 3,559 N (800 lb), the 48.93 kN (11.0 kip) actuator would work to but

with a smaller factor of safety, except for the Northridge record. Therefore, a 48.93 kN (11 kip) maximum actuator force was chosen.

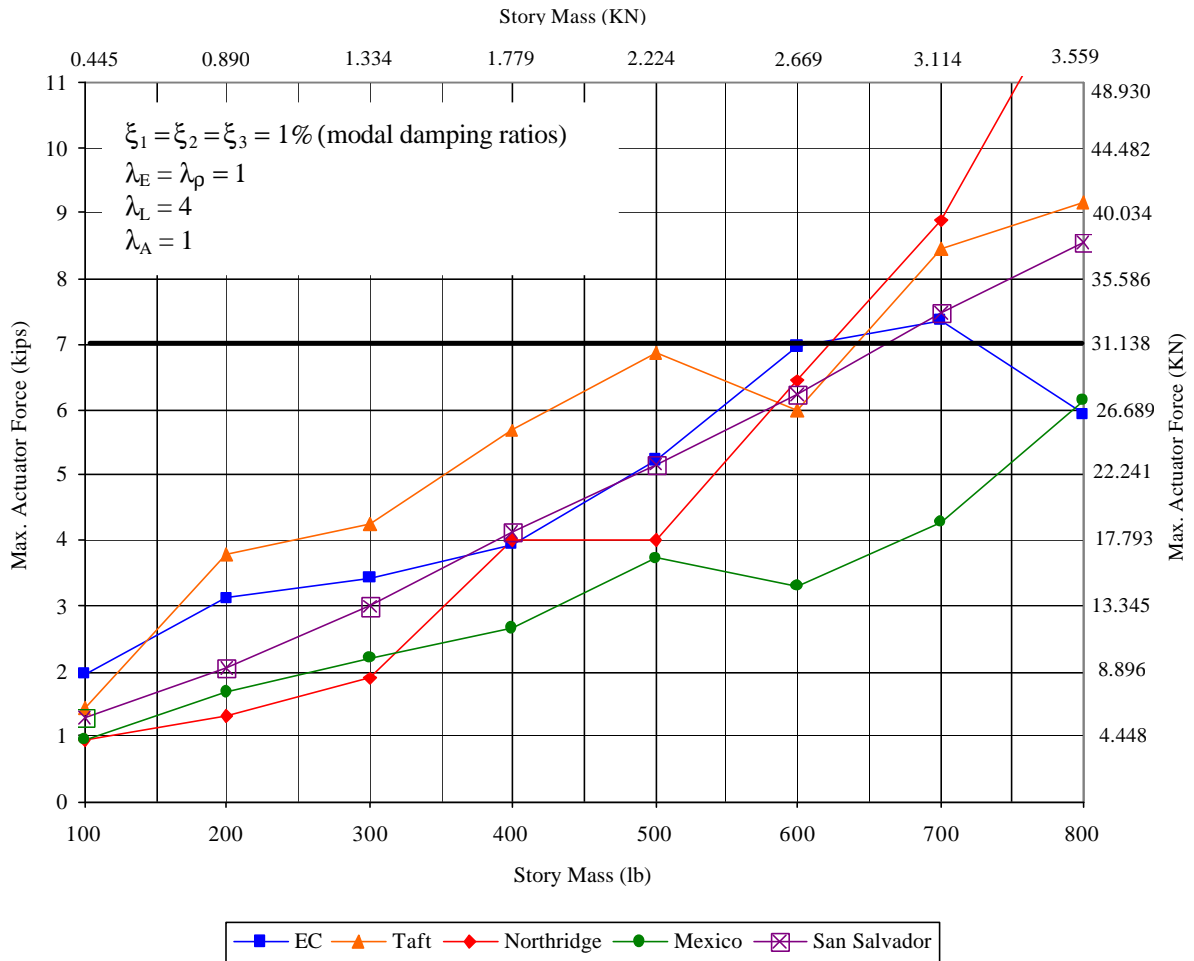


Figure 5.6 Maximum Actuator force for Five Representative Earthquake Records.

The hydraulic pressure available is  $20,684.3 \text{ kN/m}^2$  (3,000 psi) (standard), therefore the required effective piston area was determined to be:

$$A = \frac{F}{P} = \frac{48.93 \text{ kN}}{20,684.3 \text{ kN/m}^2} = 0.002366 \text{ m}^2 = 23.66 \text{ cm}^2 = 3.67 \text{ in}^2 \quad (5.7)$$

The actuator that was selected with these characteristics was an MTS Model 244.21 Hydraulic actuator rated at 48.93 kN (11 kips) and with an effective area of 25.16 cm<sup>2</sup> (3.90 in<sup>2</sup>) and a stroke of ±7.62 cm (± 3.00 inches) [20].

### 5.9. SERVO-HYDRAULIC SYSTEM

The servo-hydraulic system was designed and chosen to be able to reproduce typical seismic motions, such as those depicted in Table 5.1, and based on their compatibility with the available hydraulic system at the UPRM Structural Laboratory and between each other. From Table 5.1, it can be seen that the maximum peak ground acceleration is about 0.7g, the maximum peak ground velocity is 80.04 cm/sec (31.51 in/sec) and the maximum peak ground displacement is 21.20 cm (8.35 in). Therefore, the maximum values of acceleration, velocity and displacement at model scale, using the geometric factor of 4, would be 0.7g, 40.02 cm/sec (15.75 in/sec) and 5.3 cm (2.087 in), respectively. The maximum displacement is compatible with the span of the Model 244.21 linear hydraulic actuator of ±7.62 cm (± 3.00 in).

The maximum required flow of oil into the actuator,  $Q_{\max}$ , is calculated as follows [5]:

$$Q_{\max} = A_{\text{effective}} * V_{\max} \quad (5.8)$$

Where  $A_{\text{effective}}$  = the actuator piston effective area = 25.16 cm<sup>2</sup> (3.90 in<sup>2</sup>)

$V_{\max}$  = the maximum velocity at model scale = 40.02 cm/sec  
(15.75 in/sec)

Therefore:

$$\begin{aligned} Q_{\max} &= (25.16 \text{ cm}^2)(40.02 \text{ cm/sec}) = 1006.9 \text{ cm}^3/\text{sec} = 60.414 \text{ liters/min} \\ &= (3.90 \text{ in}^2)(15.75 \text{ in/sec}) = 61.425 \text{ in}^3/\text{sec} = 15.93 \text{ gpm} \end{aligned}$$

The servovalve selected was a dual MTS Model 252.25 two-stage servovalves, rated at 56.0 l/min (15gpm) each for a total of 112.0 l/min (30gpm) maximum flow [23]. For simulation of earthquake-like motions, the pump must be able to provide an average sustained flow equal to [5]:

$$Q_{pump} = \frac{Q_{max}}{\frac{3p}{2}} = \frac{60.414}{\frac{3p}{2}} = 12.82 \text{ l/min} \quad (5.9)$$

The Hydraulic Power Supply (pump) installed in the laboratory is a MTS Model 506.61 and is rated at 265.0 l/min (70 gpm) of steady flow [24]. A Hydraulic Service Manifold (HSM) MTS Model 293.11, with a rated capacity of 190.0 l/min (50 gpm), is mounted between the HPS and the servovalves [25]. The purpose of the HSM is to distribute the hydraulic power to the different actuator channels.

#### 5.10. CONTROLLER SPECIFICATIONS

The purpose of the controller is to regulate the position of the actuator arm [5]. The controller chosen was the TestStar IIs AP System, composed of the Model 493.01 Servo-Controller and the Control computer (PC) with the software to control the Servo-Controller. The TestStar IIs digital controller performs the control system's real time functions, including high-speed closed-loop control, data acquisition, function generation and transducer conditioning [26]. The Servo-Controller is a **PIDF** controller, it has displacement feedback and the gains of the **PIDF** algorithm can be adjusted for optimum table response for changing loading conditions [5].

The PC provides the link between the TestStar IIs digital controller and the user. The PC is where the user defines and run the applications and store and analyze data. The

software is the heart of the TestStar IIs System. The Basic TestWare program is the basic software that comes with the PC software. It let the operator to set-up and run simple monotonic and cyclic test by defining the rate, frequency, amplitude, and mean for sine, triangle, square, and ramp command signals. While the test is running, the Basic TestWare can capture the test data for analysis and display. Data can be acquired as various types, such as the peak/valley, minimum/maximum, timed data, and level crossing. All of the user's test set-ups in Basic TestWare can be saved and recalled for use at any later time.

However, for the needs of the UPRM tests, a special software called MultiPurpose TestWare was needed. This program has special attributes such as testing flexibility where the user can create his/her own test sequences and data acquisition [27]. The user is not limited as one might be with a fixed-function application. The program has a special command called "*Profile Command*" where the user can create a file made up a series of cyclic, dwell and other segment commands, read by the PC and translate them to the Servo-Controller in servovalve openings. Using this command, the earthquake time histories were generated.

#### **5.11. DATA ACQUISITION SYSTEM SPECIFICATIONS**

The Data Acquisition Computer stores the data of the accelerometers mounted on the simulator platform and reaction mass. This computer is equipped with an Iotech signal processing board and DasyLab software. We also use Dewetron's Model DAQ-PV for signal conditioning of the accelerometers. The DAQ-PV module has selectable ranges of voltages and filters to condition the accelerometer raw signal into a standardized voltage output to send to the computer's signal processing board.

The signal processing board model installed at the Data Acquisition PC (DAQ) is an Iotech model 16-bit board called DAQ BOARD-200A. It has a 100 kHz A/D converter and eight differential or sixteen single-ended analog input channels.

## **6. SERVO – HYDRAULIC SYSTEM**

### **6.1. INTRODUCTION**

Hydraulic power systems typically consist of an arrangement of hydraulic power supplies, remote service manifolds, and accessory equipment [24]. These components integrate into a hydraulic power distribution network to provide hydraulic fluid power to servo-controlled actuators. The hydraulic power supply provides the distribution system with constant-pressure, high filtered hydraulic fluid power. The distribution system consisting of hose kits, service manifolds and accessories, routes the fluid power to individual actuators within the system. The following sections discuss, in a general manner, the hydraulic power system used by the seismic simulator facility developed at the Structural Research Laboratory of the Civil Engineering Department at the University of Puerto Rico at Mayagüez. This discussion will be based on the MTS Manuals for the different parts of the hydraulic system.

The performance envelope of the shaking table is directly related to the physical limits of the hydraulic power supply (pump), servovalve, and actuator [5]. Theoretical performance envelopes will be given for the seismic simulator system.

### **6.2. HYDRAULIC POWER SUPPLY (HPS) [24]**

The MTS Model 506.61 currently provides the hydraulic power to the different testing facilities of the Structural Research Laboratory at the Civil Engineering Department. The MTS Model 506.61 hydraulic power supply (HPS) or hydraulic power unit (HPU) uses a variable volume pump to provide a source of hydraulic power for hydraulic systems having flow requirements of 265.0 l/min (70.0 gpm). It provides two levels of operation at 265.0 l/min (70 gpm): 1.0 MPa (150 psi) and 21.0 MPa (3000 psi)

for low and high-pressure, respectively. The MTS Model 506.61 model is specially designed to meet the exacting requirements of systems using servo-valves. Figure 6.1 illustrates the general form of operation of the MTS Model 506.61 hydraulic power unit through a block diagram.

The oil storage reservoir has an approximate 757.0 liters (200 gal) capacity. Oil is drawn from the storage reservoir and forced through the supercharger pump and then through the main pump. A return line brings the oil back to the reservoir to complete the cycle.

Filtering eliminates contaminants (dirt) from the hydraulic fluid to be used with dirt-sensitive servo-valves. For the MTS Model 506.61, the output fluid is filtered to 10 microns and reservoir fluid to the main pump passes through a 40-micron inlet filter. Also, a 3-micron filter bypasses fluid to the reservoir.

The fluid-to-water heat exchanger maintains the reservoir hydraulic fluid temperature below a maximum safe temperature. If fluid temperature exceeds a preset limit, a temperature-sensitive switch mounted on the reservoir will open and turn off the HPU. For the MTS Model 506.61 this preset limit is 60°C (140°F). Table 6.1 lists the main specifications for the MTS Model 506.61 hydraulic power system unit, as given by the manufacturer.

### **6.3. HYDRAULIC SERVICE MANIFOLD (HSM) [25]**

The hydraulic service manifold is a modular hydraulic pressure and flow regulation device that controls the hydraulic pressure to multiple stations independently from the main hydraulic power unit (HPU). Two hydraulic service manifolds distribute fluid power from the hydraulic power unit to the different testing facilities at the Structural

Research Laboratory. The MTS Model 293.11A hydraulic service manifold (HSM) will distribute and regulate the fluid power for the shaking table facility. It also distributes hydraulic power to the wind testing facility at the Structural Research Laboratory.

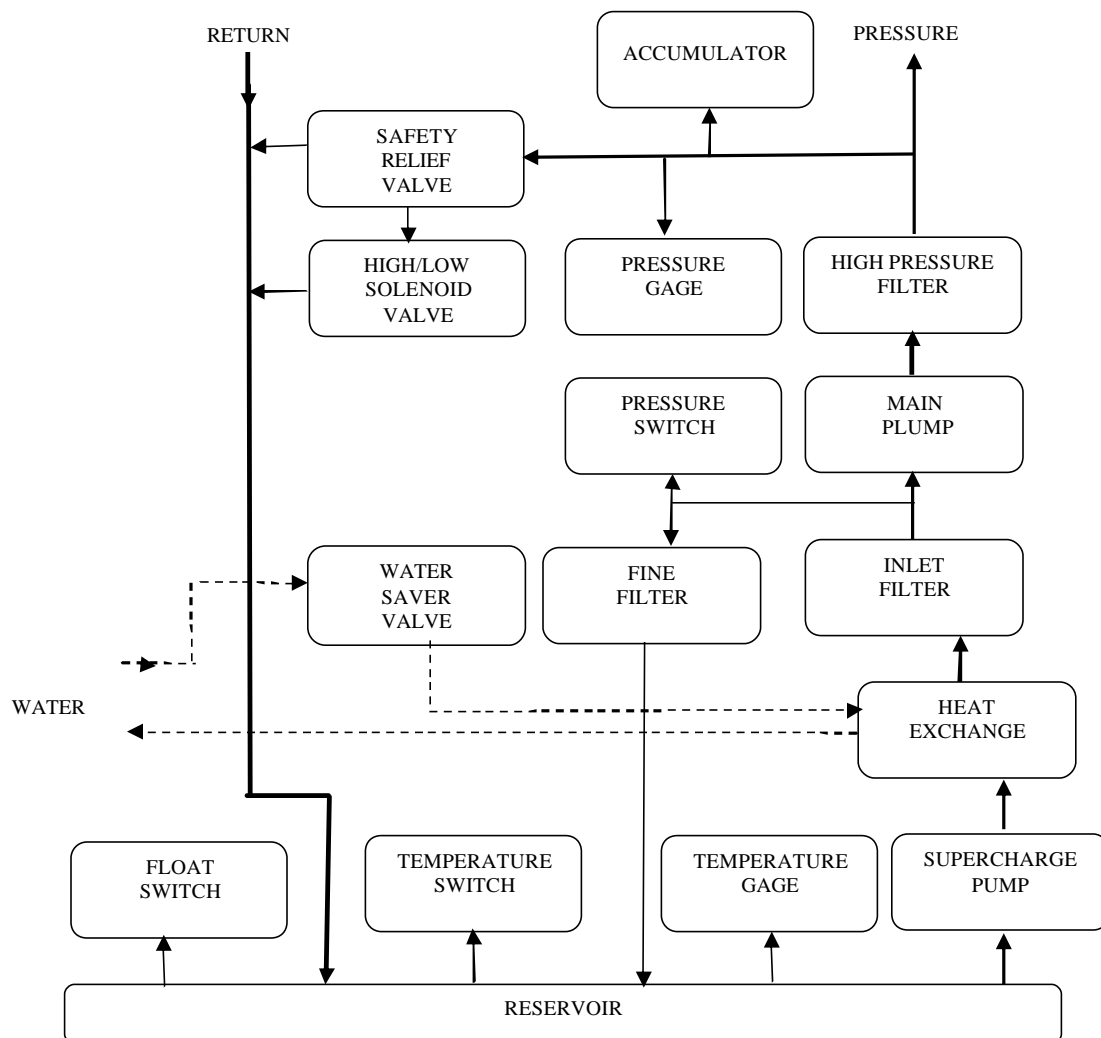


Figure 6.1 Block Diagram for MTS Model 506.61 Hydraulic Power Supply [24].

The service manifold is connected between the hydraulic power unit and the different hydraulic channels. A hydraulic channel is associated with an actuator and a servovalve system. The MTS Model 293.11A has a nominal hydraulic capacity of 190.0 l/min (50 gpm) and a control voltage of 24 volts (DC). It has two operating pressures at the

nominal flow: 1.0 MPa (150 psi) and 21.0 MPa (3,000 psi) for low and high pressure, respectively. Figure 6.2 shows the different components of the MTS Model 293.11A remote service manifold. The various components form a system of fluid flow, pressure control, filtering and accumulators.

Table 6.1 MTS Model 506.61 HPS Specifications<sup>1</sup>.

Parameter	Specifications
Reservoir Capacity, l	757.0 (200.0 gal)
Flow Capacity at: l/min	265.0 (70.0 gpm)
Pressure, MPa	21.0 (3,000 psi)
Frequency	60.0 Hz
Filtration (microns)	
Full Flow	2
Nominal/Absolute	10
Hydraulic Fluid	A/W Hydraulic 46
Pump Motor at: kW	95.0 (125.0 HP)
Frequency	60.0 Hz
Starter (3-Phase, 380V, 60Hz)	Part Winding
Inrush	380
Continuous Amps	195
Max. Ambient Operating Temperature, °C	40.0 (104°F)
Min. Ambient Operating Temperature, °C	4.4 (40°F)
Water Flow at:	
18.3 °C (65 °F)	56.78.0 l/min (15.0 gpm)
29.4 °C (85 °F)	132.0 l/min (35.0 gpm)
Height, cm	154.94 (61.0 in)
Length, cm	226.06 (89.0 in)
Width, cm	111.76 (44.0 in)
Weight, with Fluid, N	22,241.1 (5,000 lb)

Note: 1. Modified from [24].

The hydraulic fluid from the HPS enters the HSM at the pressure in port at the main manifold, where the fluid is filtered through a 10-micron filter. After filtration, the fluid passes to the control manifold (through the distribution manifold), fills the pressure accumulator and exits the HSM through the pressure out port. The control manifold distributes hydraulic fluid to and from a single hydraulic channel. The control manifold contains a low and high-pressure solenoid valves, a main valve, a slow-turn on accumulator and a pressure gage. The control manifold applies hydraulic pressure to the

servo valve, and controls whether the pressure is high or low at the HSM pressure out ports. The low and high-pressure solenoid valves allow that pressure control. High-pressure output is typically maintained at 21.0 MPa (3,000 psi). Return fluid from the actuator enters the return in port, flows through the return accumulator and exits to the HPS through the return out port. Drain ports provide a path for collecting excess fluid and returning it to the HPS.

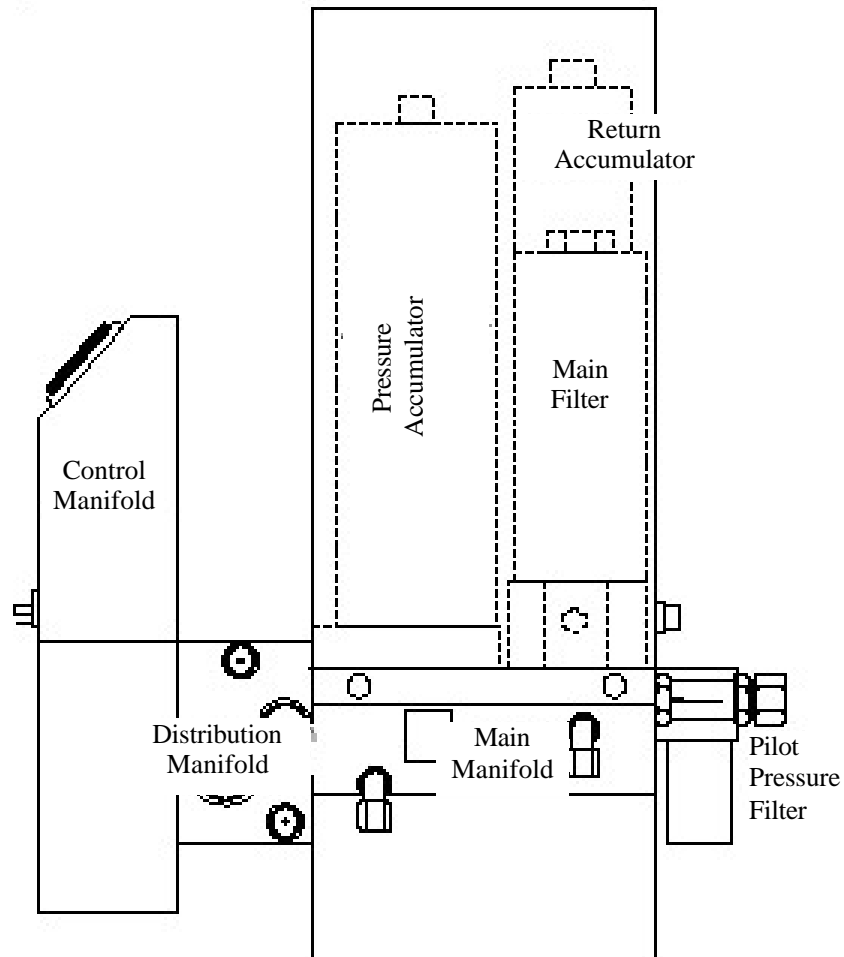


Figure 6.2 MTS Model 293.11A HSM Parts [25].

The pressure and return accumulators reduce flow fluctuations caused by changing system demands. In most cyclic test programs, the average servo valve flow requirement

is much less than the peak hydraulic requirement. Accumulators store hydraulic power during the low portion of each cycle. The type and frequency of the servovalve command signal affects the efficiency of the accumulator. Square waves cause a greater demand than sine or ramp signals. The pressure accumulator reduces the inertia and line restriction considerations. Fluid inertia is generated when the fluid flow in the lines stop at low frequencies. The return accumulator reduces movement of hoses and hammering of hard lines caused by the varying amounts of fluid being discharged into the lines as the actuator moves. Table 6.2 lists the main technical specifications for the MTS Model 293.11A hydraulic service manifold, given by the manufacturer.

Table 6.2 MTS Model 293.11A HSM Specifications<sup>1</sup>.

Division	Parameter	Specification
Model		293.11A
	Control Voltage	24 V (DC)
	Pilot Pressure	No
Environmental	Temperature	4.4°C (40°F) to 50°C (122°F)
	Humidity	0% to 80% relative, non-condensing
Dimensions	Height, cm	74.93 (29.5 in)
	Length, cm	35.56 (14.0 in)
	Width, cm	36.83 (14.5 in)
Weight	Main Manifold and Accumulators, N	689.5 (155 lb)
	Control Manifold Weight, N	35.6 (8.0 lb)
Number of Channels		2
Filtration	Main Supply	10 μ main supply
	Pilot Pressure Supply	3 μ pilot pressure supply
Operating Pressure	Variable Low Pressure, MPa	1.0 to 21.0 (150 to 3000 psi)
	High Pressure, MPa	21.0 (3000 psi)
Nominal Flow, l/min		190.0 (50 gpm)
Slow on/off Ramp Time		5.0 to 9.0 seconds
Maximum Solenoid Current		1.5 A at 24 V (DC)
Accumulators	Pressure, l	7.57 (2.0 gal)
	Return, l	0.45 (0.12 gal) standard

Note: 1. Modified from [25].

## 6.4. SERVOVALVE [23]

The servovalve provides the final control element in a closed-loop servo-hydraulic system. Figure 3.3 shows a diagram of a closed-loop servo - hydraulic system. A control signal is the driving element in a closed-loop system. The servovalve uses the control signal to operate a valve that regulates the movement of a hydraulic actuator.

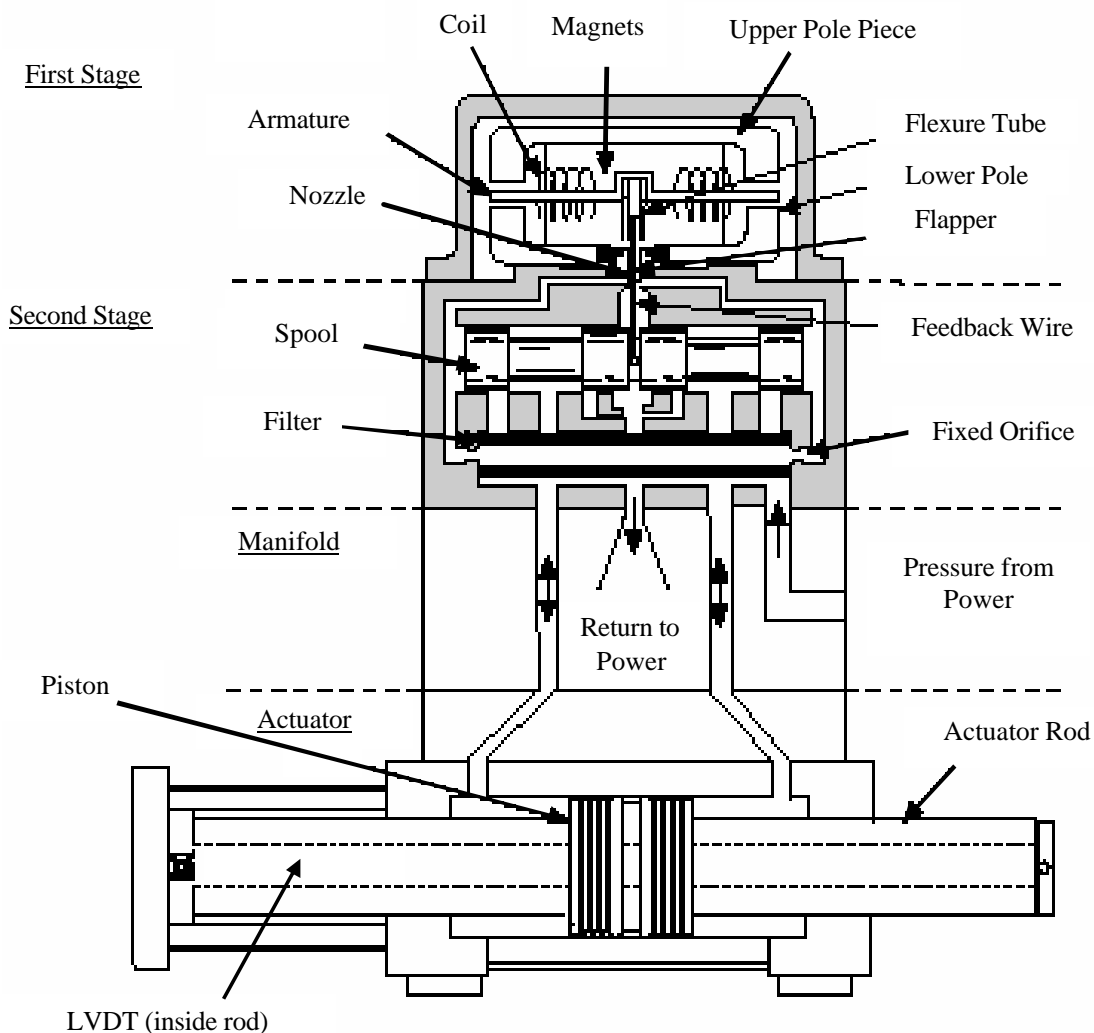


Figure 6.3 Functional Diagram of a Single Servovalve and Manifold Mounted to the Actuator [23].

The servovalve converts this control signal to a physical movement of an internal spool, allowing the controlled porting of hydraulic fluid to and from the actuator. A functional diagram of a two-stage servo valve is shown in Figure 6.3. The polarity of the control signal determines the direction the spool will move and the amplitude of the control signal determines how far the spool will move thus, controlling the direction and rate of hydraulic fluid through the servovalve. When the amplitude of the control signal reaches zero (desired actuator position) the spool returns to its null (non-flow) position, thereby stopping the flow of hydraulic fluid to and from the actuator. Single or dual servovalves can be mounted directly to the actuator or mounted to a manifold, which

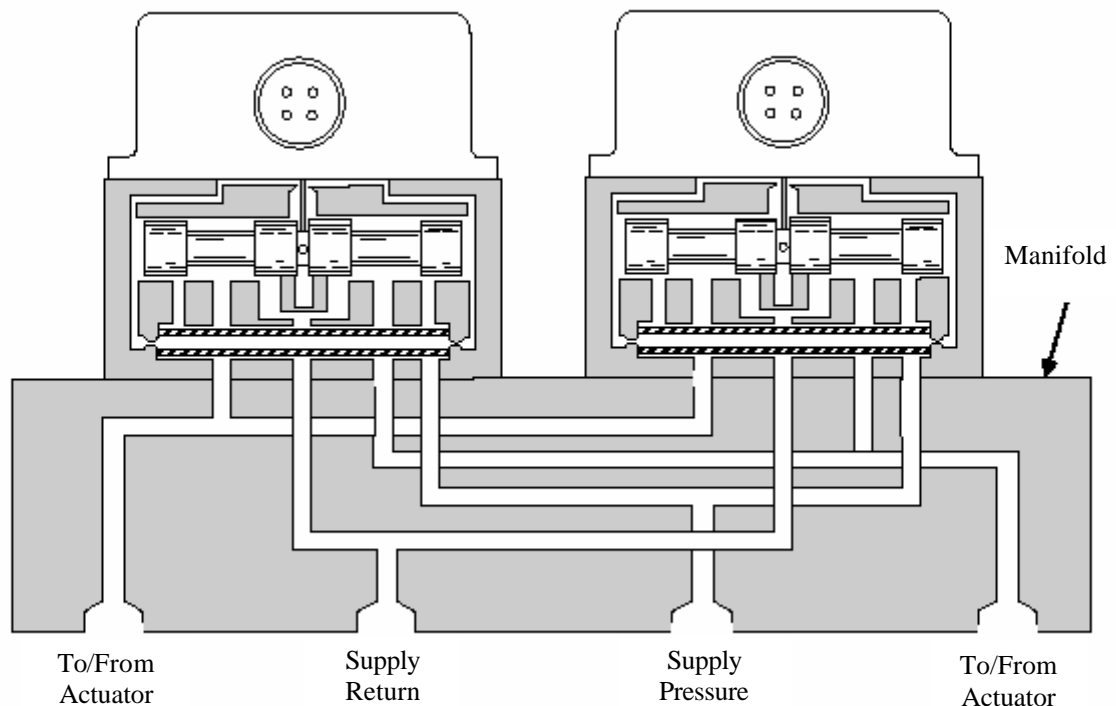


Figure 6.4 Cross-Section of Dual Servovalves Mounted to Servovalve's Manifold [23].

in turn is mounted to an actuator. The manifold, in the case of dual servovalves, is a metal block that connects the ports of each servovalve to the ports of the actuator, as

shown in Figure 6.4. The manifold doubles the hydraulic flow rate of the two servovalves.

Two MTS Model 252.25 two-stage servovalves will regulate the hydraulic flow of the linear actuator to be used to drive the shaking table at the Structural Research Laboratory. The full flow rating of each MTS Model 252.25 servovalve is 57.0 l/min (15 gpm) for a 6.9 MPa (1,000 psi) pressure drop across the servovalve. The maximum operating pressure and standard operating pressures are 31.0 MPa (4,500 psi) and 21.0 MPa (3,000 psi), respectively. Table 6.3 gives the main technical specifications for the MTS Model 252.25 two-stage servovalves, provided by the manufacturer.

Table 6.3 MTS Model 252.25 Servovalves Specifications<sup>1</sup>.

Parameter	Specification
Maximum Operating Pressure, MPa	31.0 (4500 psi)
Minimum Operating Pressure, MPa	1.4 (200 psi)
Operating Temperature Range, °C	-40 to 135.0 (-40°F to +275°F)
Rated Full-Flow Input Signal Current	
Series	25 mA
Differential	50 mA
Parallel	50 mA total
Coil Resistance	80 Ω per coil
Weight, N	10.23 (2.3 lb)
Servovalve Flow Ratings	
Full-Flow Rating, l/min <sup>1</sup>	190.0 (15.0 gpm)
90 Point at 10% Command	160 Hz
Null Flow, l/min <sup>2</sup>	2.27 (0.60 gpm)

Notes: 1. Flow ratings are for 7.0 MPa (1000 psi) pressure drop across the servovalve.

2. The maximum internal null flow is specified at 21.0 MPa (3000 psi).

The null flow at the first stage is 0.76 l/min (0.20 gpm).

The MTS flow versus frequency performance curve of the Model 252.25 two-stage servovalve is shown in Figure 6.5. Flows versus frequency performance curves indicate the typical performance capabilities of the servovalve at various frequencies. The curves are derived by driving the servovalve, at the indicated frequency, with a sine wave control signal and  $\pm$  full current to the coil.

The full flow rating of 190.0 l/min (15 gpm) is maintained up to a frequency of 30 Hz, and then drops to 7.57 l/min (2 gpm) at a frequency of 600 Hz. At frequencies higher than 30 Hz, servovalve performance is a function of variables introduced by system components, actuator response and characteristics of the specimen.

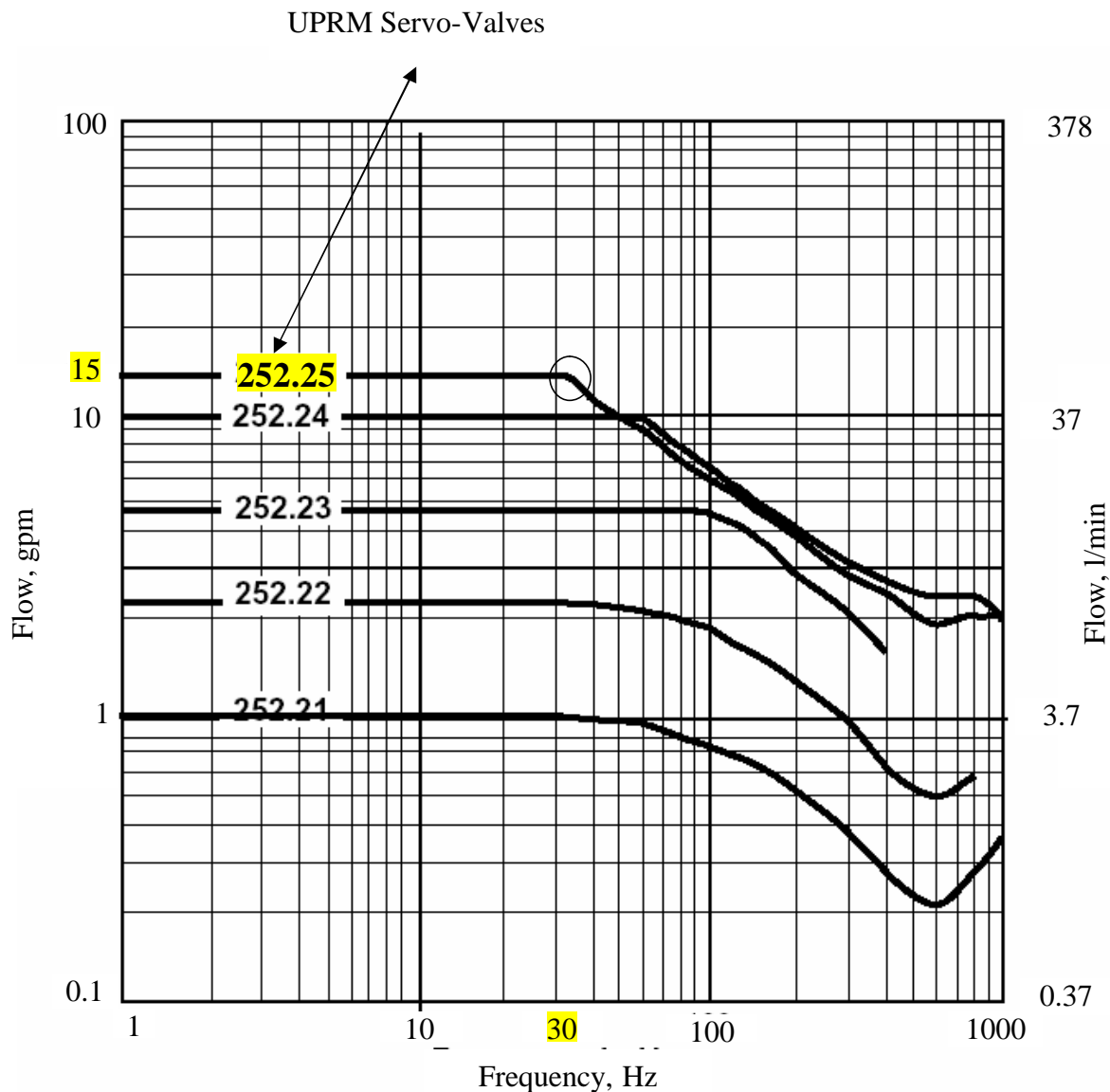


Figure 6.5 MTS Theoretical Performance Curves for the Series 252 Servovalves [23].

## 6.5. LINEAR ACTUATOR [20]

The slip table of the shaking table facility at the Structural Research Facility will be driven by a MTS Model 244.21 linear actuator. A linear actuator consists of a cylinder that contains a piston. The MTS Model 244.21 actuator is a double-acting and double-ended actuator that operates under precision servovalve control in a closed-loop servo-hydraulic system. Double-acting means the hydraulically powered piston can extend (tension) or retract (compression). A double-ended actuator can provide equal power in tension and compression.

The linear actuator system consists of force (load cell) and displacement (LVDT assembly) transducers, high-pressure fluid ports, cushions and swivel-end connections.

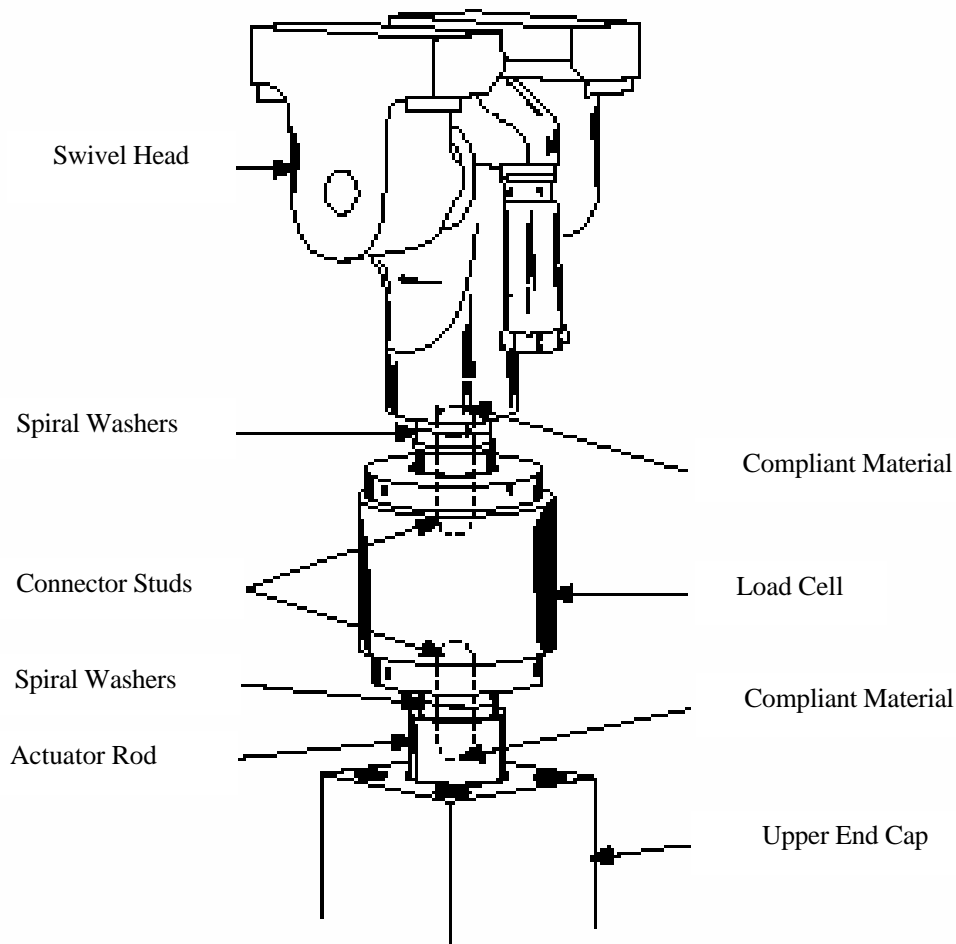


Figure 6.6 Force Transducer [20].

Figure 3.8 shows the different components of the MTS Model 244.21 linear actuator. The actuators force and displacement transducers are shown in Figure 6.6 and 3.8, respectively.

As previously discussed, actuator piston rod movement is accomplished by supplying high pressure hydraulic fluid to one side of the actuator piston and opening the other side to the return line. High-pressure hydraulic fluid is ported into the cylinder through the retraction port or the extension port. The differential pressure across the piston forces the piston rod to move. The amount of hydraulic fluid, and the speed and direction of piston rod movement is controlled by the servovalve. When the piston rod contacts an external reaction point (test specimen) then a force is applied to that reaction point. The force equals the effective piston area times the actuating pressure. The force applied is measured with a force transducer, in this case a load cell as shown in Figure 6.6. The load cell is connected at the end of the actuator's piston rod and in turn to a swivel mounting head. The swivel head connects the actuator-load cell system to the test specimen (slip table). Spiral washers are used to provide fatigue-resistant connections between elements of the force train and to minimize backlash. Backlash is caused by loose fitting or worn stud threads.

The MTS Model 244.21 actuator has a double-ended piston rod. The double-ended piston has equal areas on both sides for balanced performance. As illustrated in Figure 3.8, the hollow piston rod has an internally mounted LVDT that indicates the actuator piston rod displacement. The LVDT, an electromechanical device, provides an output voltage proportional to the displacement of the moveable core extension. The core extension moves as the piston rod moves.

The MTS Model 244.21 actuator has a piston rod diameter of 6.985 cm (2.75 in) and an effective actuator area of 25.16 cm<sup>2</sup> (3.90 in<sup>2</sup>). The theoretical maximum applicable force for a 21.0 MPa (3,000 psi) operating pressure is 49.24 N (11.7 kips). However, the nominal maximum force given by the manufacturer is 48.93 N (11 kips). The maximum dynamic stroke of the actuator is 15.24 cm (6.0 in), while in static conditions the maximum stroke is 17.27 cm (6.8 in).

## **6.6. PERFORMANCE ENVELOPES**

The performance of the hydraulic system is dependent on the frequency content of the commanded motion [5]. There are two types of commanded signals of interest in the area of shaking tables and they are harmonic and random signals. Two other physical limitations play a major role in determining the performance envelope of the shaking table system and they are the span and force [5]. The theoretical performance envelope curves for the UPRM hydraulic system will be given. The following procedure is derived from Muhlenkamp [5].

### **6.6.1. FLOW LIMITS FOR HARMONIC AND RANDOM ACTUATOR MOTION**

The HPS is able to provide a constant flow of hydraulic flow to the HSM and then to the servovalves. When the command signal is harmonic and the ratio of the  $q_{\text{peak}}$  to  $q_{\text{avg}}$  is 1.571, this indicates that accumulators are needed to help provide the additional (57%) hydraulic fluid during peak flow periods.

When the command signal is random, like an earthquake ground motion, the flow rate time history is characterized by a very peaked (jagged) and random behavior. The manufacturer, MTS, specifies that with accumulators,  $q_{\text{peak}}$  is about three times the  $q_{\text{peak}}$  value for harmonic loading [5]. That is,

$$q_{\max}^{seismic} = 3q_{\max}^{harmonic} = 4.71q_{\max}^{pump} \quad (6.1)$$

This indicates that accumulators help to reach an actuator  $q_{peak}$  equal to 4.71 times the pump maximum steady flow.

The reproduction of earthquake ground motions containing high velocity components will simultaneously require a high fluid flow rate and a large volume of fluid [5, 19]. In order for the accumulator to provide for such additional fluid demands, it must be designed for the proper flow rate and volume capacity. For harmonic flow conditions, this volume of fluid is [5]:

$$V_{accum} = 0.421AC \quad (6.2)$$

where  $A$  is the piston's effective area and  $C$  is the harmonic signal amplitude.

To find the maximum table velocity we simply use the basic fluid mechanics principle and the following equation:

$$v_{\max} = \frac{Q_{\max}}{A_p} \quad (6.3)$$

where  $Q_{\max}$  is the maximum flow rate into the actuator and  $A_p$  is the effective piston area. The maximum flow rate into the actuator depends on the pump, accumulator and servovalve characteristics, as discussed earlier. A list of the hydraulic flow rates available from the different components of the UPRM servo-hydraulic system is shown in Table 6.4.

Table 6.4 Components of the Servo-Hydraulic System.

Component	Model	Specification
Pump (HPS)	MTS 506.61	265.0 l/min (70 gpm)
Service Manifold (HSM)	MTS 293.11A	190.0 l/min (50 gpm)
Accumulators	MTS 111	7.57 l (2.0 gal) Pressure 0.45 l (0.12 gal) Return
Servovalves	MTS/Moog 252.25	Dual/ 56.78 l/min = 113.56 l/min  Dual/15 gpm = 30 gpm

Therefore, the maximum mean velocity generated by the actuator  $v_{\max}$  is:

$$v_{\max} = \frac{Q_{\max}}{A_p} = \frac{1892.67 \text{ cm}^3/\text{sec}}{25.16 \text{ cm}^2} = 75.23 \text{ cm}/\text{sec} = \frac{115.5 \text{ in}^3/\text{sec}}{3.90 \text{ in}^2} = 29.62 \text{ in}/\text{sec}$$

However, the ability of the servovalves to provide their full flow rate capacity diminishes beyond motions with frequencies of about 30 Hz as illustrated in Figure 6.5.

### 6.6.2. SPAN AND FORCE LIMITS

The maximum displacement capacity of the seismic simulator is the span or stroke of the actuator. Span is the maximum distance that the piston can travel [5], which is 15.24 cm (6.0 in),  $\pm 7.62$  cm ( $\pm 3.0$  in) from the center position, for the dynamic stroke of the MTS Model 244.21 actuator. For harmonic flow conditions, span and frequency are inversely proportional. Therefore the maximum span decreases for increasing frequency [5].

The maximum acceleration of the seismic simulator is limited by the properties of the servo-hydraulic system and the mass that the system is driving. The maximum force that

the actuator can produce is 48.93 kN (11 kip). For a given table mass and using Newton's Second Law, the maximum table acceleration is:

$$a_{\max}^{bare} = \frac{F_{\max}}{W_{table} / g} = \frac{F_{\max}}{W_{table}} g \quad (6.4)$$

where  $a_{\max}^{bare}$  is the maximum bare table acceleration,  $F_{\max}$  represents the maximum actuator force, and  $W_{table}$  represents the weight of the bare table, and  $g$  is the gravitational acceleration constant, 981 cm/sec<sup>2</sup> (386.4 in/sec<sup>2</sup>). Therefore, the maximum bare table acceleration is:

$$a_{\max}^{bare} = \frac{48,930N}{9,786N} g = \frac{11,000lbs}{2,200lbs} g = 5.0g$$

However, when the table is loaded with a test structure, the maximum acceleration diminishes. Given a test structure mass, for example 3,113 N (700 lb), and considering the simulator platform and test structure to behave as a rigid mass, the maximum acceleration is:

$$a_{\max}^{700} = \frac{48,930N}{12,899N} g = \frac{11,000lbs}{2,900lbs} g = 3.8g$$

With the same considerations as above but with a test structure with lumped masses of 3,558 N /floor (800 lbs /floor), the maximum acceleration is:

$$a_{\max}^{800} = \frac{48,930N}{23,575N} g = \frac{11,000lbs}{5,300lbs} g = 2.1g$$

It should be noted that the friction force between the sliding bearings and rails is neglected in Equation 6.4. The MTS Theoretical Performance Envelopes for the bare

table are shown in Figure 6.7 through Figure 6.9. Figure 6.7 shows the displacement vs. frequency performance envelope. Figure 6.8 shows the velocity vs. frequency performance envelope and Figure 6.9 displays the acceleration vs. frequency performance envelope. The blue curve shows a 0.0 N (0.0 kip) force and the green curve shows a 48.93 KN (11.0 kip) force.

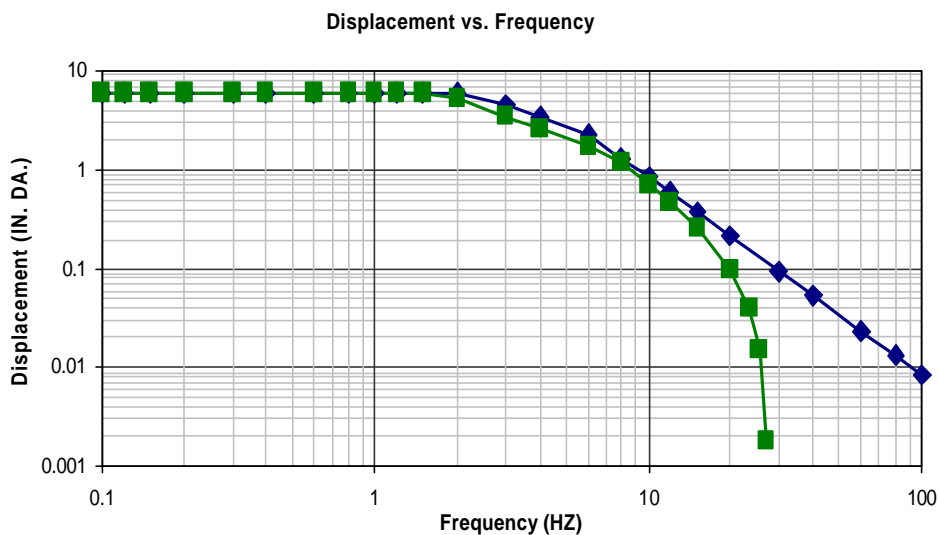


Figure 6.7 Displacement vs. Frequency Performance Envelope.

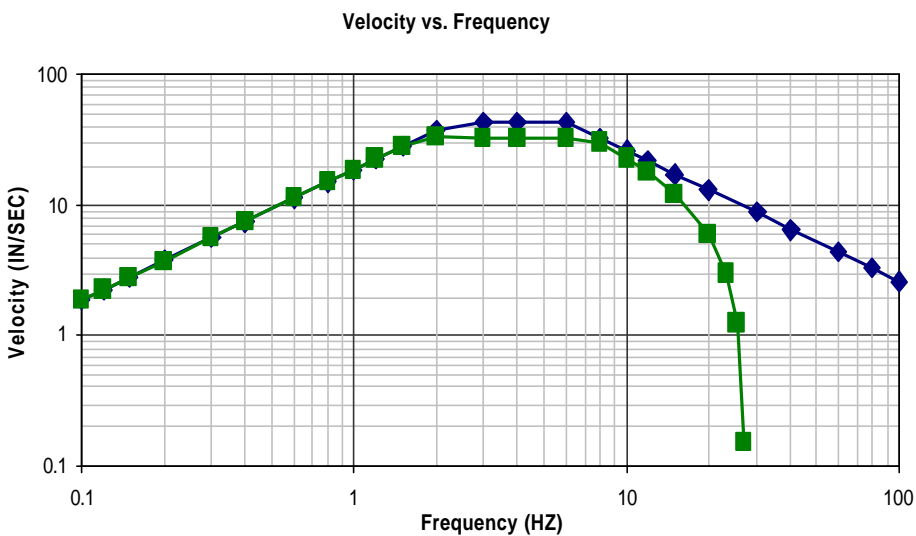


Figure 6.8 Velocity vs. Frequency Performance Envelope.

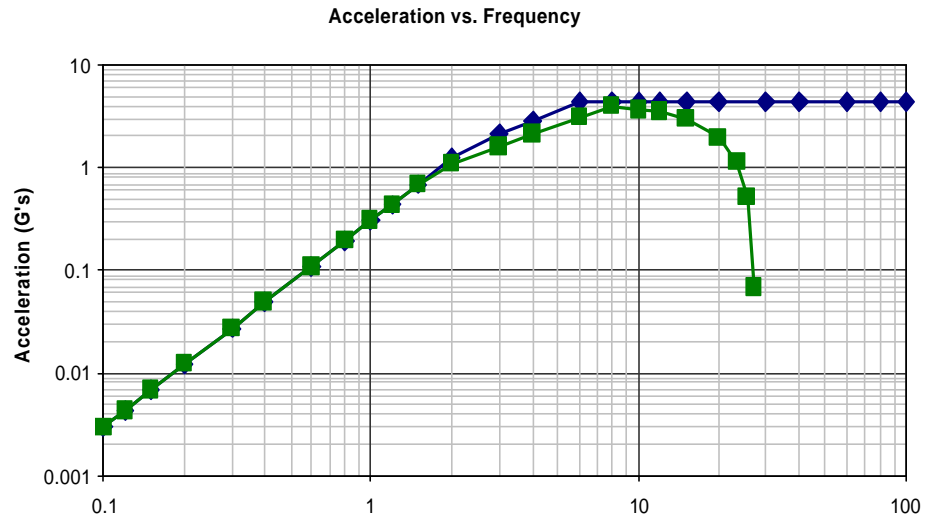


Figure 6.9 Acceleration vs. Frequency Performance Envelope.

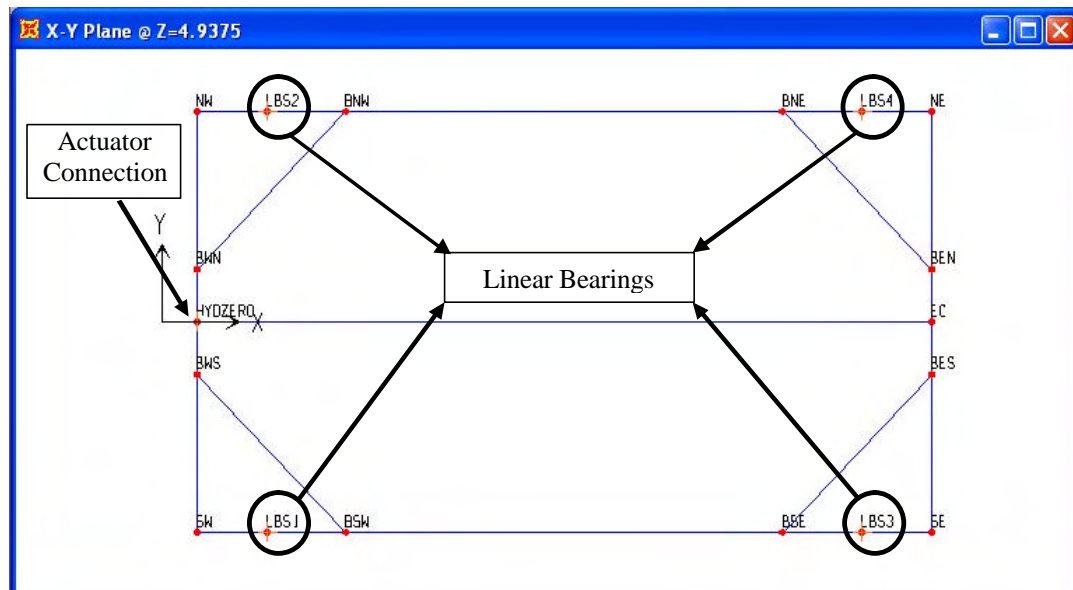
## 7. DYNAMIC MODELS OF SEISMIC SIMULATOR

### 7.1. COMPONENTS OF SEISMIC SIMULATOR

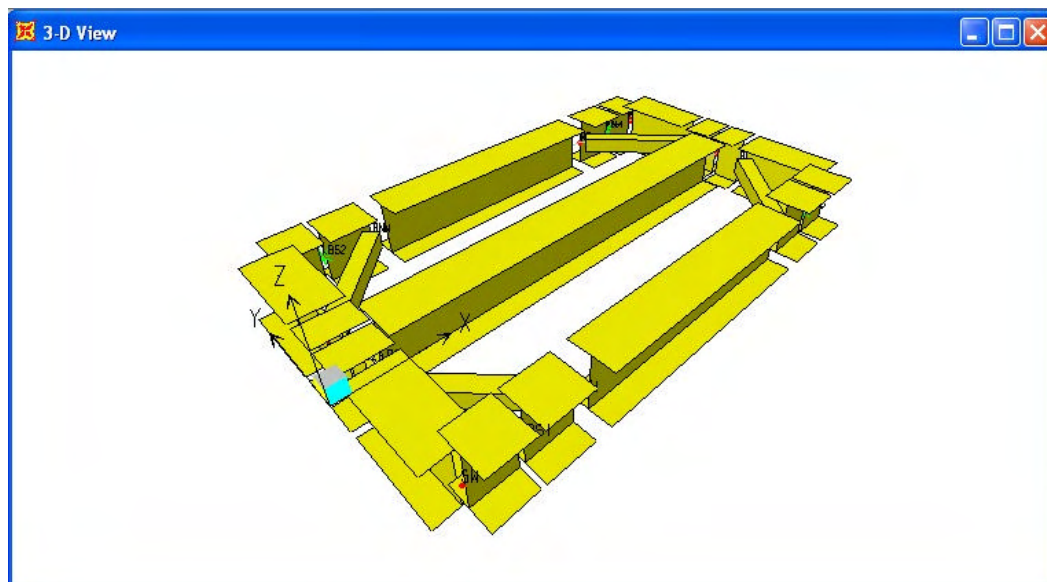
#### 7.1.1. SIMULATOR PLATFORM (SLIP TABLE)

As discussed earlier, the simulator platform consists of a bolted steel frame made up of three longitudinal W10x33 wide flange beams, four diagonal ST 3x3x0.25 tube section beams at the corners, and three 1.905 cm (0.75 in) thick steel plates at the top. Figure 5.2 shows the simulator platform. The top plate has 32 attachment points consisting of 2.06375 cm (0.8125 in) diameter holes for bolts with a diameter of 1.905cm (0.75 in) and a length of 5.08 cm (2.0 in).

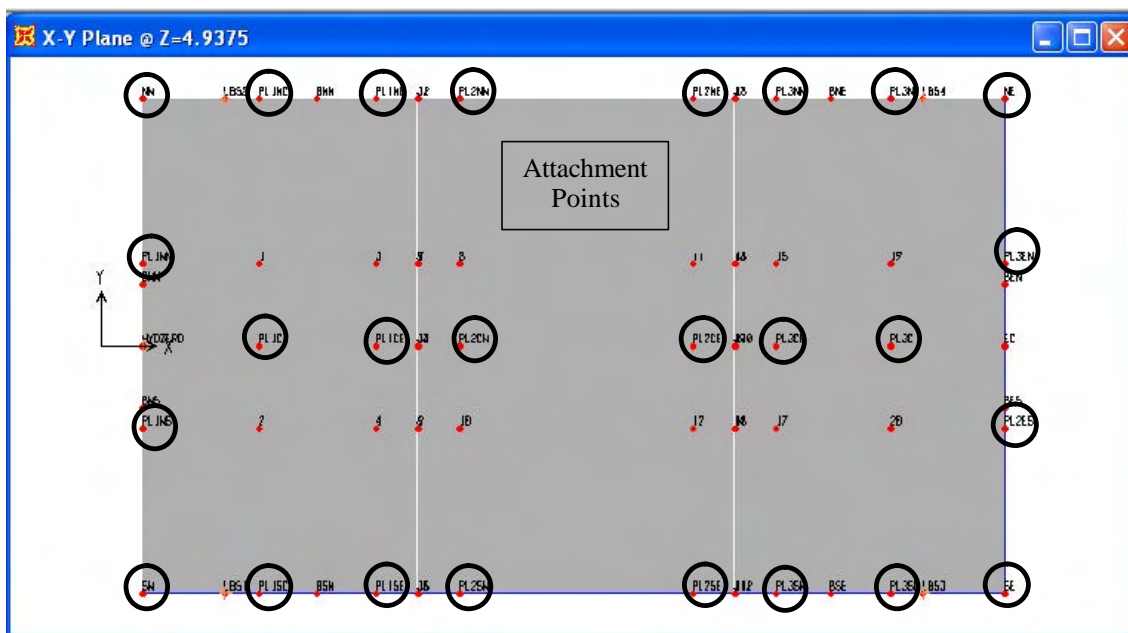
The natural frequencies of the simulator platform were obtained by creating a model in the finite element analysis program SAP2000. Figure 7.1 shows the model of the simulator platform.



(a) Plan View of Simulator Platform Model without the Steel Plates.



(b) 3D View of Model of Simulator Platform without the Steel Plates.

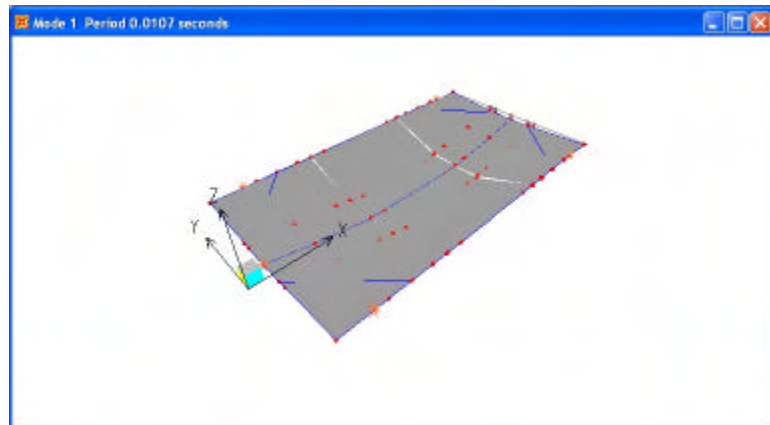


(c) Plan View of Model of Simulator Platform with the Steel Plates.

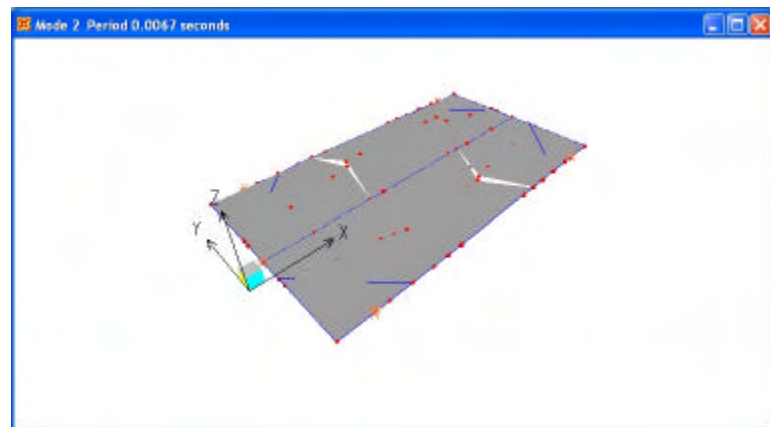
Figure 7.1 Simulator Platform Model.

Figure 7.1 (a) shows a plan view of the simulator platform steel frame without the steel plates. It also shows the location of the linear bearings and how they were modeled. Furthermore it shows the location of the actuator connection. The linear bearings were restrained against all rotations and against translations in the global Y-direction and Z-direction. They were unrestrained in the global X-direction, that is, in the direction of motion. The actuator connection was restrained against translation in the X-direction. The steel frame of the simulator platform was modeled using frame elements. The steel plates were modeled using shell elements and were placed at the centerline of the model. Figure 7.1 (b) shows a 3D view of Figure 7.1 (a). Figure 7.1 (c) shows the steel plates mounted on the steel frame, directly on the centerline, and also illustrates where the bolts were attached.

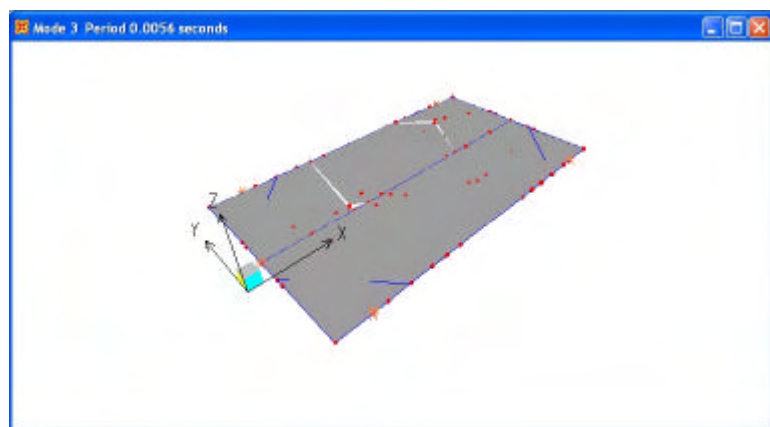
By means of a modal analysis, the first three mode shapes of the simulator platform were found and are shown in Figure 7.2. The natural periods of the first three modes are: 0.0107, 0.0067 and 0.0056 seconds. These correspond to the following frequencies: 93.5, 149 and 179 Hz. The maximum theoretical frequency range of operation of the table is approximately 0-32 Hz. MTS recommends that the table's fundamental natural frequency be at least three times the maximum operating frequency, or about 96 Hz [5]. In this case, the fundamental natural frequency (93.5 Hz) is 2.92 times higher than the theoretical highest excitation frequency (32 Hz). If we compare the first mode frequency (93.5 Hz) with the highest expected operational frequency range of the table, that is the 20 Hz range, the ratio would be 4.7. Thus, the platform could be considered to have enough rigidity and can be modeled as a rigid body up to that operational frequency.



(a) First Mode Shape.



(b) Second Mode Shape.



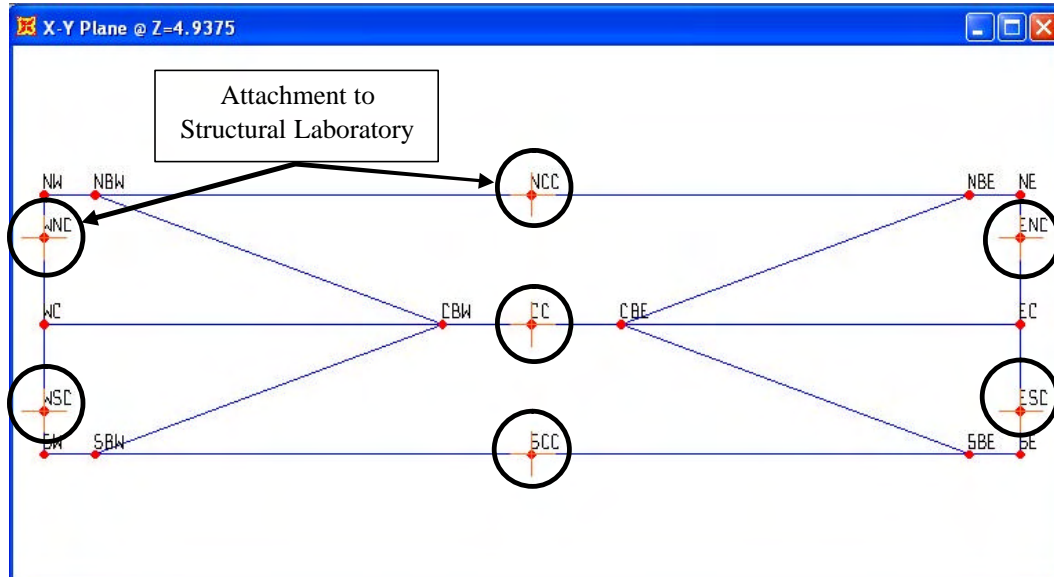
(c) Third Mode Shape.

Figure 7.2 First Three Modes of Simulator Platform.

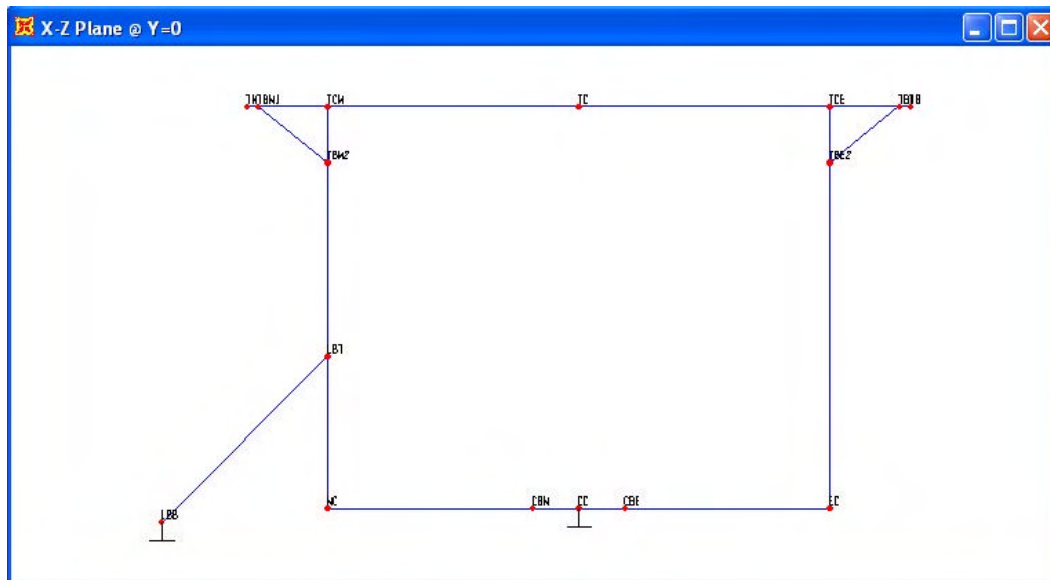
### 7.1.2. REACTION FRAME

The reaction frame, as illustrated in Figures 3.1 and 3.2, can be divided as a bottom frame and a top frame. The bottom frame also consists of a bolted steel frame of three longitudinal W10x33 wide flange beams and four diagonal ST 3x3x0.25 tube section beams at the corners. The bottom frame is bolted to the Structural Laboratory's floor. The top frame consists of a bolted frame of two W10x33 columns and a W10x33 beam. The primary purpose of the top frame is to carry an electric chain hoist to carry the test structure elements.

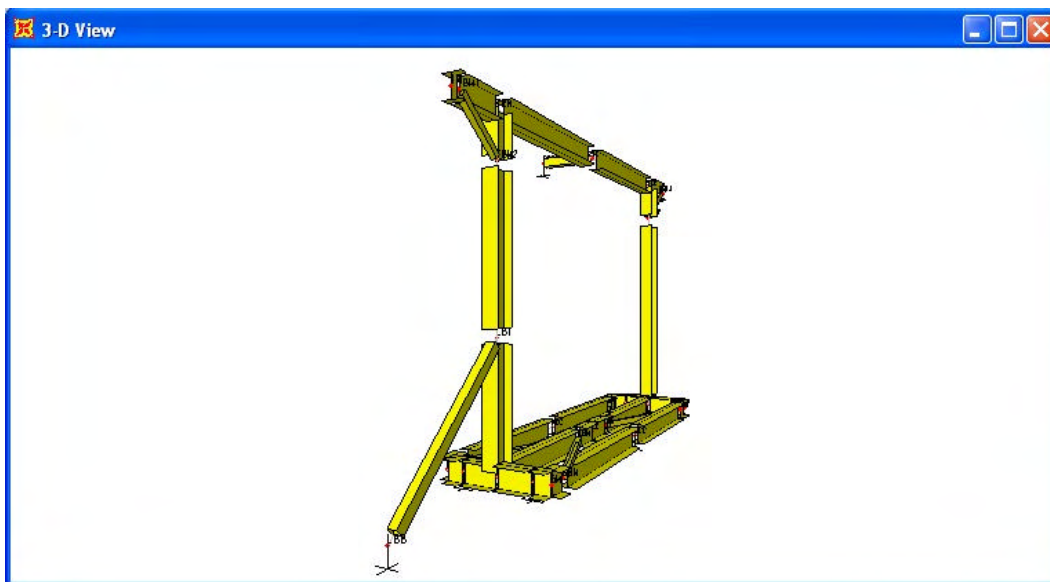
The natural frequencies of the reaction frame were obtained creating a model in the finite element analysis program SAP2000. Figure 7.3 shows the model of the reaction frame.



(a) Plan View of Bottom Frame.



(b) Elevation View of the Reaction Frame.

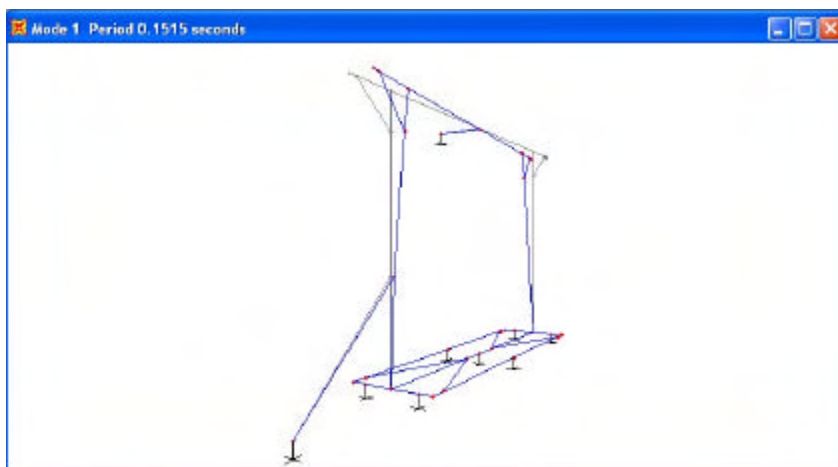


(c) 3D View of Reaction Frame.

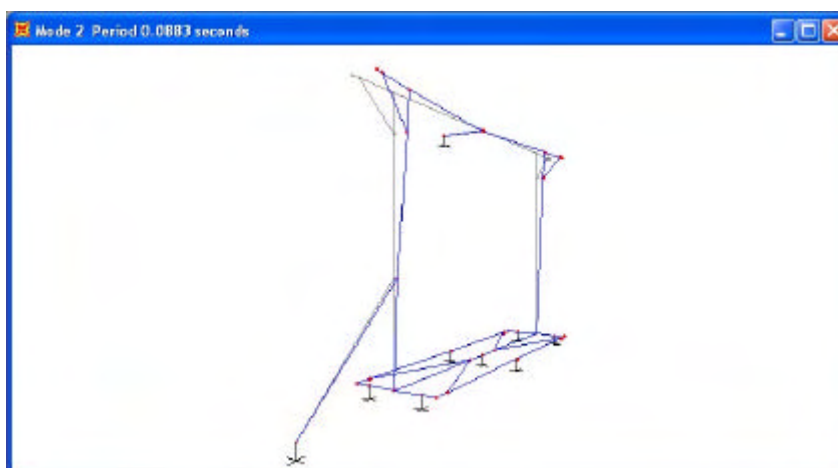
Figure 7.3 Reaction Frame Model.

Figure 7.3 (a) shows the bottom steel frame of the reaction frame. It also shows the locations where the reaction frame is connected to the Structural Laboratory floor. The connection to the laboratory floor was restrained against all rotations and against all translations, that is, it was modeled as a fixed joint. The bottom steel frame of the reaction frame was modeled using frame elements. Figure 7.3 (b) shows an elevation view of the reaction frame with the top frame also included. The latter was also modeled with frame elements. Figure 7.3 (c) shows a 3D version of Figure 7.2 (b).

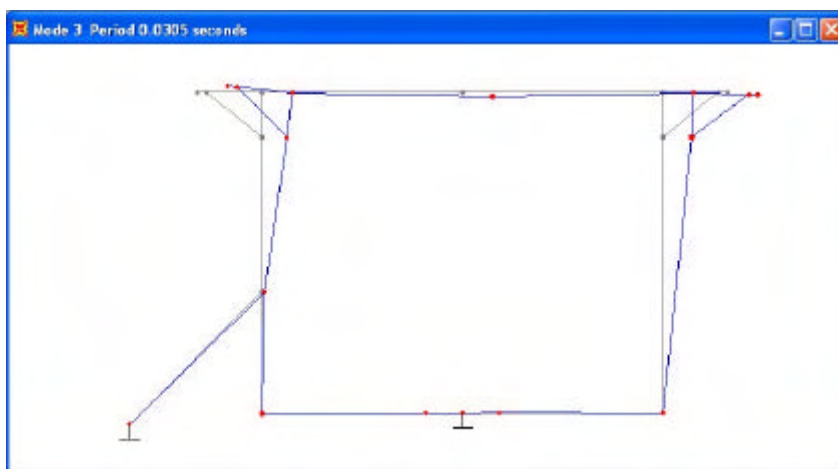
Using modal analysis, the first three mode shapes of the simulator platform were calculated and are shown in Figure 7.4. The natural periods of the first three modes are: 0.1515, 0.0883 and 0.0305 seconds, which correspond to frequencies of 6.6, 11 and 33 Hz. The three fundamental modes of the system show a flexibility of the top frame of the reaction frame. The two natural frequencies of the first two modes (6.6 and 11 Hz) are in the operating range of the shaking table and there could be some interaction when operating the table at these frequencies. We recommend that the top frame be isolated from the system or made to be less flexible.



(a) First Mode Shape.



(b) Second Mode Shape.



(c) Third Mode Shape.

Figure 7.4 First Three Modes of the Reaction Frame.

### 7.1.3. HYDRAULIC ACTUATOR OIL COLUMN DYNAMICS

The dynamic characteristics of the servo-hydraulic system are assumed to be primarily dependent on the actuator oil column stiffness and frequency [19]. Consider the actuator and oil system as a single degree of freedom mass/spring/damper system, as shown in Figure 7.5. To derive the equation for the oil column stiffness and frequency let us start by considering the actuator schematic shown in Figure 7.6 (a). This approach to derive the oil column stiffness and frequency is based on Twitchell [19].

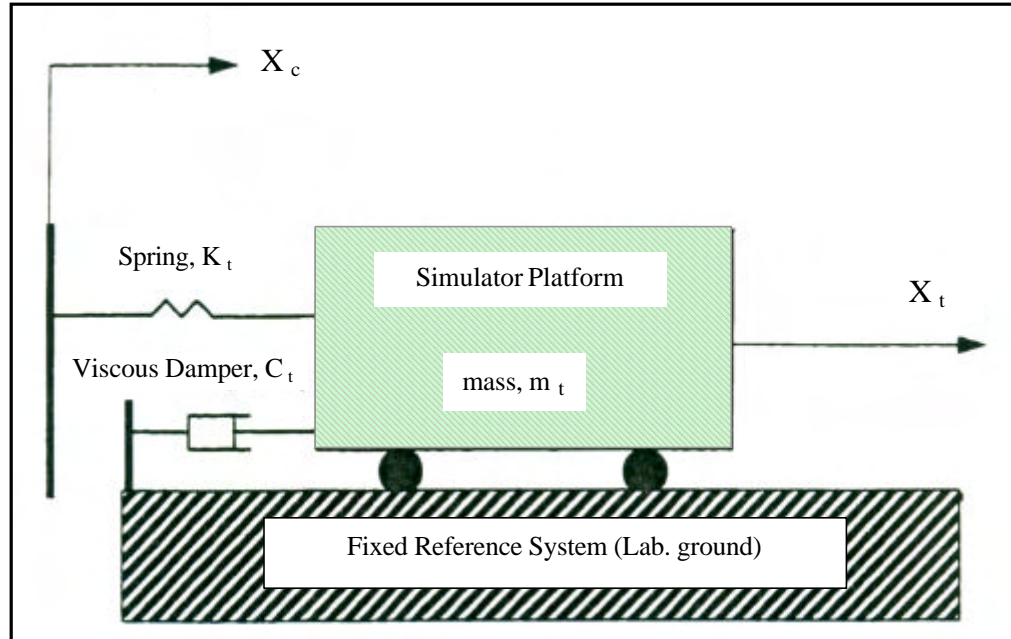
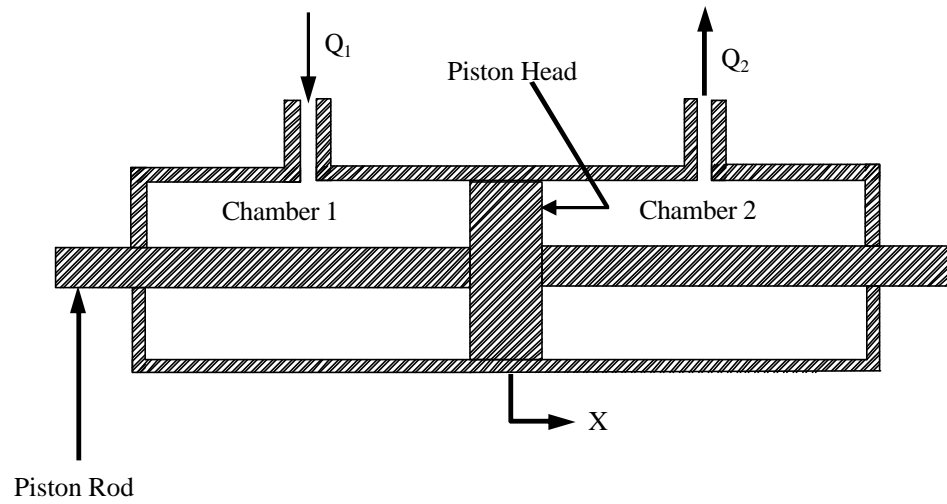
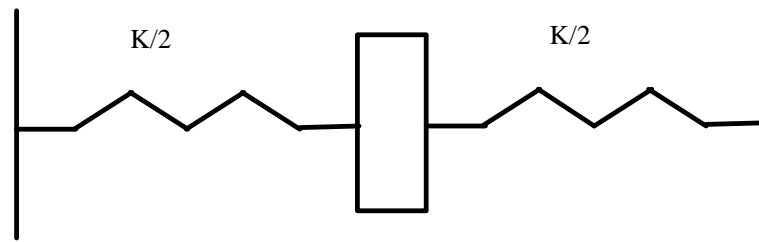


Figure 7.5 Equivalent SDOF of Actuator and Oil System [9].

From Figure 7.6 (a),  $Q_1$  and  $Q_2$  can be defined as the fluid flow into chamber 1 and fluid flow out of chamber 2, respectively. Also from Figure 7.6 (b), it can be seen that the actuator's oil column can be represented by an equivalent spring system. The fluid spring is characterized by the value of the bulk modulus [28]. The bulk modulus,  $\beta$ , of a liquid has been shown to be [19, 28]:



(a) Actuator Oil Column.



(b) Equivalent Spring System.

Figure 7.6 Schematic of Hydraulic Actuator [9, 19].

$$\mathbf{b} = -\Delta P \left( \frac{V}{\Delta V} \right) \quad (7.1)$$

where  $V$  is the total volume of the fluid within the actuator and  $\Delta V$  is the change in fluid volume due to a change in fluid pressure,  $\Delta P$ . The negative sign indicates a decrease in volume with pressure increase. Therefore the change in fluid volume,  $\Delta V$ , can be defined as:

$$\Delta V = -\Delta P \left( \frac{V}{\mathbf{b}} \right) \quad (7.2)$$

The change in fluid volume can be further simplified by observing the actuator schematic in Figure 7.2. For example, the change in fluid volume of chamber 1,  $\Delta V_1$ , can be defined as:

$$\Delta V_1 = A(\Delta X) \quad (7.3)$$

where  $A$  is the effective actuator piston head cross-sectional area and  $\Delta X$  is the change in position of the actuator piston head. Equating Equations 7.2 and 7.3, we obtain an expression for the change in position of the piston head,  $\Delta X$ , as:

$$\Delta X = \frac{\Delta V_1}{A} = -\Delta P_1 \left( \frac{V_1}{\mathbf{b}} \right) \left( \frac{1}{A} \right) \quad (7.4)$$

The differential pressure between chambers 1 and 2 multiplied by the effective piston head area gives the net force acting on the piston head,  $\Delta F$ :

$$\Delta F = A(\Delta P) = A(\Delta P_2 - \Delta P_1) \quad (7.5)$$

Therefore, an expression for the stiffness of the actuator oil column,  $K_{oil}$ , can be obtained from Equations 7.4 and 7.5 utilizing  $F = K*U$ :

$$K_{oil} = \frac{\Delta F}{\Delta X} = \left( \begin{array}{c} \frac{A(\Delta P_2 - \Delta P_1)}{-\Delta P_1 \left( \frac{V_1}{b} \right) \left( \frac{1}{A} \right)} \end{array} \right) = -\frac{A^2 b}{V_1} \left( \frac{\Delta P}{\Delta P_1} \right) \quad (7.6)$$

Servovalves direct hydraulic fluid to the actuator such that the pressure in chamber 2 decreases when the pressure in chamber 1 increases [19]. Therefore,

$$\Delta P_1 = -\Delta P_2 \quad (7.7)$$

Substituting Equation 7.7 into Equation 7.6 results in:

$$K_{oil} = -\frac{A^2 b}{V_1} \left( \frac{-2\Delta P_1}{\Delta P_1} \right) = \frac{2A^2 b}{V_1} \quad (7.8)$$

The total volume of hydraulic fluid in the actuator can be simplified as the sum of the fluid volume in chambers 1 and 2. In the null position ( $X=0$ ), the fluid volume in chamber 1 is equal to the fluid volume in chamber 2 [9, 19, 28]. As a result, for small displacements of the actuator near the null position, the stiffness of the actuator oil column can be defined as [9, 19]:

$$K_{oil} = \frac{2A^2 b}{V_1} = \frac{2A^2 b}{\frac{V}{2}} = \frac{4A^2 b}{V} \quad (7.9)$$

where  $V$  is the total volume of fluid within the actuator.

The natural frequency of the oil column,  $f_{oil}$ , for the unloaded seismic simulator can be obtained by using the equation for the natural frequency of a single degree of freedom system:

$$f_{oil} = \frac{1}{2\mathbf{p}} \sqrt{\frac{K_{oil}}{M_{unloaded}}} = \frac{1}{2\mathbf{p}} \sqrt{\frac{4A^2\mathbf{b}}{VM_{unloaded}}} \quad (7.10)$$

This equation assumes that the actuator behaves as a linear elastic spring and that there is no friction at the bearing/rail interface [19].

Table 7.1 gives the physical properties of the servo-hydraulic system needed to calculate the dynamic properties of the servo-hydraulic system.

Table 7.1 Physical and Dynamic Properties of the UPRM Servo-Hydraulic System.<sup>1</sup>

Property	Value
Effective Piston Area, A	25.16 cm <sup>2</sup> (3.90 in <sup>2</sup> )
Total Fluid Volume, V	911.75 cm <sup>3</sup> (55.64 in <sup>3</sup> )
Bulk Modulus of Hydraulic Fluid, $\beta$	1.45 GPa (210,000 lbf/in <sup>2</sup> )
Mass of Simulator Platform, $M_{unloaded}$	9.98 kg (5.69 lb-sec <sup>2</sup> /in)
Oil Column Stiffness, $K_{oil}$	402.2 kN/cm (229,634 lb/in)
Natural Frequency of Oil Column, $f_{oil}$	32.0 Hz

Note: 1) Modified from [19].

The oil column frequency depends on many factors such as the specimen mass, the oil pressure and temperature. Therefore, its numerical value could shift somehow depending on the changes in the factors mentioned above.

The oil column frequency is inherent in the system, it acts like a spring and there will always be some residual vibration at that frequency.

## **8. SHAKING TABLE CONSTRUCTION**

### **8.1. INTRODUCTION**

Most of the shaking table components were manufactured “out-of house” and assembled “in-house” later on. The hydraulic power components and the electronic control system were purchased from the MTS Corporation. Some were assembled by the research team, the rest was assembled and calibrated by MTS personnel. The construction process was divided into the following parts:

1. Assembly of Reaction Frame
2. Assembly of Simulator Platform
3. Connection of Reaction Frame to Structural Laboratory floor
4. Mounting of Linear Bearing System
5. Leveling and Alignment of Linear Bearing System
6. Mounting of Simulator Platform
7. Connection of Hydraulic Actuator

### **8.2. ASSEMBLY OF REACTION FRAME**

The assembly of the reaction frame consisted of forming the bolted frame of the W10x33 beams and of the ST 3x3x0.25. For additional stiffness, a lateral bracing was added and connected to the column on the west side and to the floor, as shown in Figure 8.1.

### **8.3. ASSEMBLY OF SIMULATOR PLATFORM**

The assembly of the simulator platform consisted of forming the bolted frame of the W10x33 beams and of the ST 3x3x0.25. For added stiffness a new W10x33 beam was welded to the sides of the platform as shown in Figure 8.2.



Figure 8.1 Lateral Bracing of Reaction Frame.



Figure 8.2 New Beam Welded to Simulator Frame.

#### **8.4. CONNECTION OF REACTION FRAME TO FLOOR**

The connection to the laboratory floor consisted of two types: the middle connection and the west and east side connections, as shown in Figure 5.1. These connections were made of steel bars PL 2.0 in x 0.25 in and the middle connection of L3.0 in x 3.0 in x 0.25in angles. They were welded together and to the flanges of the W10x333 beams for the west and east side connections. For the middle connection they were welded to the top and bottom of the web on the inside of the beam. After welding, they were bolted to the floor using 1.5875 cm (0.625 in) diameter and 10.16 cm (4.0 in) long bolts.

#### **8.5. MOUNTING OF THE LINEAR BEARING SYSTEM**

The linear bearing system was mounted to top flange of the W10x33 beams with bolts after being carefully aligned and leveled.

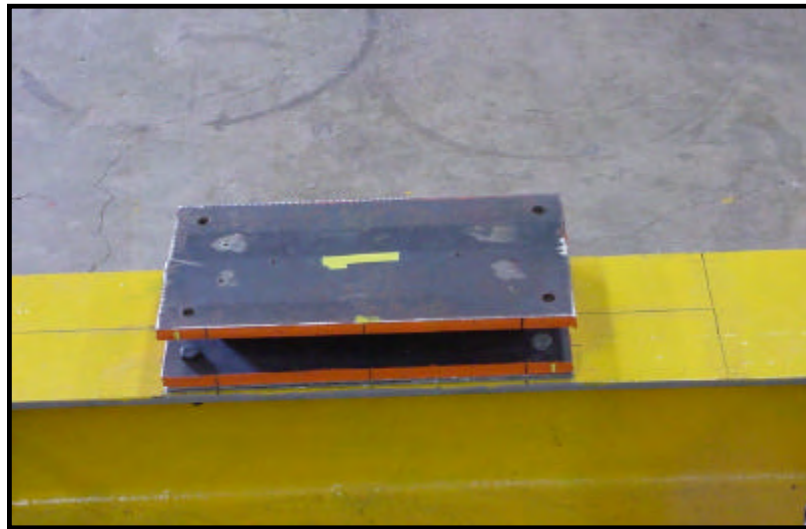


Figure 8.3 Linear Bearing System #1 Mounted to the Reaction Frame.

## 8.6. LEVELING AND ALIGNMENT OF LINEAR BEARING SYSTEM

It was important the four linear bearing systems behave as a unit. For this to happen, the individual bearing systems had to be leveled and aligned with each other. Also, the two lines of bearings had to run straight and parallel. Alignment, or Optical Tooling, is the geometric orientation of various components of a system such that all components can work harmoniously as they were designed to. If alignment and leveling is not carefully done, the misalignment can create additional friction to the movement of the simulator platform or induce damage of the equipment (linear bearings). Some of the instruments used for our measurements were: a precision sight level, tape measure (millimeters), carpenter's square, digital calipers (15.24 cm (6.0in) to 76.5 cm (30 in)), chalk line, a plumb bob and a machinist level.

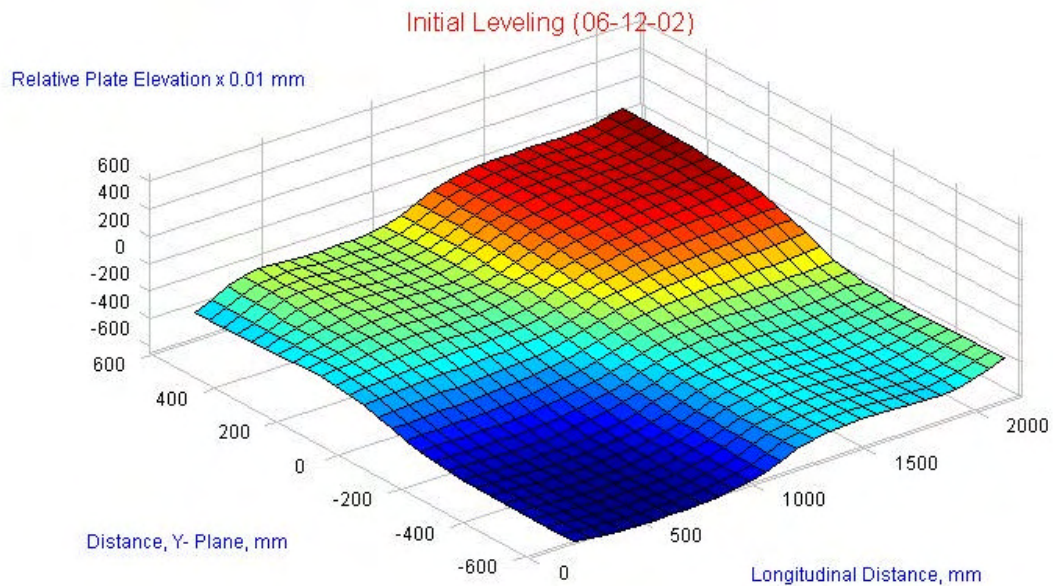


Figure 8.4 Top Flange's Surface Initial Leveling.

Leveling is the measure of the possible deviation of a horizontal plane formed by the four linear bearing systems. Figure 8.4 shows how the surface of the top of the flanges was before any work was done. This figure shows that the north-east part of the frame is higher than the rest of the frame, shown by the red color, and that the lowest part is the south-west part of the frame, shown by the blue color.

The four linear bearing systems were put in place and were leveled using the information of the initial leveling. For leveling, 1/8, 1/16 and 1/32 of an inch steel plates were used. Figure 8.5 shows the next leveling. Figure 8.6 shows the last leveling.

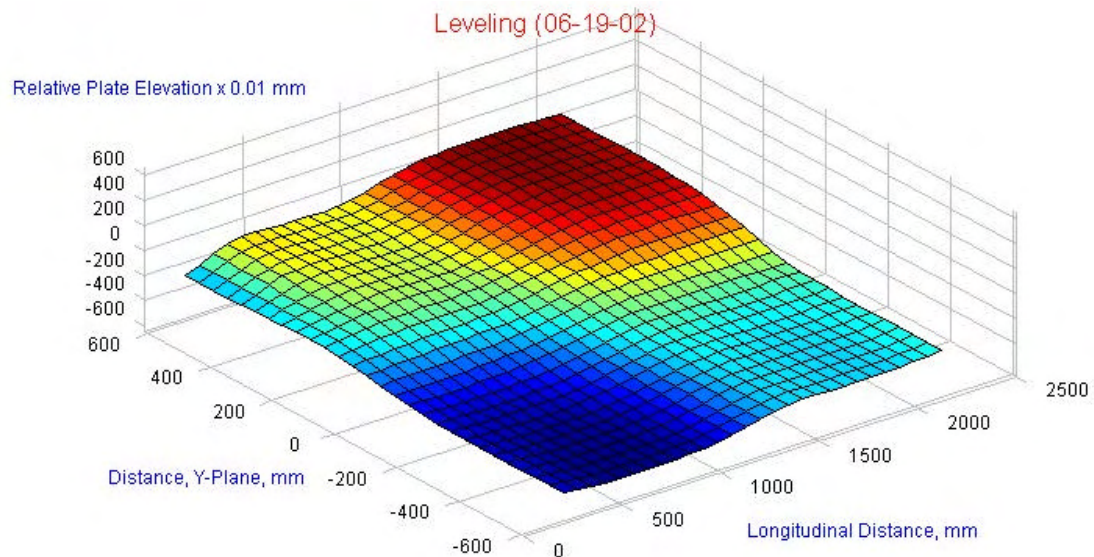


Figure 8.5 Next Leveling of 4-Linear Bearing Systems.

The last leveling shows a flat surface with parts slightly lower than the rest (blue color) and parts slightly higher than the rest (red color). Figure 8.7 illustrates where the elevations were taken to make the elevation profiles. Figure 8.8 shows the elevation profiles of the two lines of bearings at the beginning and at the end of the leveling process. At the end of the leveling process, the elevation deviation of the two lines of bearings was 0.8 mm (0.0315 in).

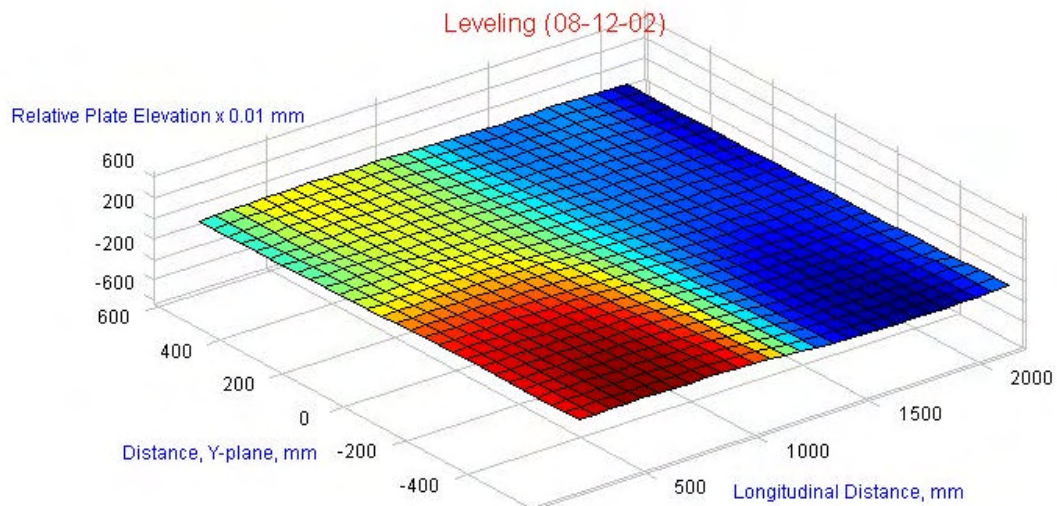


Figure 8.6 Last Leveling of 4-Linear Bearing Systems.

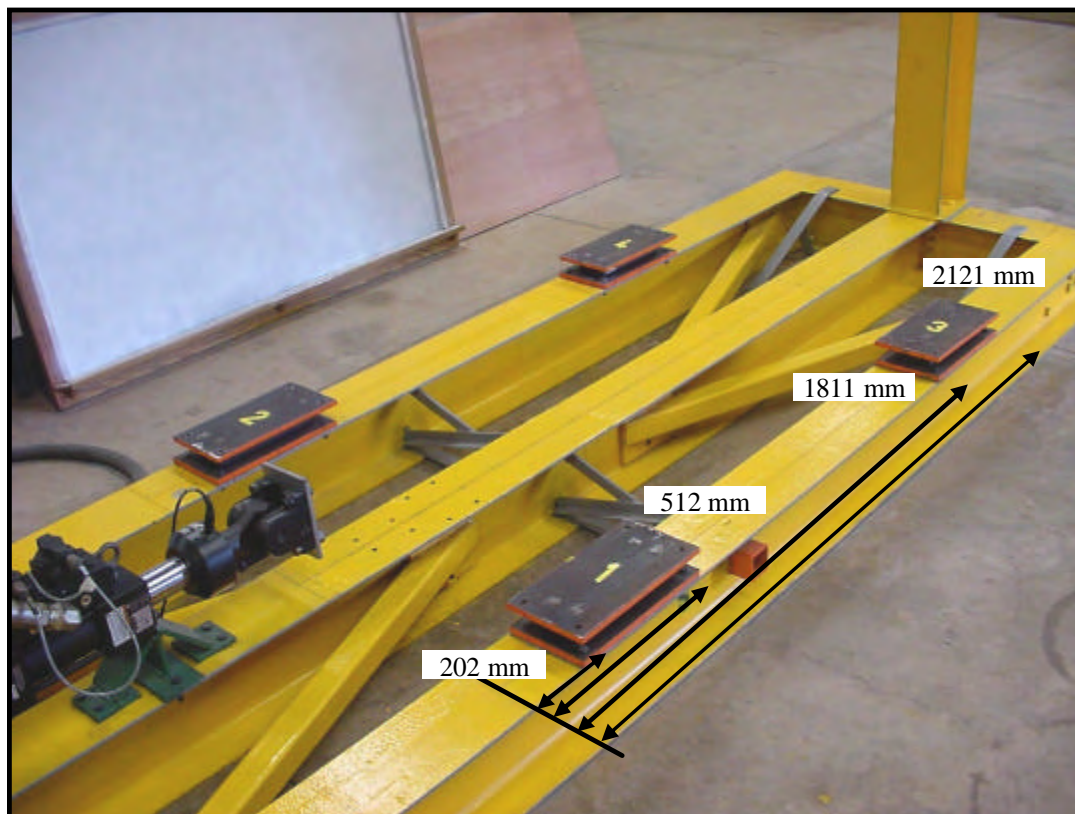
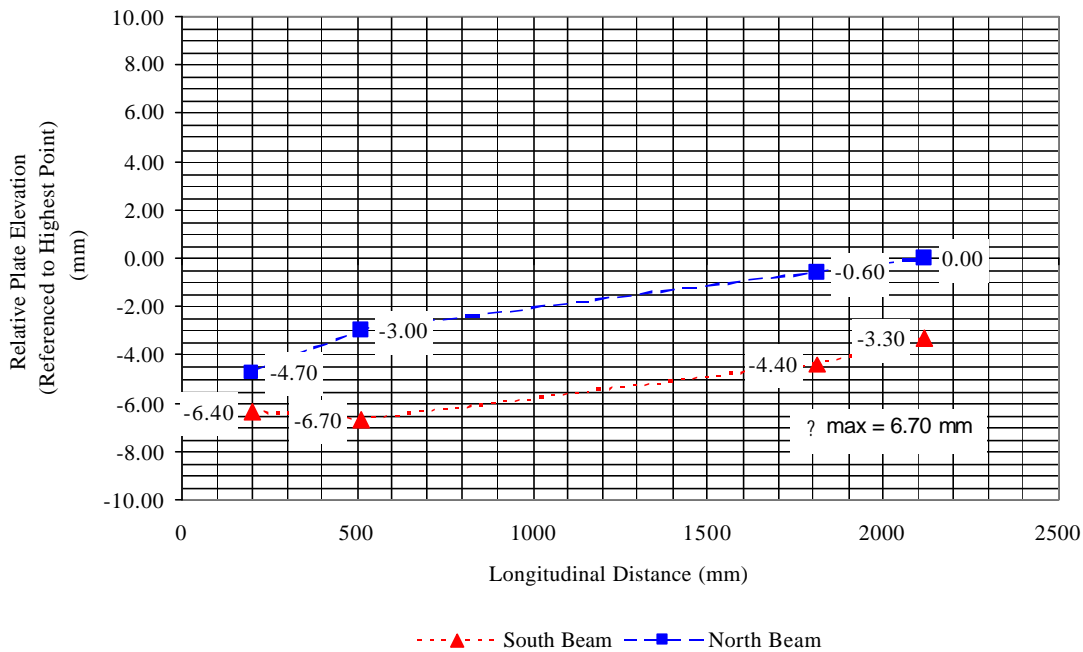
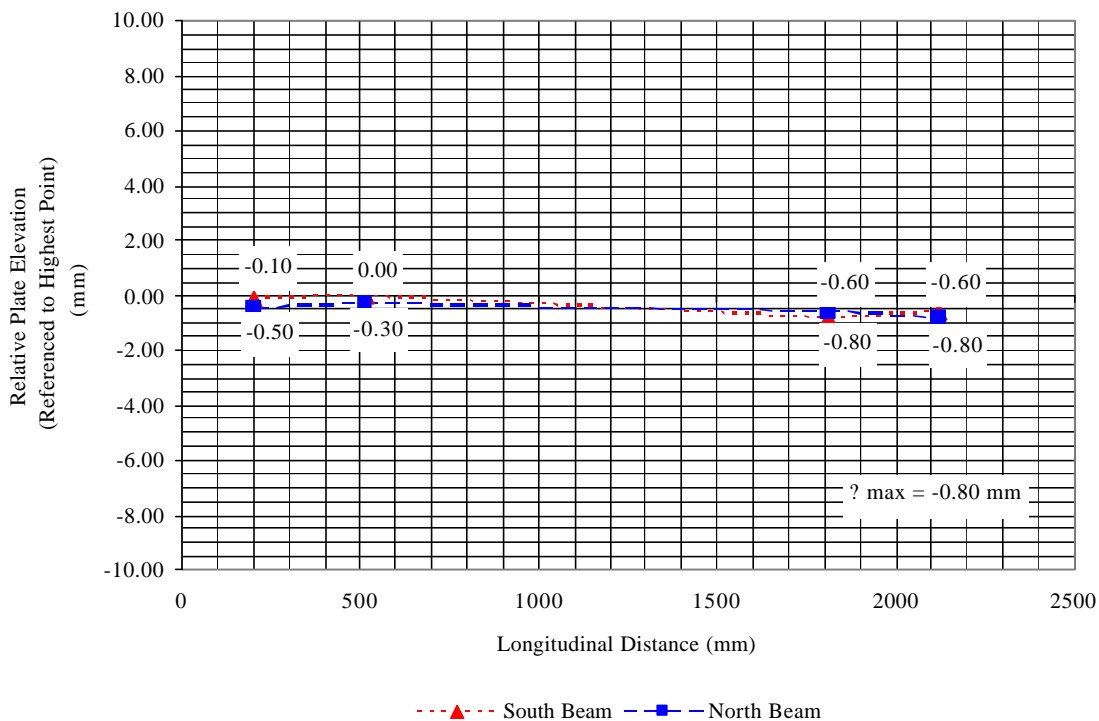


Figure 8.7 Elevations Layout.



(a) Initial Elevation Profile.



(b) Elevation Profile at the End of the Leveling Process.

Figure 8.8 Elevation Profiles of the Two Lines of Bearings.

The two lines of bearings were fixed to run straight and parallel, with a maximum absolute deviation between the CL of the bearing to the CL of the actuator of,  $\pm 0.05$  mm ( $\pm 0.001968$  in).

### 8.7. MOUNTING OF SIMULATOR PLATFORM

After the 4-Linear Bearing Systems were properly aligned and level, the simulator platform was bolted to the top plate of the bearing systems, as shown in Figure 8.9.

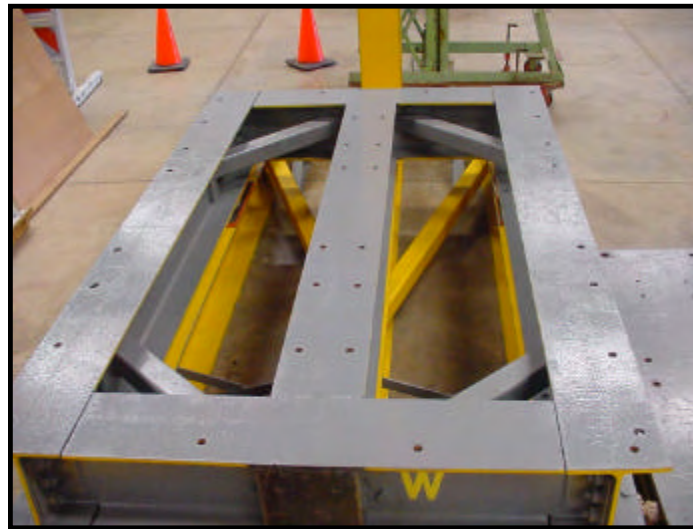


Figure 8.9 Simulator Platform Bolted to the Top Plate of the 4-LBS.

Then, the steel plates were bolted to the simulator frame, as shown in Figure 8.10.



Figure 8.10 Steel Plates Attached to Simulator Frame.

## 8.8. CONNECTION OF HYDRAULIC ACTUATOR

Once the simulator platform was mounted to the bearings, the actuator was fastened to a steel plate welded on the west side of simulator platform, as illustrated in Figure 8.11.



Figure 8.11 Attachment of Actuator to Simulator Platform.

## **9. MEASURES OF SHAKING TABLE PERFORMANCE**

### **9.1. INTRODUCTION**

In the case of a newly assembled shaking table, like the one at the UPRM Civil Engineering Department, it is necessary an evaluation of the accuracy of the input motion reproduction by the table. Furthermore, it is necessary to conduct a complete study of the table behavior in order to determine the calibration parameters for which the table can provide the best accuracy in earthquake reproduction [9].

### **9.2. EXPERIMENTAL TESTS FOR DETERMINATION OF SHAKING TABLE PERFORMANCE**

A comprehensive investigation of table performance should use several types of input motions. The following discussion on the types of input motion is based on Mills [3].

The different types of input motion should include the following:

1. A Square wave
2. A Sinusoidal wave
3. White noise, modified by high and low-pass filtering
4. Actual earthquake time histories, with various model scaling factors

Each form of input motion provides a specific insight into the shake table response characteristics. Also, each type of test should be carried out for different parameters such as frequency, amplitude and payload conditions (bare table, rigid payload and flexible SDOF/MDOF payload).

An initial subjective determination of the quality of shake table reproduction was obtained by carrying out preliminary experimental tests. The preliminary tests involved the following input motions:

1. Square wave - provided information on the bare (unloaded) shaking table stability and rate of response.
2. Sinusoidal wave - provided the amplitude spectra envelope of the shaking table response and the frequency performance limitations.

These tests were carried out only in the bare table condition.

### 9.3. CALIBRATION PARAMETERS

The right calibration parameters or control gain settings for the different shake table payload conditions are found by a process called tuning. Tuning is discussed on the MTS manual titled “Controller Installation & Calibration” and the following discussion is based on this manual. Tuning affects the response and stability of the servo-control loop. Proper tuning improves the performance of the system by reducing error and phase lag [21]. Figure 9.1 illustrates this concept.

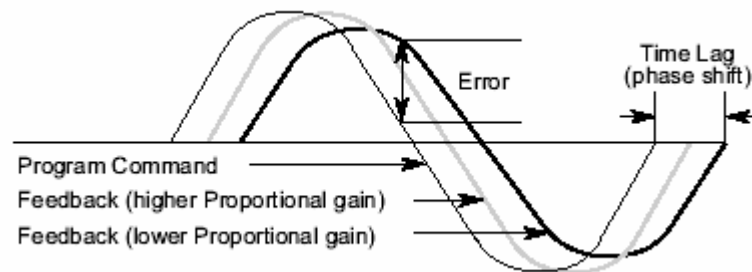


Figure 9.1 Definitions of Error and Phase Lag [21].

A control mode uses a program command and sensor feedback to control the servovalve [21]. For the purpose of tuning our system we utilized displacement control. This control mode uses the LVDT on the actuator as feedback signal. The TestStarAP controller uses a group of gain controls – proportional, integral, derivative and feed forward gain. These controls are called PIDF [21]. One does not need to use all of the

controls to properly tune a system. In fact, most testing can be accomplished with just proportional gain adjustment [21]. Proportional gain was used during our tests to tune the system. The five available gain controls have different functions.

### 9.3.1. PROPORTIONAL GAIN (P)

Proportional gain introduces a control factor that is proportional to the error signal. Proportional gain increases system response by increasing the effect of the error signal on the servovalve. Figure 9.2 shows the effects of proportional gain.

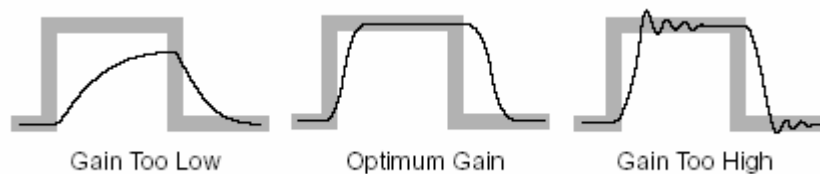


Figure 9.2 Effects of Proportional Gain on Sensor Feedback [21].

As proportional gain increases, the error decreases and the feedback signal tracks the command signal more closely. Too much proportional gain can cause the system to become unstable. In the other direction, too little proportional gain can cause the system to become sluggish. The MTS rule of thumb for proportional gain is to adjust gain as high as it will go without going unstable.

### 9.3.2. INTEGRAL GAIN (I)

Integral gain introduces “an integral of the error signal” that gradually, over time, increases the low-frequency response of the servovalve command. Integral gain maintains the mean level at high-frequency operation. Figure 9.3 shows the effects of integral gain. Higher integral gain settings increase system response. Too much integral

gain can cause a slow oscillation (hunting). The MTS rule of thumb is to set the integral gain to 10% of the proportional gain setting.

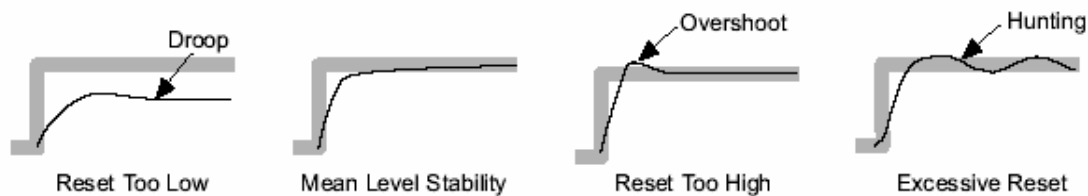


Figure 9.3 Effects of Integral Gain on Sensor Feedback [21].

### 9.3.3. DERIVATIVE GAIN (D)

It introduces a “derivative of the feedback signal”. This means it anticipates the rate of change of the feedback and slows the system response at high rates of change. It reduces ringing, provides stability and reduces noise at higher proportional gain settings. Too much derivative gain can create instability at high frequencies, and way too much gain may cause a ringing or screeching sound. Too little derivative gain can make a rumbling sound. The correct amount of derivative gain results in the system running quietly. Figure 9.4 shows the effect of derivative gain.

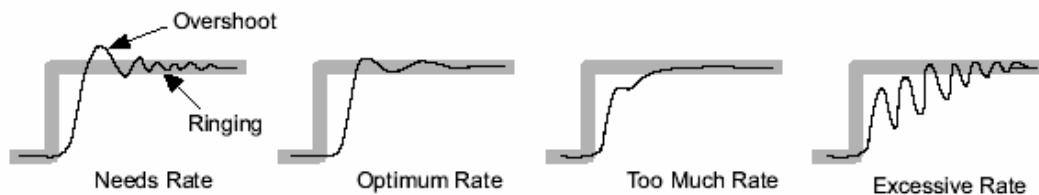


Figure 9.4 Effects of Derivative Gain on Sensor Feedback [21].

### 9.3.4. FEED FORWARD GAIN (F)

Feed forward gain is like derivative gain except that it introduces a derivative of the command signal. It anticipates how much valve opening is needed to reach the required response and adds that to the valve command – like compensating for phase lag. Feed

forward gain helps the servo-control loop to react quickly to an abrupt change in the command. Figure 9.5 shows the effect of feed forward gain.

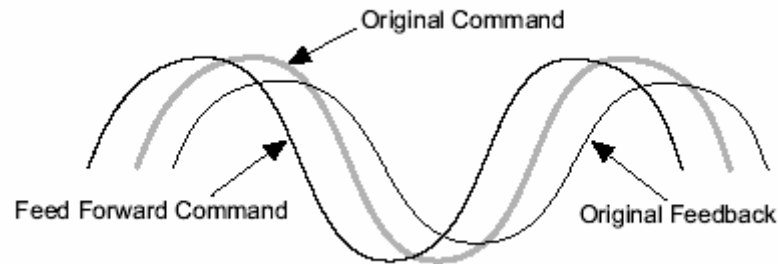


Figure 9.5 Effects of Feed Forward Gain on Sensor Feedback [21].

### 9.3.5. TUNING PROGRAM

The purpose of a tuning program is to produce a command that reflects the most demanding system response expected from a test. Square and ramp waveforms are preferred for initial tuning due to the fact that these waveforms have abrupt changes and excite the system at frequencies likely to be unstable with excessive gain. Final tuning can be done with the actual program for the test. MTS uses for a typical tuning program a low-amplitude (5% to 10% command), low-frequency (1 Hz to 2 Hz) square waveform [21].

For the purpose of obtaining the gain settings we utilize the square waveform and the sinusoidal waveform.

### 9.4. SQUARE WAVE

Shake table rate of response and stability can be investigated using square wave input [3]. The sensitivity settings for optimum table response can be found with this input motion. Figure 9.6 shows the effects of sensitivity on a square waveform.

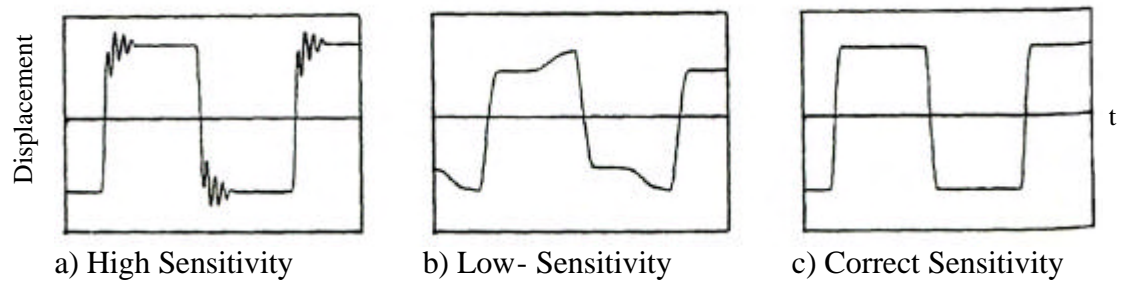


Figure 9.6 Effects of Sensitivity on a Square Waveform [3].

As seen from Figure 9.6, too much sensitivity can cause the system to become unstable as shown by the oscillations. On the other hand, too low sensitivity will cause a lack of ability to track the command signal. This characteristic should be investigated for various amplitudes and frequencies [3].

We used a single frequency and single amplitude for our tests to find the gain settings. For our tuning program, MTS technician Brad Schroenghamer recommended to use a square waveform of 0.1 Hz and amplitude of 5% of full range, which is  $\pm 0.3175$  cm ( $\pm 0.125$  in). For tracking the waveform we used the scope that comes with TestStarAP controller software. Figure 9.7 shows P-gain ( $K_p$ ) tuning for our system.

It can be seen that as we increase the  $K_p$  the feedback signal (blue curve) tracks the command signal (red curve) more closely. Utilizing MTS criteria for  $K_p$  tuning, we can see some oscillation with  $K_p = 2.5$ , marked with the two circles. Figure 9.8 shows a close-up of the oscillations at  $K_p = 2.5$ . Therefore, the correct  $K_p$  is a number between 2.0 and 2.5. Figure 9.9 shows the  $K_p$  between 2.0 and 2.5. Figure 9.9 illustrates that the value of  $K_p$  before oscillation is  $K_p = 2.4$ .

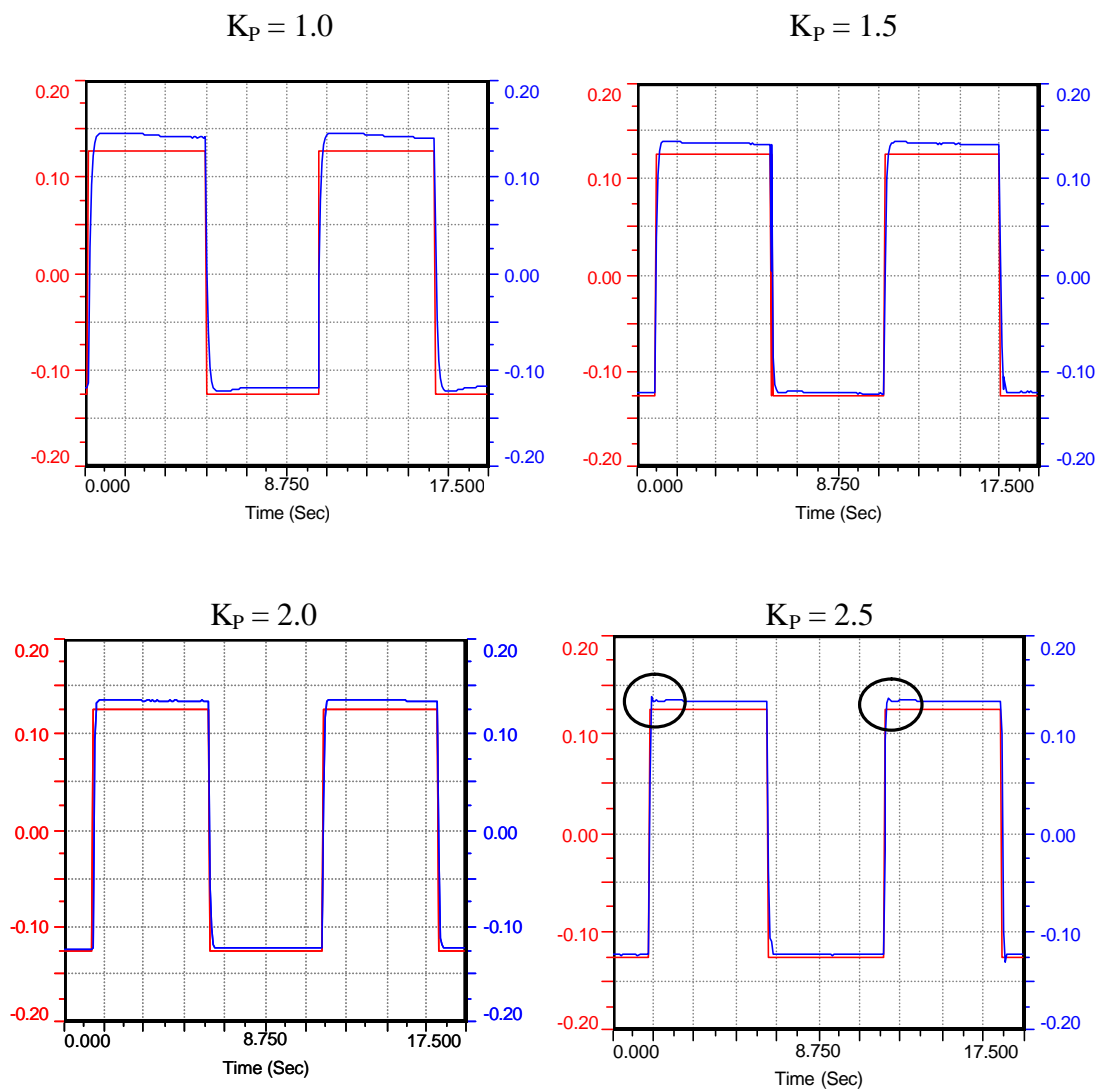
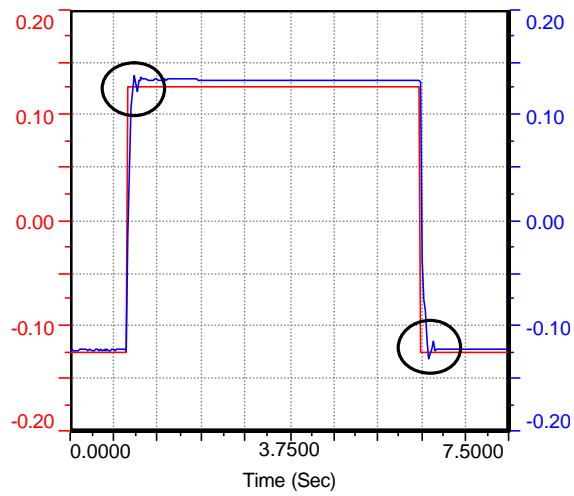
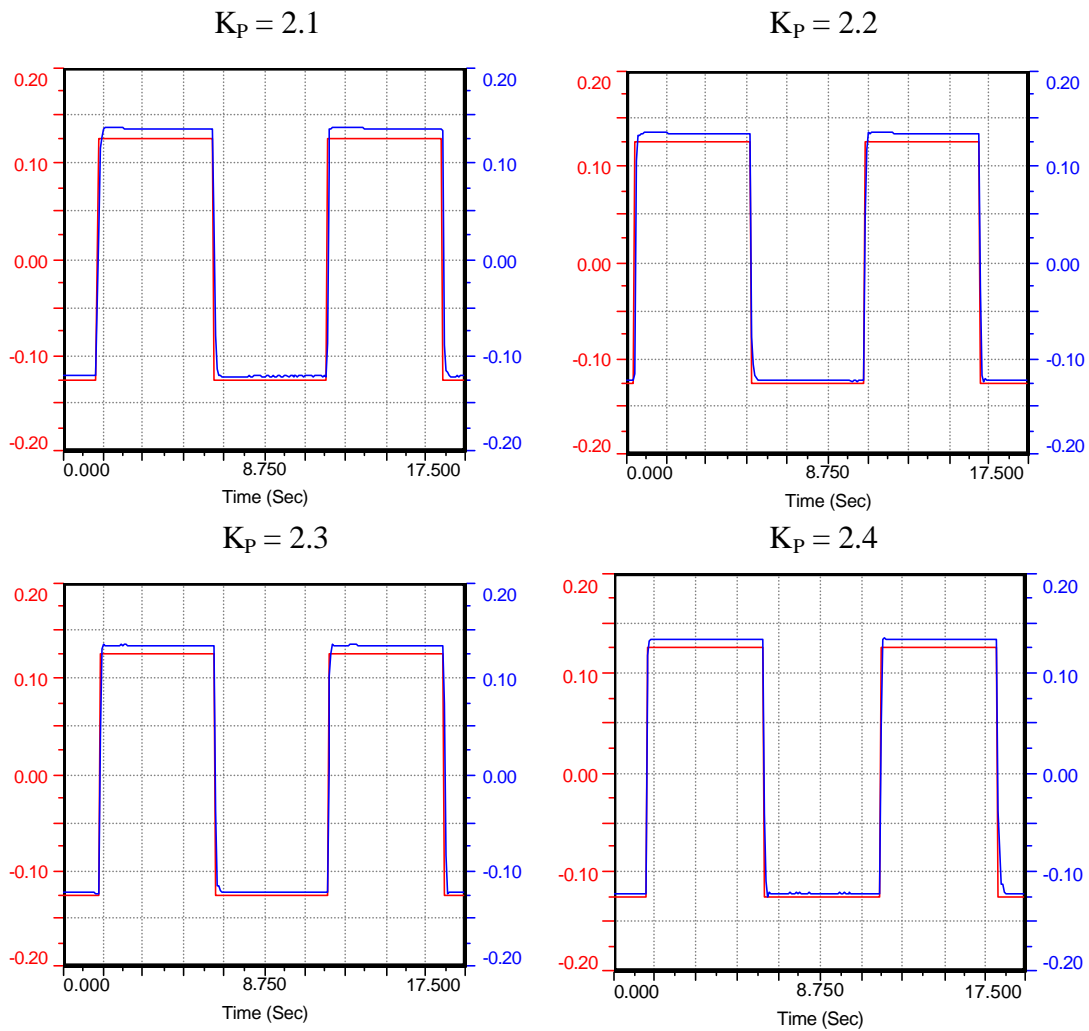


Figure 9.7 P-Gain ( $K_p$ ) Tuning for a Square Wave.

Figure 9.10 shows the effect of the I-gain ( $K_I$ ) on the waveform with  $K_p = 2.4$ . It can be seen that the feedback signal tracks the command more closely, due to the effect of the  $K_I$  gain. We used  $K_I = 0.250$  for Figure 9.10 which is approximately 10% of the  $K_p = 2.4$  recommended by MTS. We conclude that for this tuning program the right control gain settings are  $K_p = 2.4$  and  $K_I = 0.250$ .

Figure 9.8 Close-Up of Oscillations at  $K_P = 2.5$ .Figure 9.9 Scope Graphics for  $K_P = 2.1$  to 2.4.

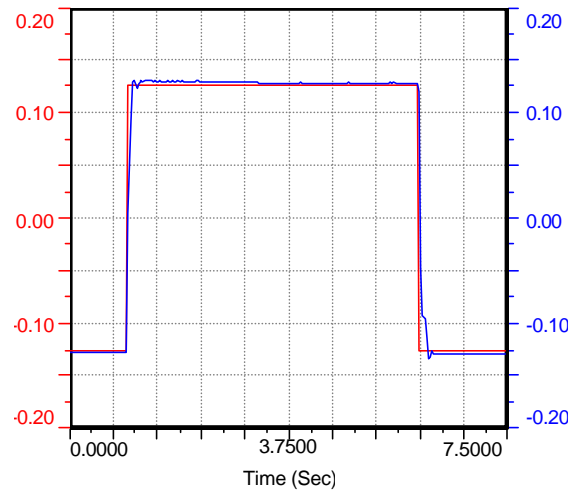


Figure 9.10 Effect of  $K_I$  on the Waveform.

## 9.5. SINUSOIDAL WAVE

### 9.5.1. COMPARISON OF INPUT/RESPONSE AMPLITUDE

An initial test would involve comparison of input amplitude to response amplitude at various frequencies of motion [3]. We used frequencies from 1.0 Hz to 18.0 Hz and single amplitude for our tests to find the gain settings. For our tuning program, MTS technician Brad Schroenghamer recommended to use the sine waveform of different frequencies and amplitude of 10% of full range, which is  $\pm 0.635$  cm ( $\pm 0.250$  in). For tracking the waveform we used the scope that comes with TestStarAP controller software. We also used a time meter that gave timed peak/valley feedback data to calculate error from command signal. Figure 9.11 shows the command error (peak) vs. P-gain ( $K_P$ ) tuning for 1.0 to 10.0 Hz. Figure 9.12 shows the command error (valley) vs. P-gain ( $K_P$ ) tuning for 1.0 to 10.0 Hz. From the Figures 9.11 and 9.12, it can be seen that from 1.0 to 6.0 Hz the error diminishes greatly as we increase the  $K_P$ . Also, we noticed

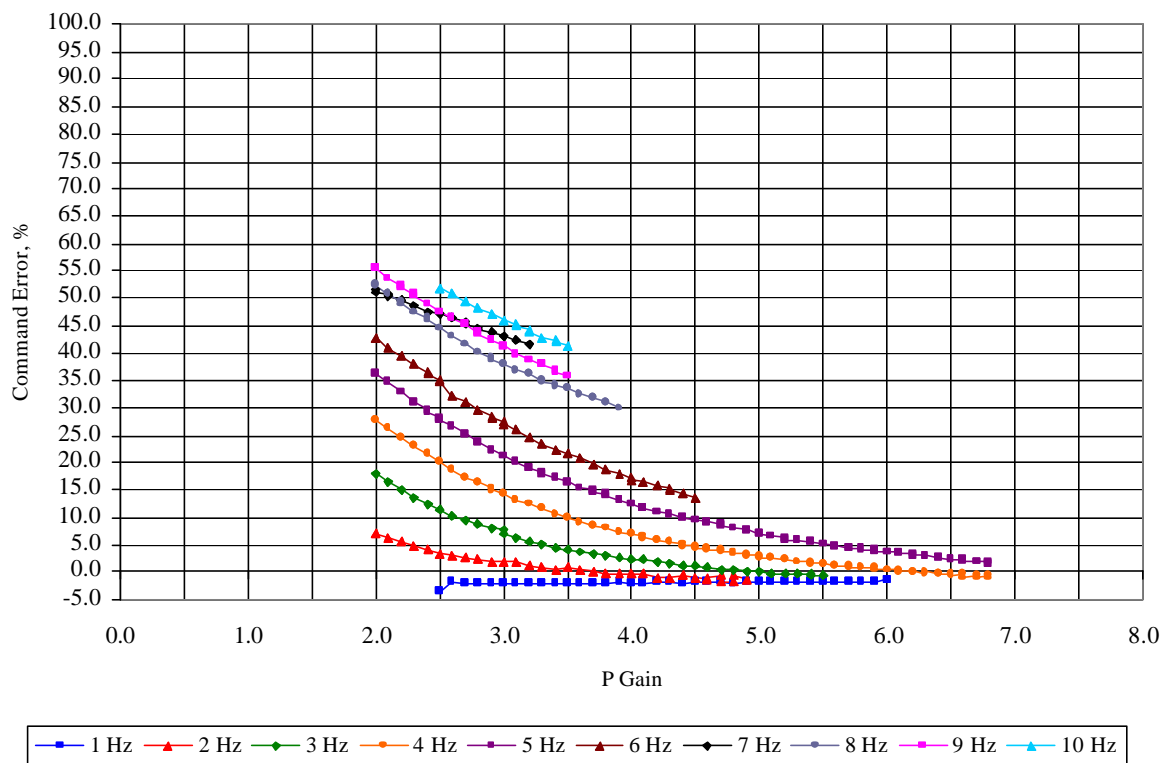


Figure 9.11 Command Error (peak) vs. P-gain ( $K_p$ ) Tuning for 1.0 to 10.0 Hz.

that as the frequency increases the  $K_p$  needed to decrease the error increases. From  $K_p = 4.5$  to 6.0 the peak error goes from 15% for 6.0 Hz to 5% for 5.0 Hz.

For the higher frequencies, from 7.0 to 10.0 Hz, the highest  $K_p$  goes from 3.5 to 3.9 and a peak error that goes from 50% to 40% for 10.0 Hz

From  $K_p = 4.5$  to 6.0 the valley error goes from 20% for 6.0 Hz to 10% for 6.0 Hz. For the higher frequencies, from 7.0 to 10.0 Hz, the highest  $K_p$  goes from 3.5 to 3.9 and a valley error that goes from 60% to 50% for 10.0 Hz. In these frequencies we did not go higher with the  $K_p$  because some kind instability was showing in the system. It is recommended that in future tests in these frequencies to go higher with the  $K_p$  until the system goes almost unstable.

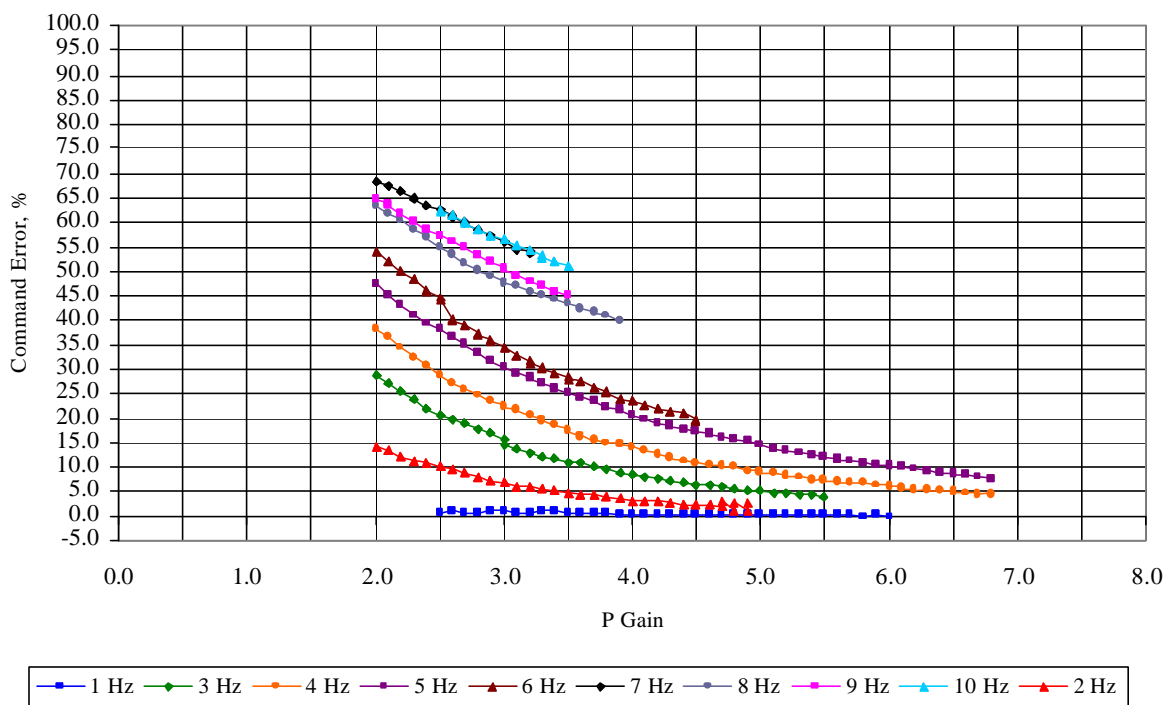


Figure 9.12 Command Error (valley) vs. P-gain ( $K_p$ ) Tuning for 1.0 to 10.0 Hz.

We also tested the system for higher frequencies. We tested from 11.0 Hz to 18.0 Hz, at single amplitude also of 10% of full range that is  $\pm 0.635$  cm ( $\pm 0.250$  in). For tracking the waveform we used the scope that comes with TestStarAP controller software, also. To calculate the error from the command signal, we used the data from each test saved by the Data Acquisition System Software, DasyLab. Figure 9.13 shows the command error (peak) vs. P-gain ( $K_p$ ) tuning for 11.0 to 18.0 Hz. Figure 9.14 shows the command error (valley) vs. P-gain ( $K_p$ ) tuning for 11.0 to 18.0 Hz. According to Figure 9.13 the peak command error increased as the frequency increased. Also, we noticed that the error decreased almost linearly with  $K_p$  and the error decreased more slowly than for the lower frequencies (1 to 10 Hz). In addition, we noticed that some frequencies are grouped together. The lowest peak command error is 40% for 11.0 Hz at  $K_p = 4.0$ . The highest peak command error is 85% for 16, 17 and 18 Hz at  $K_p = 2.0$ .

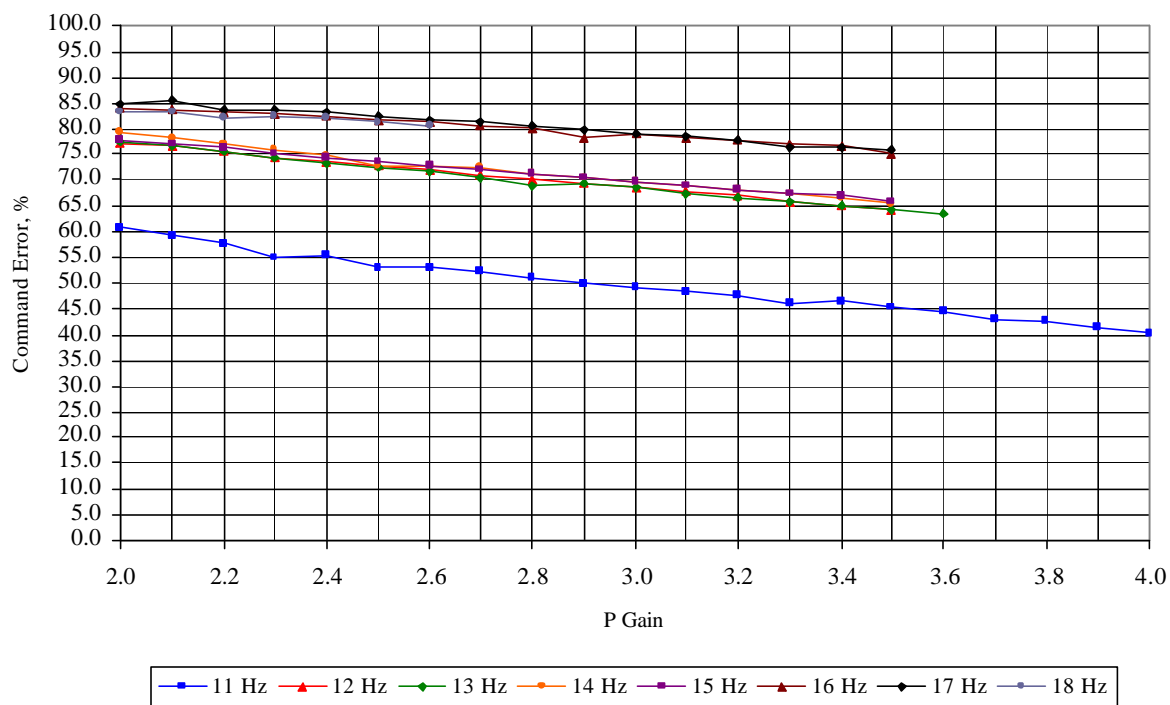


Figure 9.13 Command Error (peak) vs. P-gain ( $K_p$ ) Tuning for 11.0 to 18.0 Hz.

From Figure 9.14 the valley command error also increased as the frequency increased. Also we noticed that the error decreased almost linearly with  $K_p$  and the error decreased more slowly than for the lower frequencies (1 to 10 Hz). Moreover, we noticed that some frequencies are grouped together. The lowest peak command error is 50% for 11.0 Hz at  $K_p = 4.0$ . The highest peak command error is 93% for 16, 17 and 18 Hz at  $K_p = 2.0$ . The valley command error is greater than the peak command error. We recommend that these tests are run for higher  $K_p$  than we did. We only did the tests until some instability was showing on the system.

For tracking the waveform we used the scope that comes with TestStarAP controller software. Using the scope we can see how  $K_p$  changed the waveform. We only are going to show the graphs for the following frequencies: 1 Hz, 5Hz, 10Hz, 15 Hz and 18 Hz.

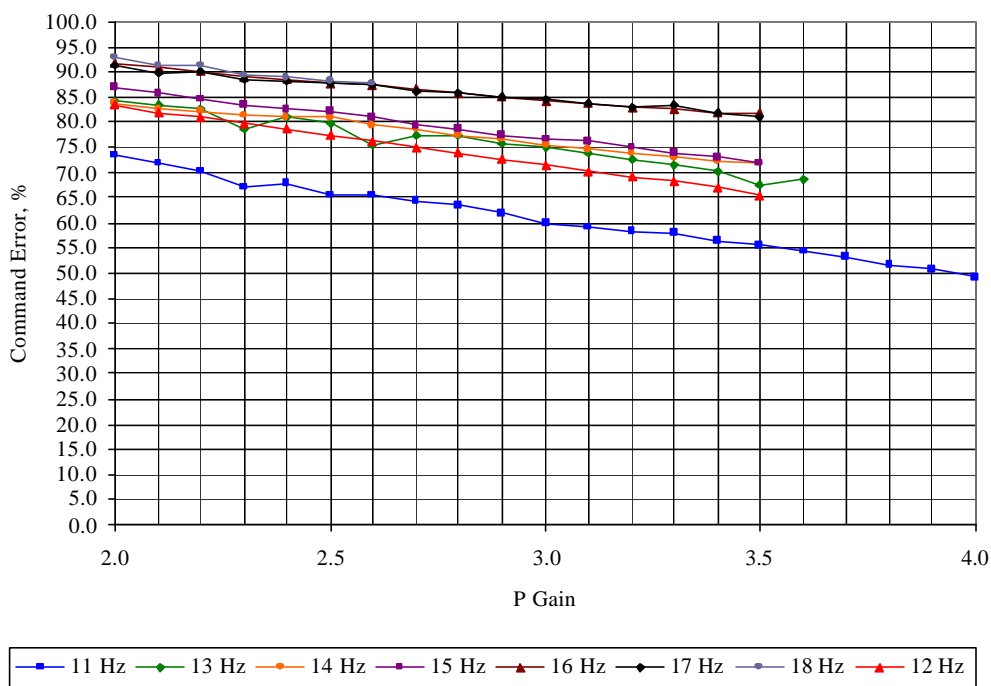
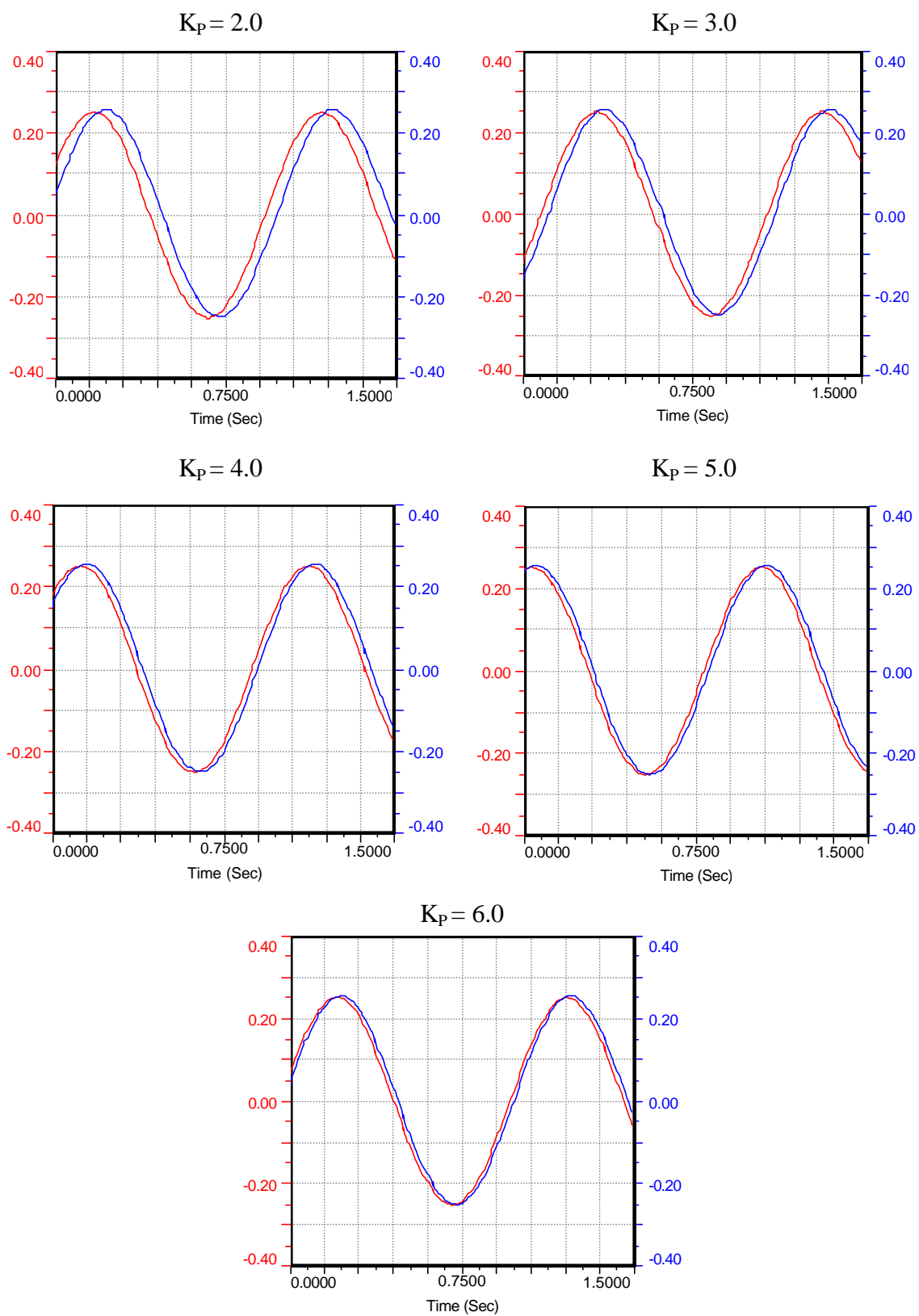
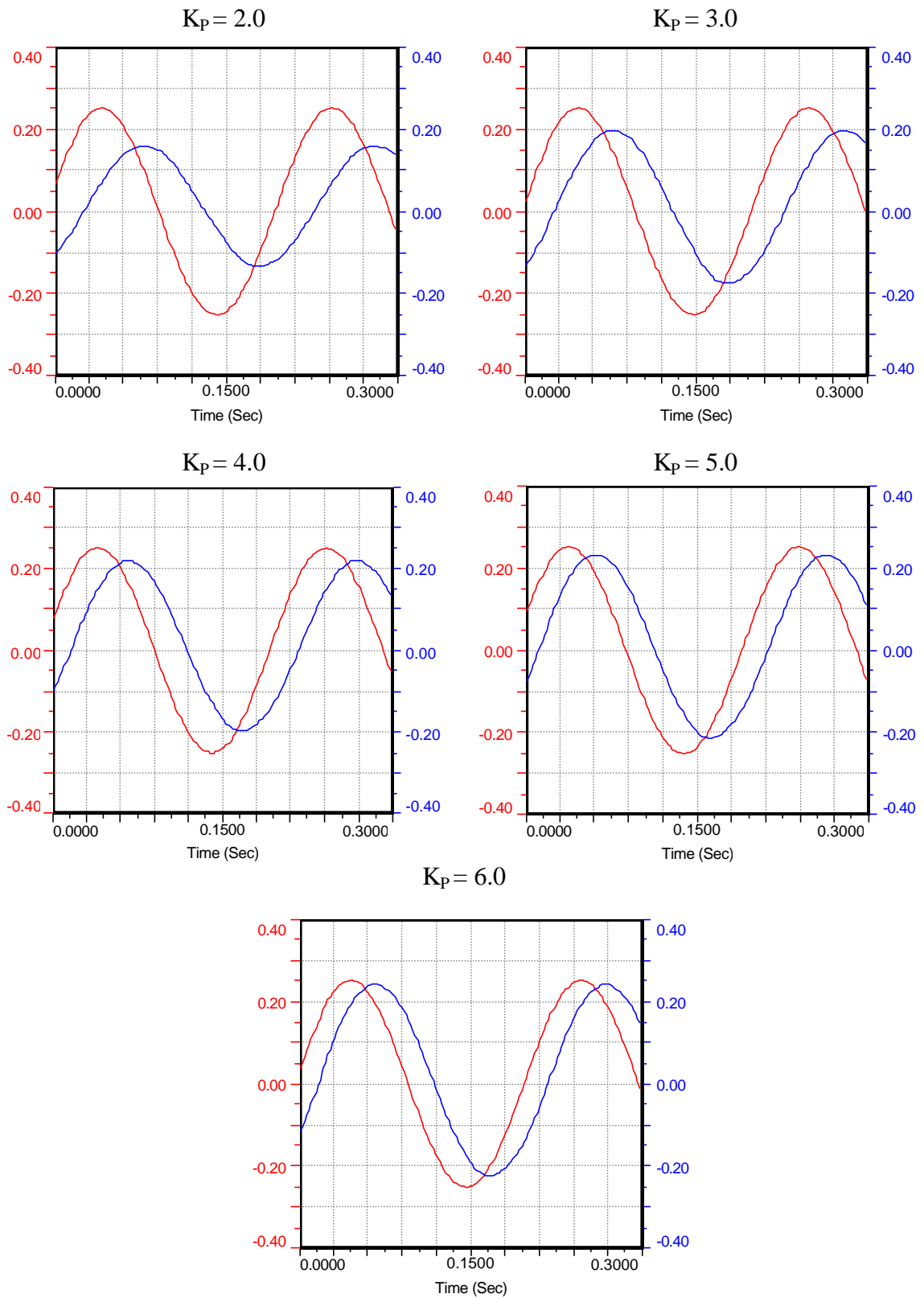


Figure 9.14 Command Error (valley) vs. P-gain ( $K_P$ ) Tuning for 11.0 to 18.0 Hz.

Figure 9.15 shows the effect of  $K_P$  on the 1.0 Hz sinusoidal waveform. Figure 9.16 shows the effect of  $K_P$  on the 5.0 Hz sinusoidal waveform. Figure 9.17 shows the effect of  $K_P$  on the 10.0 Hz sinusoidal waveform. Figure 9.18 shows the effect of  $K_P$  on the 15.0 Hz sinusoidal waveform. Figure 9.19 shows the effect of  $K_P$  on the 18.0 Hz sinusoidal waveform. It can be seen that as we increase the  $K_P$  the feedback signal (blue curve) tracks the command signal (red curve) more closely. Figure 9.15 illustrates that the value of  $K_P$  that best tracks the command signal for 1.0 Hz is  $K_P = 6.0$ . At the same value of  $K_P = 6.0$  at 5.0 Hz, the feedback signal tracks the amplitudes of the waveform more closely but the  $K_P$  does not correct the phase lag showing on Figure 9.16. Figures 9.17, 9.18 and 9.19 show that the values of  $K_P = 2.0$  to 3.0 for these frequencies do not correct the command error nor the phase lag. Further tests are needed to find the right values.

Figure 9.15 Effect of  $K_P$  on 1.0 Hz Sinusoidal Waveform.

Figure 9.16 Effect of  $K_P$  on 5.0 Hz Sinusoidal Waveform.

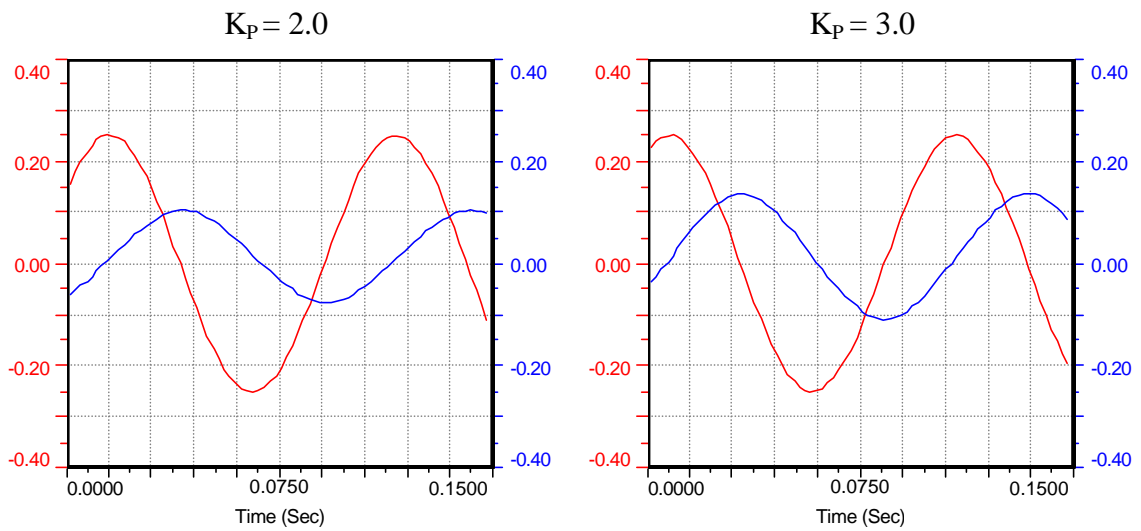


Figure 9.17 Effect of  $K_P$  on 10.0 Hz Sinusoidal Waveform.

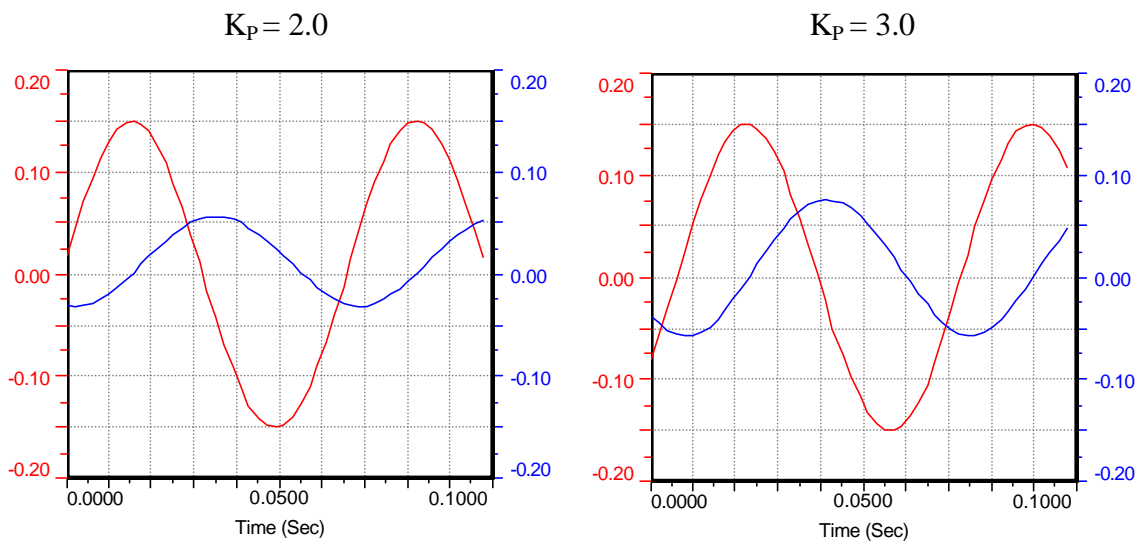


Figure 9.18 Effect of  $K_P$  on 15.0 Hz Sinusoidal Waveform.

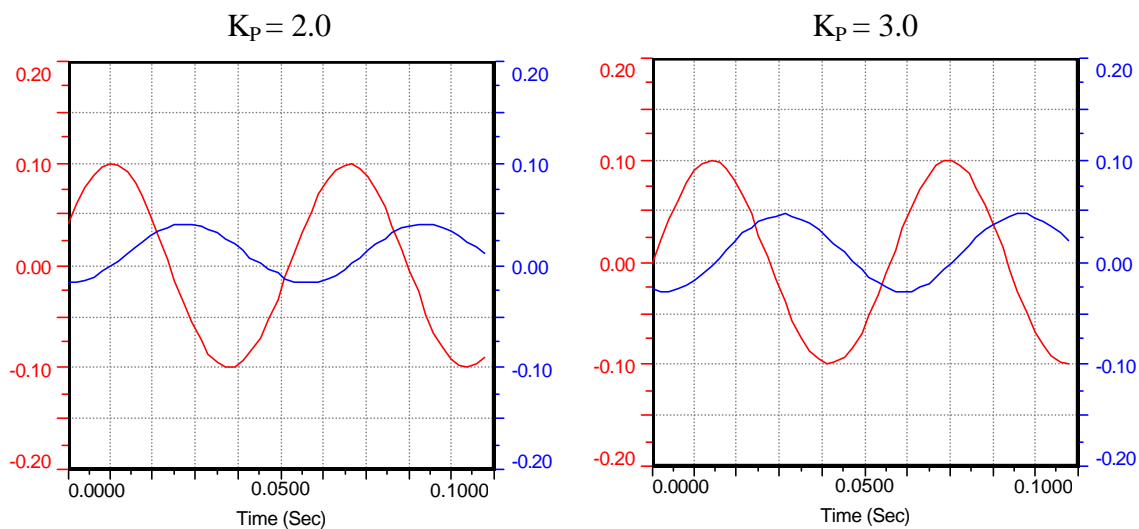


Figure 9.19 Effect of  $K_P$  on 18.0 Hz Sinusoidal Waveform.

### 9.5.2. CHECKING FOR ROTATIONAL MODES OF VIBRATION

From this test series shake table resonances could be found, such as for rocking or rotational mode of vibration, by finding appropriate locations and orientations of measuring devices, such as accelerometers [3]. Figure 9.20 illustrates this concept.

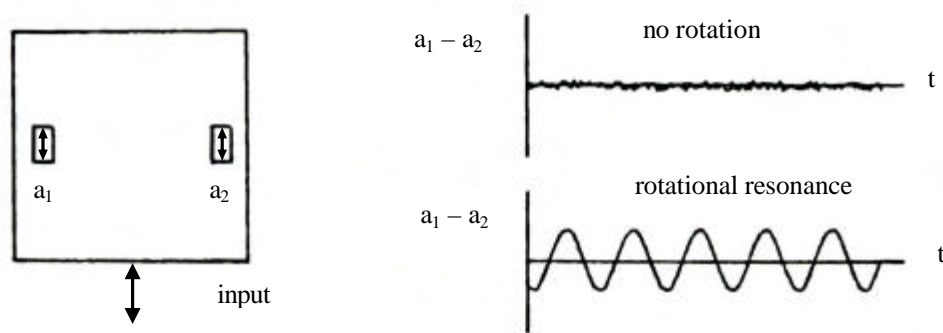


Figure 9.20 Shake Table Rotational Modes [3].

For our system we used accelerometers as our measuring device and positioned them in different locations, as illustrated in Figure 9.21.

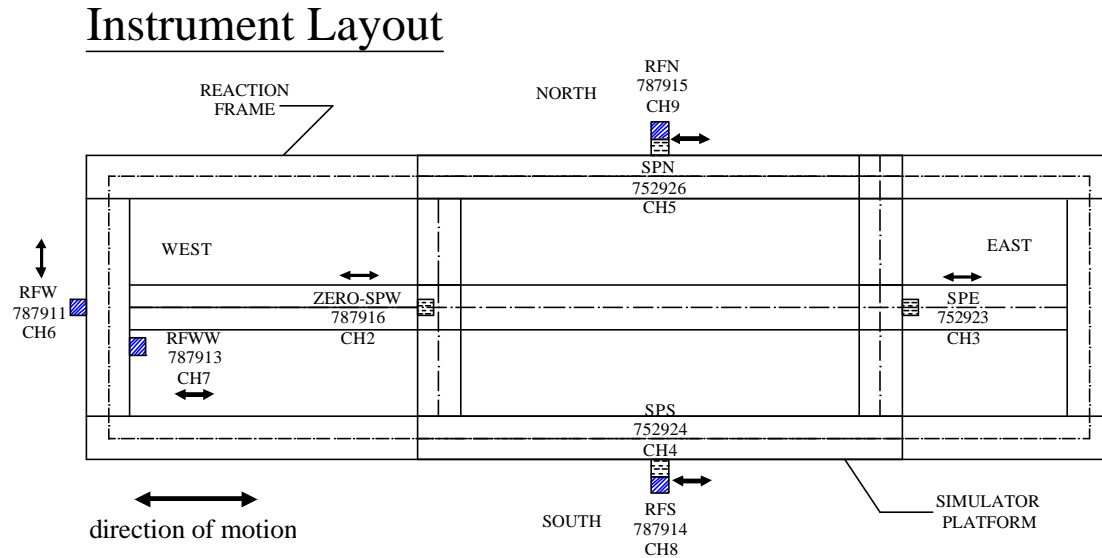
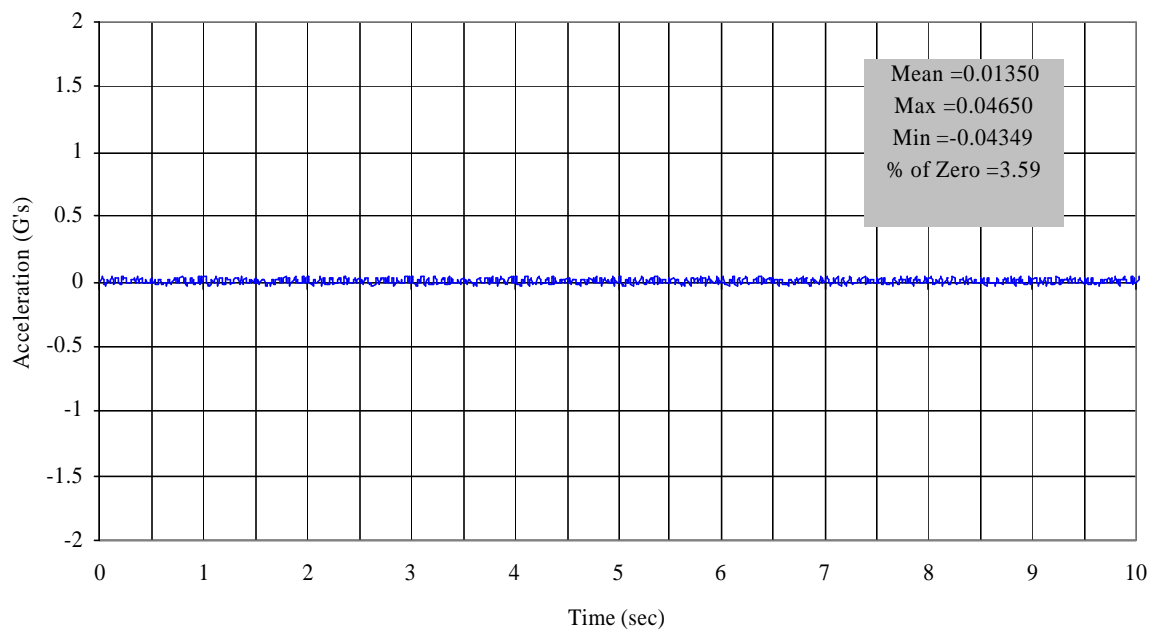


Figure 9.21 Accelerometers Layout.

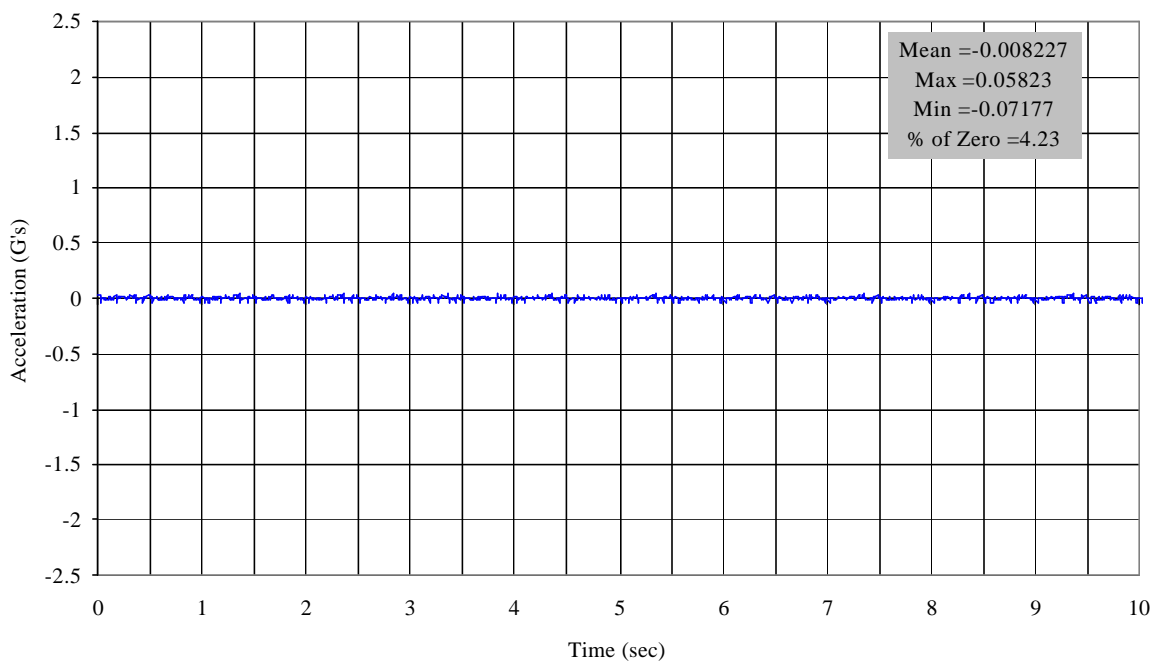
Mills [3] specifies that these modes should be located and identified for future consideration of possible contribution to the response of specific models.

In our case, for the frequencies from 11.0 Hz to 18.0 Hz, we checked (RFN – RFS) for the reaction frame and (SPN – SPS) for the simulator platform. We only are going to show the graphics for the following frequencies: 11.0 Hz, 15.0 Hz, and 17.0 Hz. For the frequency of 11.0 Hz we are going to show how the curves change with changing  $K_p$ . For frequencies 15.0 Hz and 17.0 Hz we are going to show the curves for  $K_p = 3.5$ , because it is the  $K_p$  where the system shows more response.

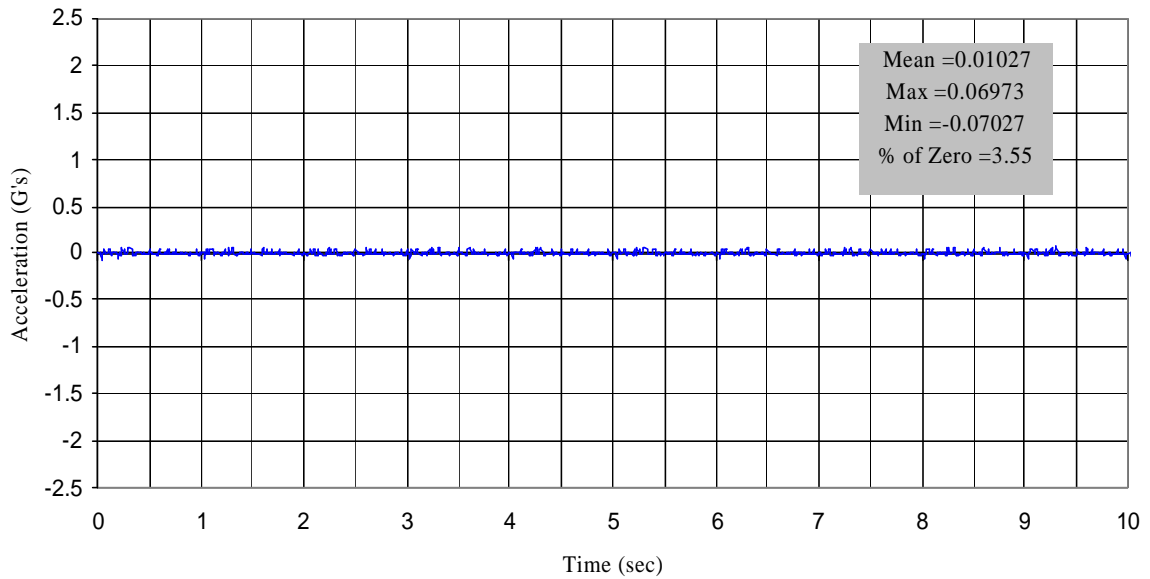
Figure 9.22 shows that there is no rotation on the reaction frame. It also shows that there is no significant change on the % of Zero-SPW Acceleration with changing  $K_p$ . This percent was taken as the ratio of maximum amplitude of RFN-RFS acceleration to



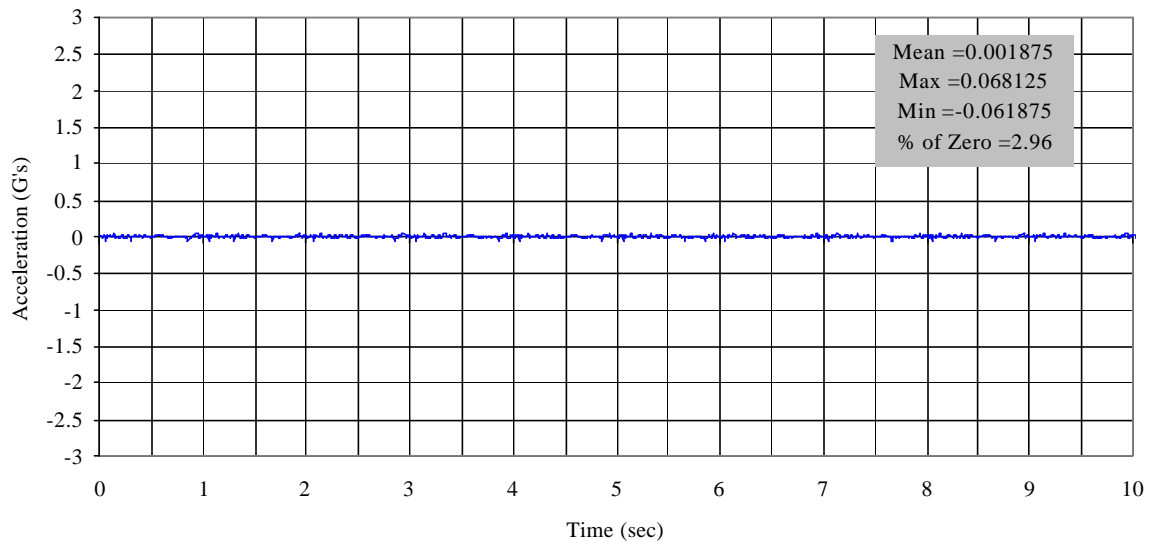
(a) RFN-RFS for 11.0 Hz Sine Wave -  $K_p = 2.0$ .



(b) RFN-RFS for 11.0 Hz Sine Wave -  $K_p = 2.5$ .



(c) RFN-RFS for 11.0 Hz Sine Wave -  $K_p = 3.0$ .



(d) RFN-RFS for 11.0 Hz Sine Wave -  $K_p = 3.5$ .

Figure 9.22 Effect of  $K_p$  on RFN-RFS for 11.0 Hz.

the maximum amplitude of the Zero-SPW acceleration. This percent went from 2.96 to 4.23.

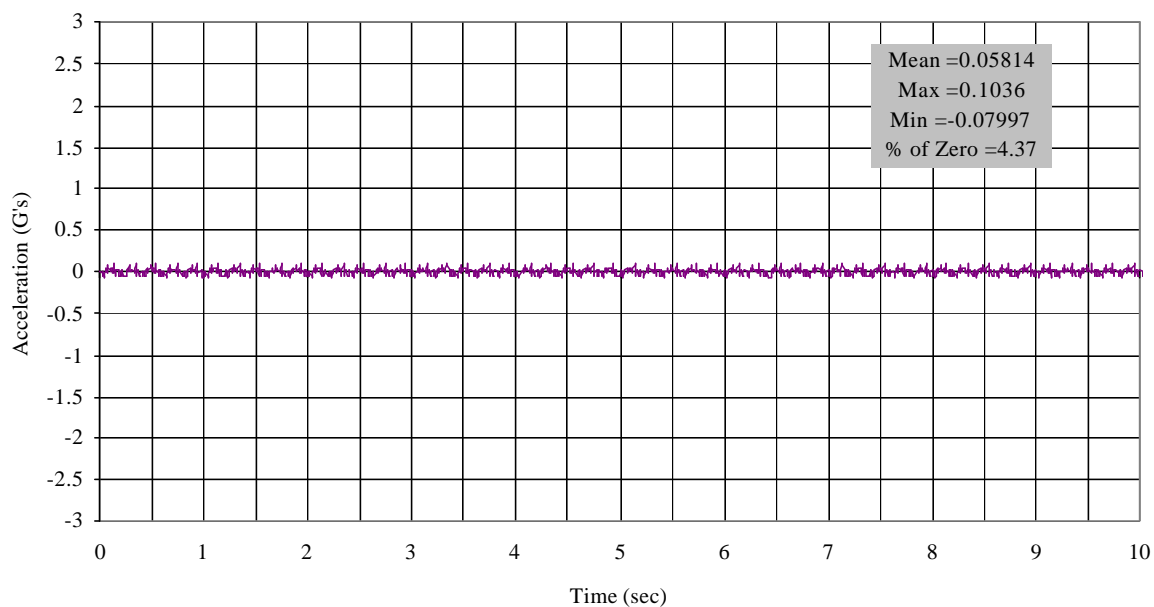


Figure 9.23 RFN-RFS for 15.0 Hz Sine Wave -  $K_p = 3.5$ .

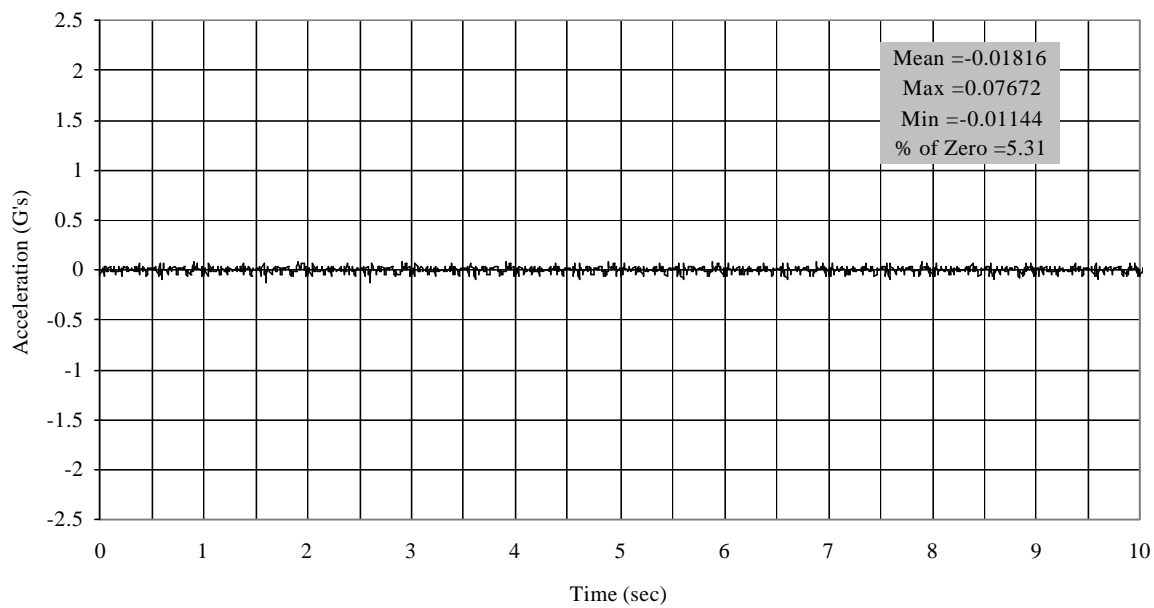


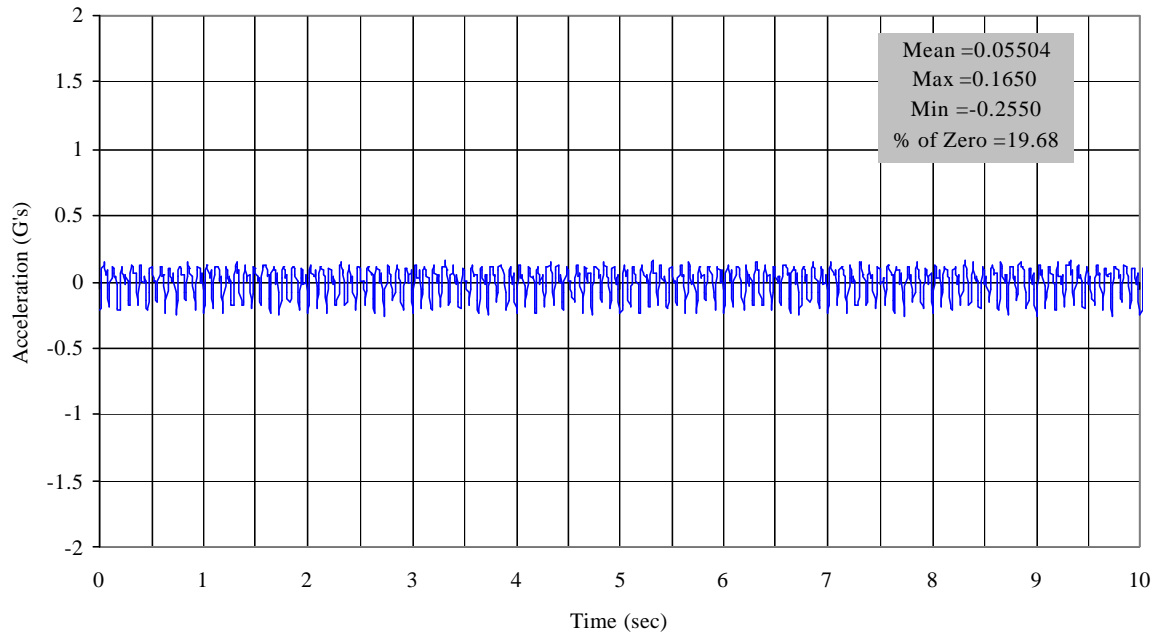
Figure 9.24 RFN-RFS for 17.0 Hz Sine Wave -  $K_p = 3.5$ .

Figures 9.23 and 9.24 show RFN-RFS for 15.0 Hz and 17.0 Hz, respectively. These figures show there is no rotation of the reaction frame at these frequencies, also. The % of Zero amplitude went from 4.37 to 5.31. At this point, we conclude there is no rotation of the reaction frame.

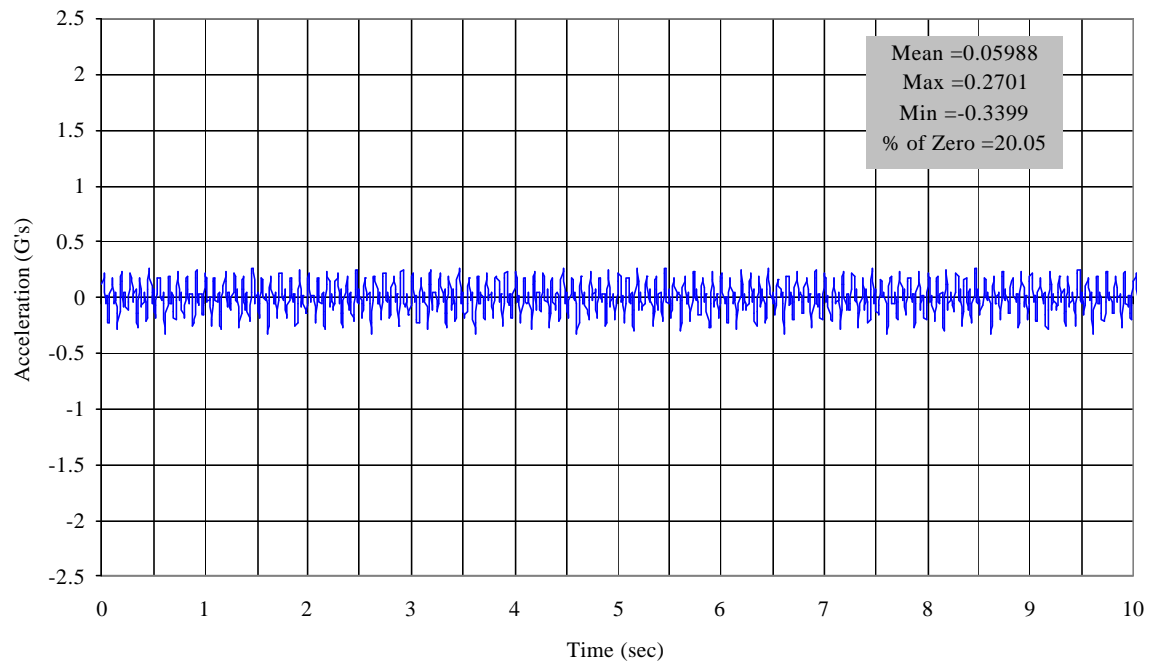
Figure 9.25 shows the effect of  $K_p$  on SPN –SPS for 11.0 Hz. This figure illustrates there is some rotation on the simulator platform. It also illustrates there is no significant change of % of Zero amplitude with changing  $K_p$  until  $K_p = 3.5$ . This percent went from approximately 20% for  $K_p = 2.0, 2.5$  and  $3.0$  to almost 15% for  $K_p = 3.5$ .

Figures 9.26 and 9.27 show SPN-SPS for 15.0 Hz and 17.0 Hz, respectively. These figures show there is rotation of the simulator platform at these frequencies, also. The % of Zero amplitude went from almost 14% to 20% for 15.0 Hz and 17.0 Hz, respectively. At this point, we conclude there is some rotation on the simulator platform.

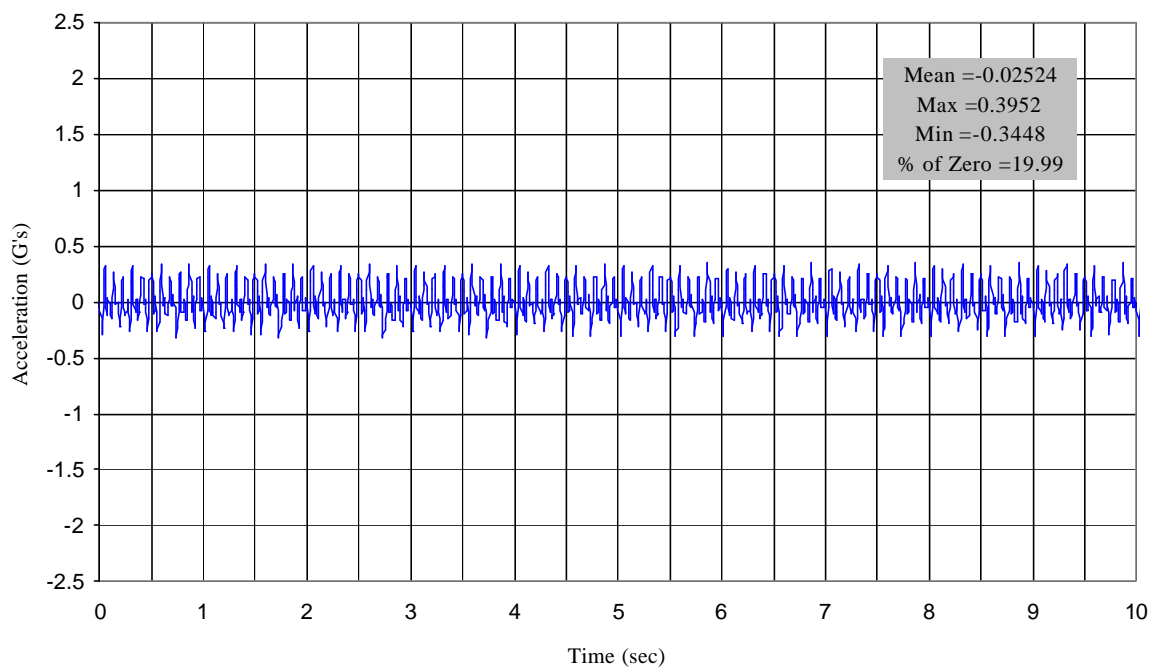
To quantify if this rotation is small or large other measures of behavior have to be considered. Let's consider looking at the curves of the three accelerometers: Zero-SPW, SPN and SPS for the frequencies being studied. Figure 9.28, 9.29 and 9.30 show the curves of the acceleration of the three accelerometers for 11.0 Hz, 15.0 Hz and 17.0 Hz, respectively. The  $K_p$  for these curves is 3.5. Looking at the curves it can be seen that the rotation is small and is revealed at the differences in acceleration amplitudes of the three accelerometers. In addition, the rotation shown in one accelerometer, SPS, is larger than the rotation shown in the other accelerometer, SPN. It can be seen from the figures, also, that the acceleration peak and valleys of Zero-SPW and SPN are almost the same. Only SPS shows a significant difference in magnitude of the peaks and valleys compared to Zero-SPW.



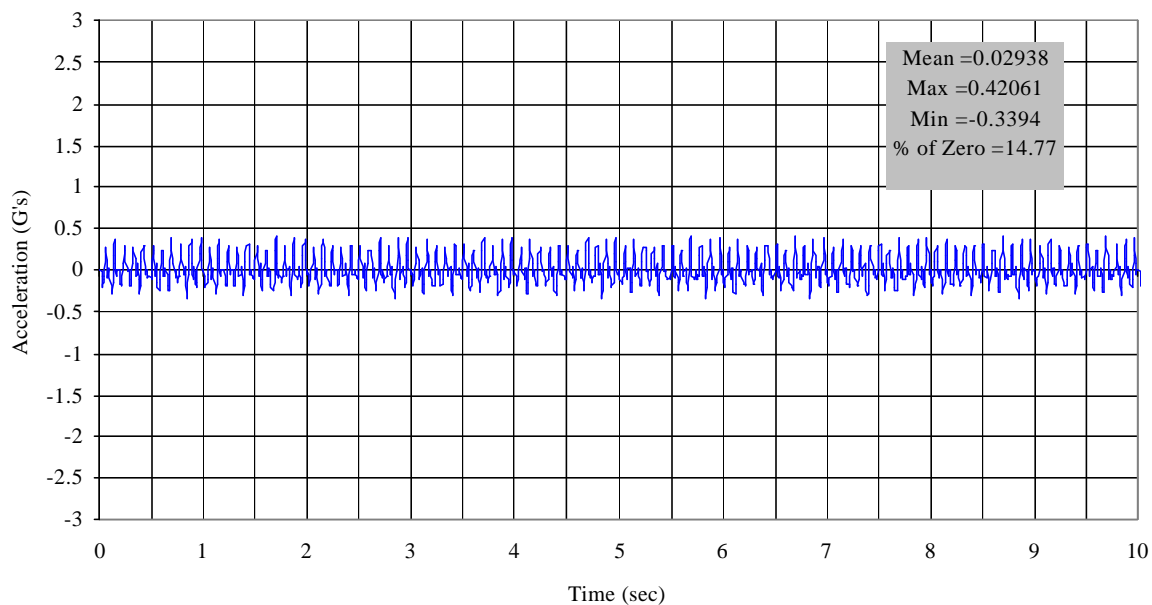
(a) SPN-SPS for 11.0 Hz Sine Wave -  $K_p = 2.0$ .



(b) SPN-SPS for 11.0 Hz Sine Wave -  $K_p = 2.5$ .



(c) SPN-SPS for 11.0 Hz Sine Wave -  $K_p = 3.0$ .



(d) SPN-SPS for 11.0 Hz Sine Wave -  $K_p = 3.5$ .

Figure 9.25 Effect of  $K_p$  on SPN-SPS for 11.0 Hz.

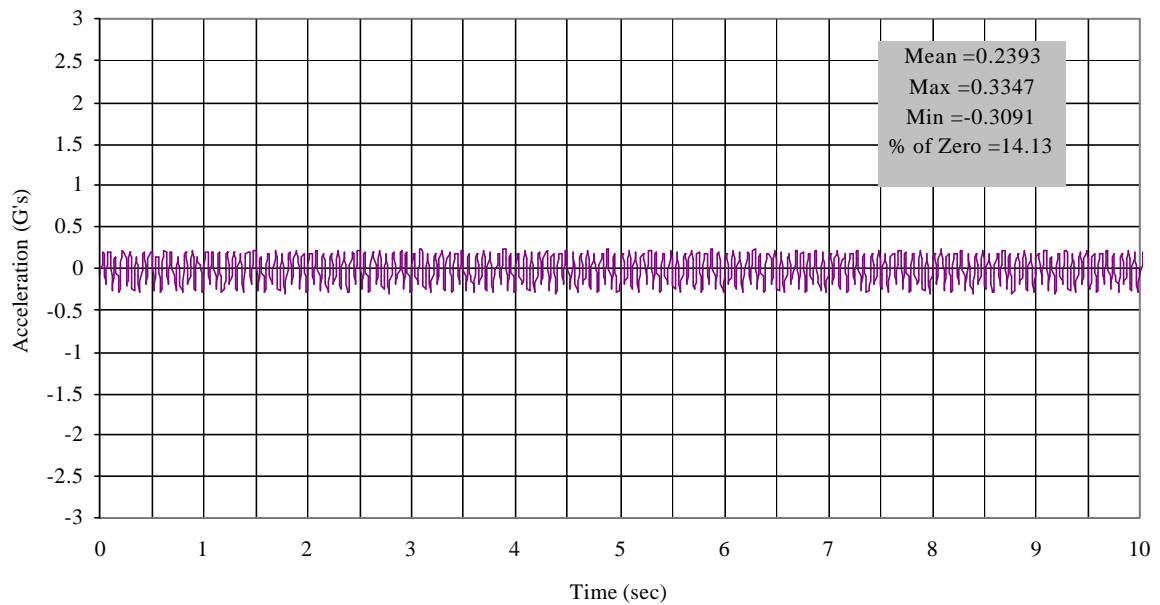


Figure 9.26 SPN-SPS for 15.0 Hz Sine Wave -  $K_p = 3.5$ .

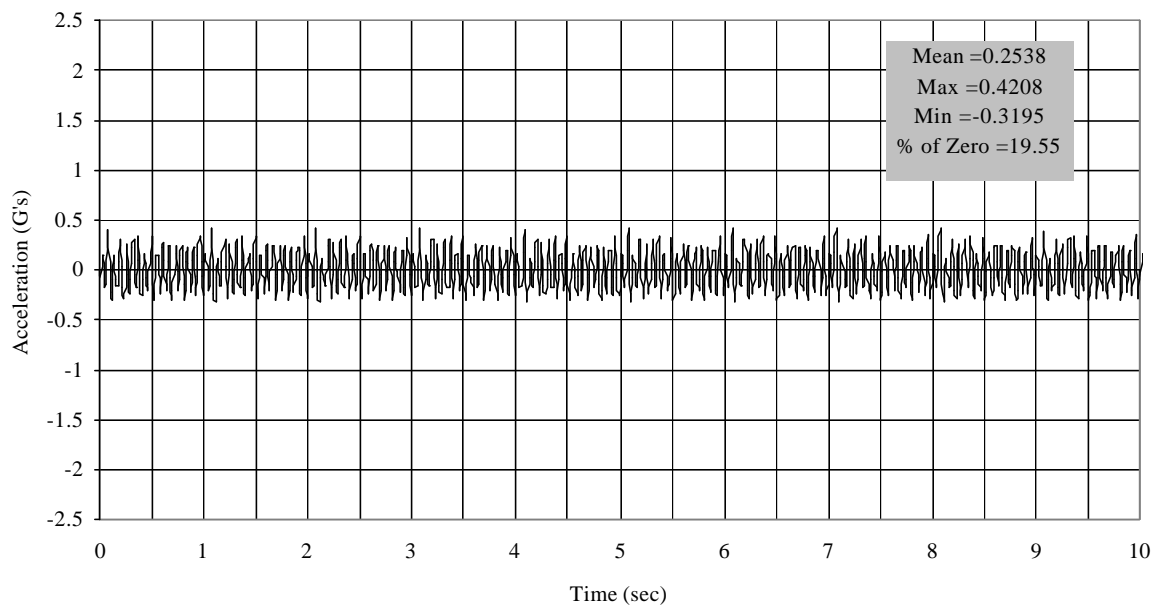


Figure 9.27 SPN-SPS for 17.0 Hz Sine Wave -  $K_p = 3.5$ .

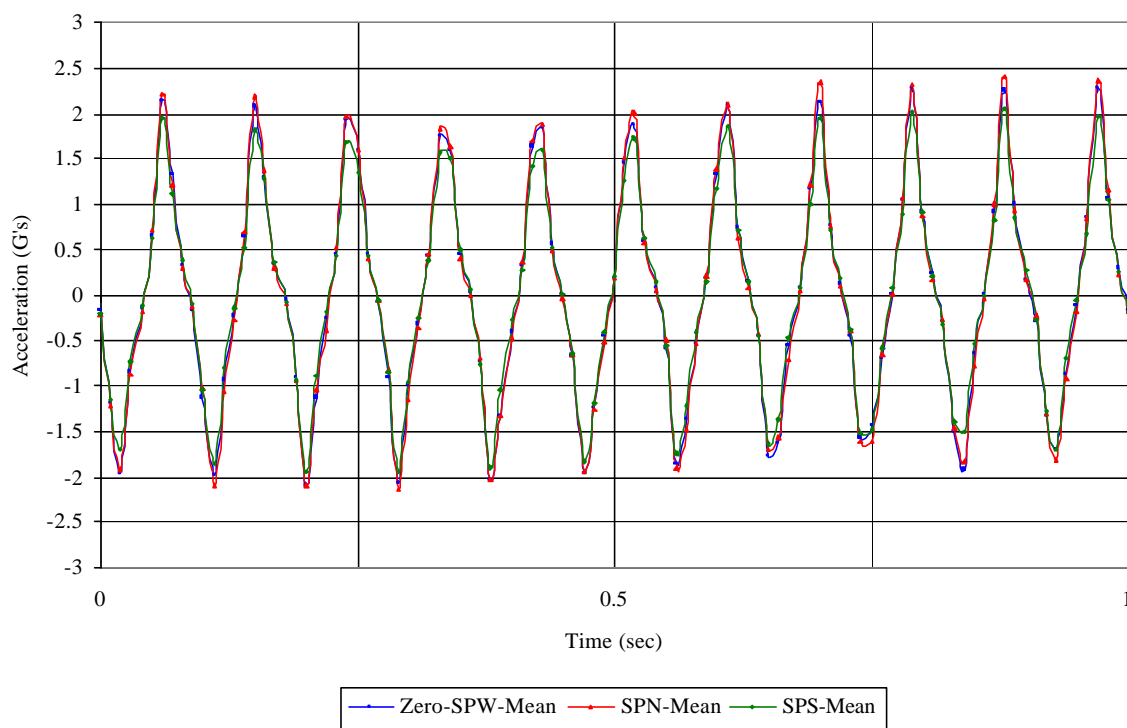
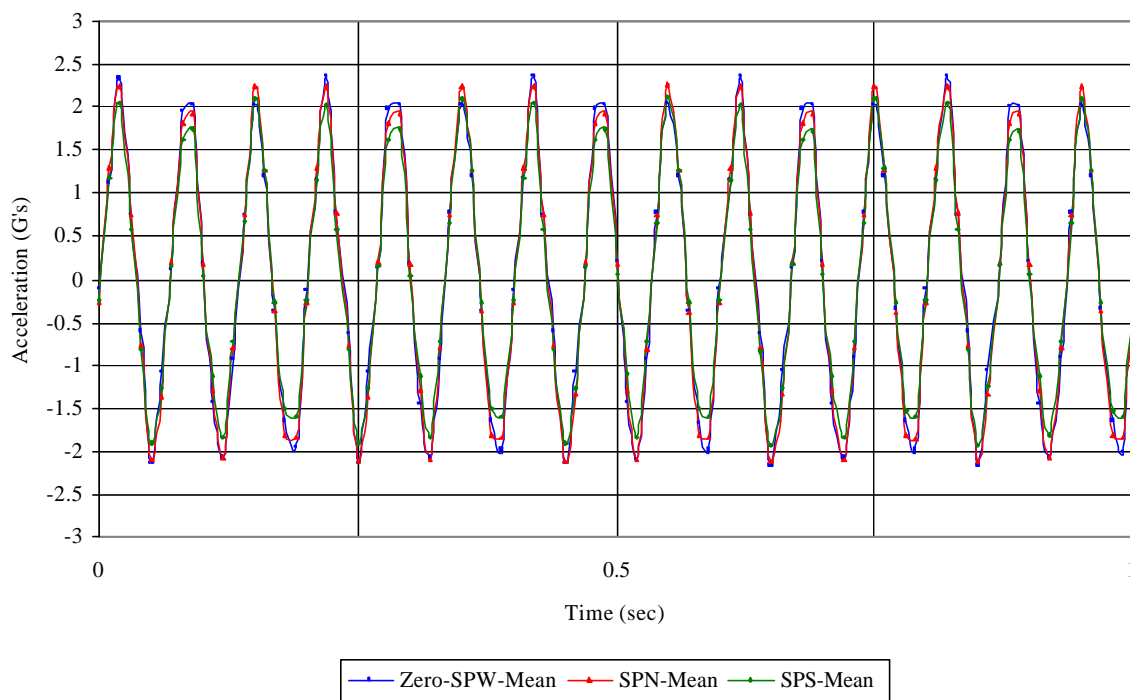


Figure 9.28 Close-Up of 11.0 Hz Sine Wave Acceleration for SPN, SPS and Zero-SPW.



.Figure 9.29 Close-Up of 15.0 Hz Sine Wave Acceleration for SPN, SPS and Zero-SPW.

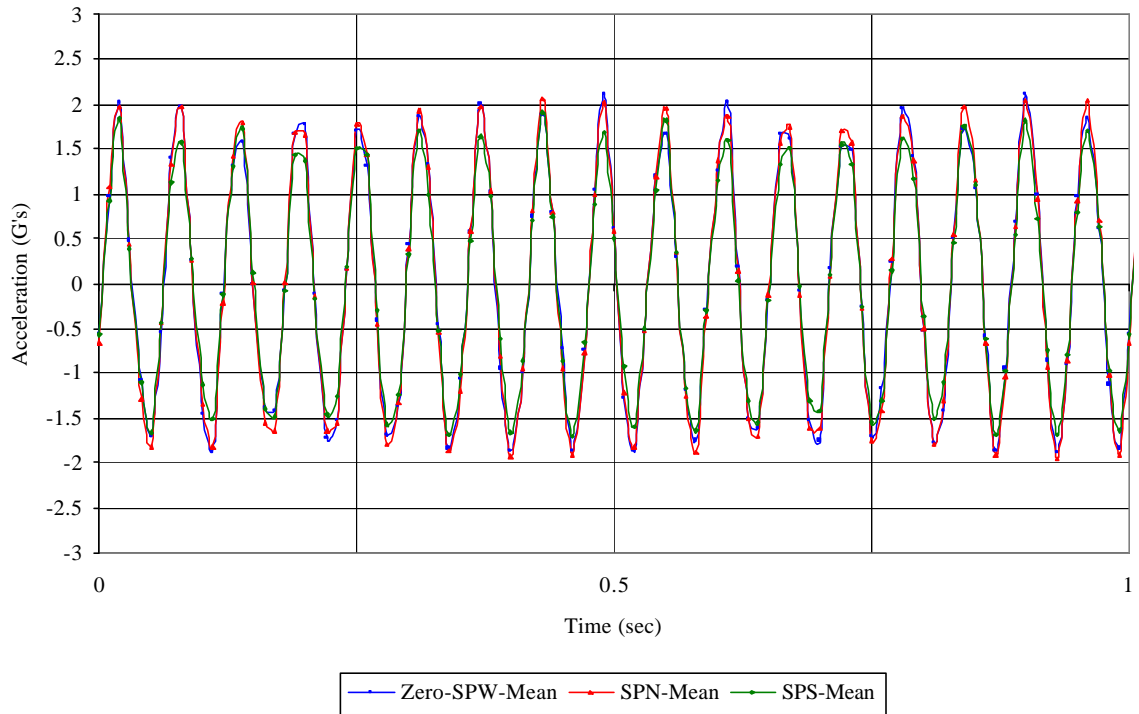


Figure 9.30 Close-Up of 17.0 Hz Sine Wave Acceleration for SPN, SPS and Zero-SPW.

This difference in rotation between the accelerometers may be due to the following factors: mass eccentricity of the platform, a small eccentricity of the actuator applying the displacement or a small misalignment of the linear roller bearings.

The acceleration of SPN is larger than the acceleration of SPS. This behavior is in agreement with the equations of acceleration for a rigid mass that have both translation and rotation, as shown in Figure 9.31. The equations for displacement for point 1 and point 2 are:

$$d_1 = u - \frac{a}{2} * \mathbf{q} \quad (9.1)$$

$$d_2 = u + \frac{a}{2} * \mathbf{q} \quad (9.2)$$

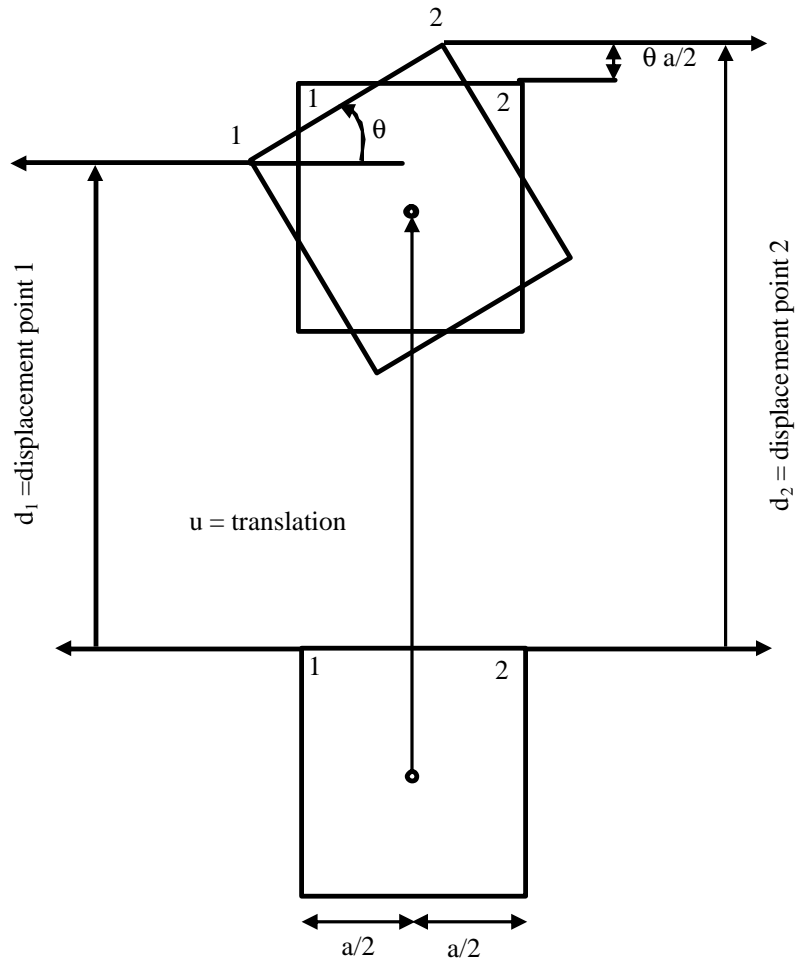


Figure 9.31 Rigid Mass with Translation and Rotation.

Therefore the equations for acceleration for points 1 and 2 are the following:

$$a_1 = \ddot{u} - \frac{a}{2} * \ddot{\mathbf{q}} \quad (9.3)$$

$$a_2 = \ddot{u} + \frac{a}{2} * \ddot{\mathbf{q}} \quad (9.4)$$

Looking at the equations, SPS is similar to  $a_1$  and SPN is similar to  $a_2$ . To obtain the angular acceleration we simply subtract the translational acceleration (Zero-SPW) from

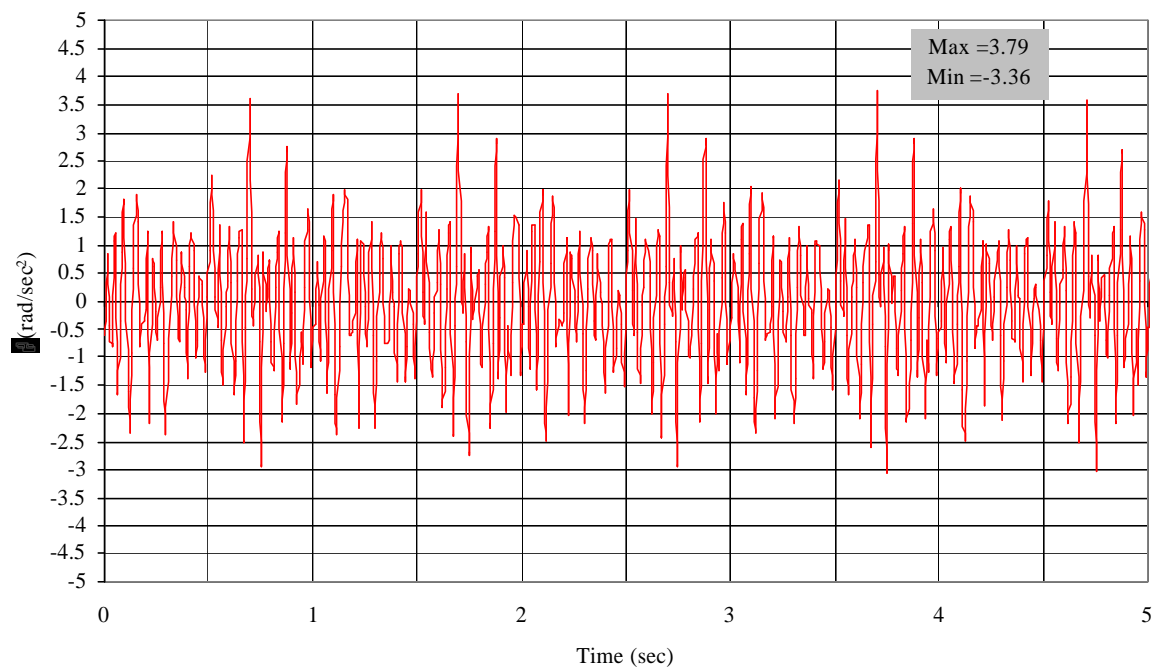
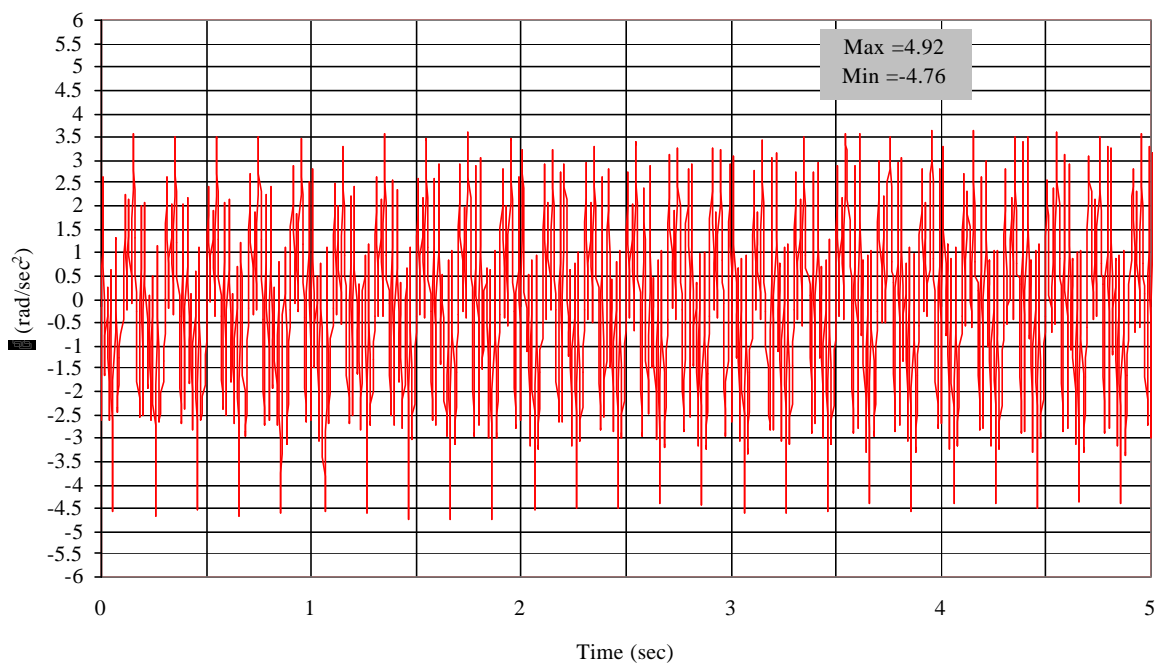
$a_1$  (SPS) and  $a_2$  (SPN) and divide by  $2/a$ . After following the procedure mentioned above we obtain the following equations:

$$(a_2 - \ddot{u}) * \frac{2}{a} = \ddot{q} \quad (9.5)$$

$$(a_1 - \ddot{u}) * -\frac{2}{a} = \ddot{q} \quad (9.6)$$

Figures 9.32, 9.33 and 9.34 show the curves of angular acceleration using the accelerometer SPN for the following frequencies: 11.0 Hz, 15.0Hz and 17.0 Hz. These curves have a  $K_p = 3.5$ . The maximum values of each signal are 3.79, 4.92 to 5.058 rad/sec<sup>2</sup> for sine waves with frequencies 11.0 Hz, 15.0 Hz and 17.0 Hz, respectively. The minimum values of each curve are -3.36, -4.76 to -3.89 rad/sec<sup>2</sup> for 11.0 Hz, 15.0 Hz and 17.0 Hz, respectively.

Figures 9.35, 9.36 and 9.37 show the time variation of the angular acceleration using accelerometer SPS for the following frequencies: 11.0 Hz, 15.0Hz and 17.0 Hz. These curves have a  $K_p = 3.5$ . The maximum values of each curve are 4.86, 6.61 to 8.03 rad/sec<sup>2</sup> for 11.0 Hz, 15.0 Hz and 17.0 Hz, respectively. The minimum values are -6.91, -9.52 to -6.44 rad/sec<sup>2</sup> for 11.0 Hz, 15.0 Hz and 17.0 Hz, respectively.

Figure 9.32 (SPN-Zero)-11.0 Hz Sine Wave -  $K_p = 3.5$ .Figure 9.33 (SPN-Zero)-15.0 Hz Sine Wave -  $K_p = 3.5$ .

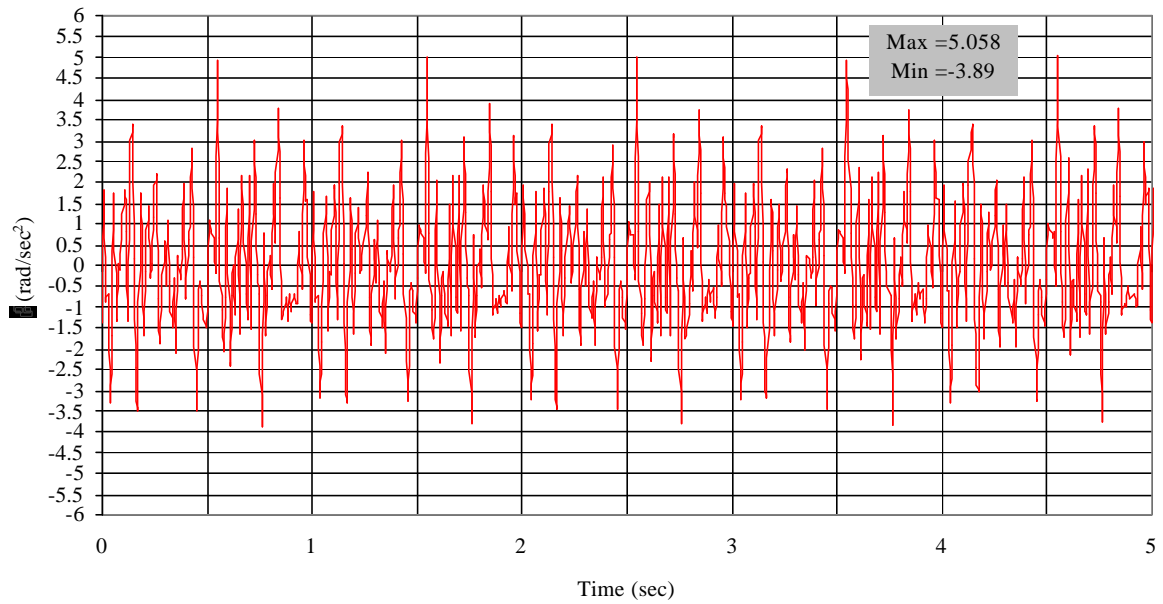


Figure 9.34 (SPN-Zero)-17.0 Hz Sine Wave -  $K_p = 3.5$ .

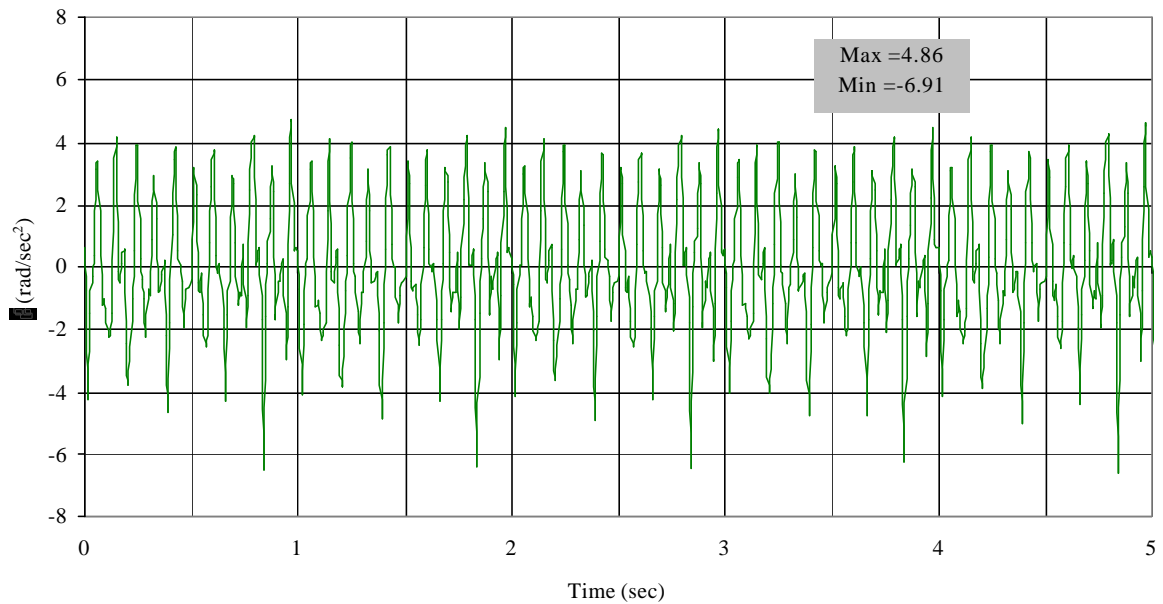
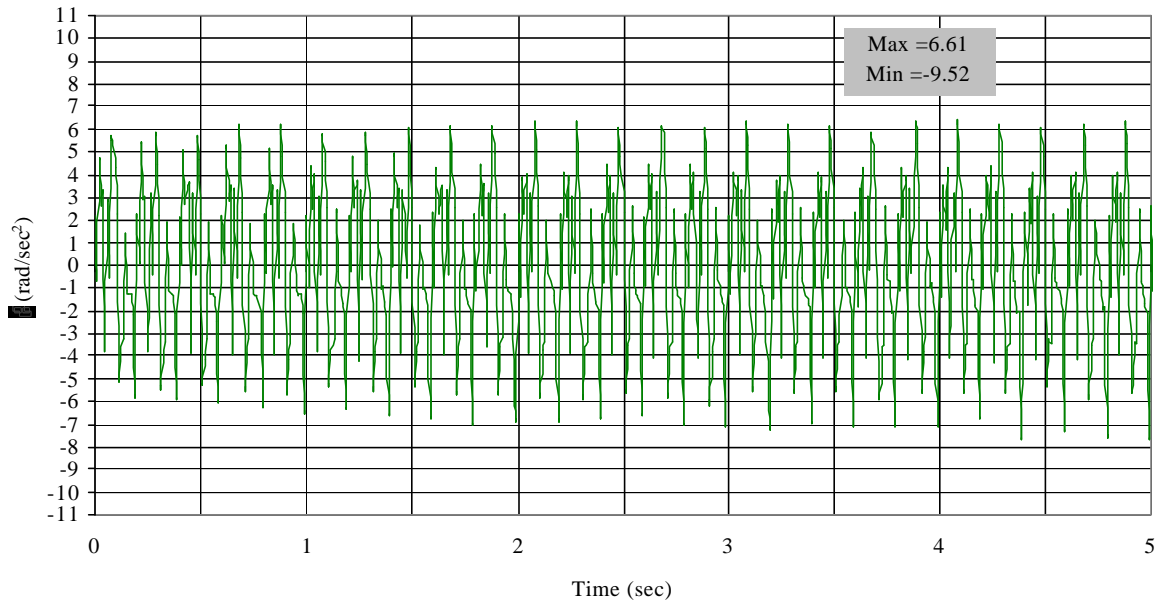
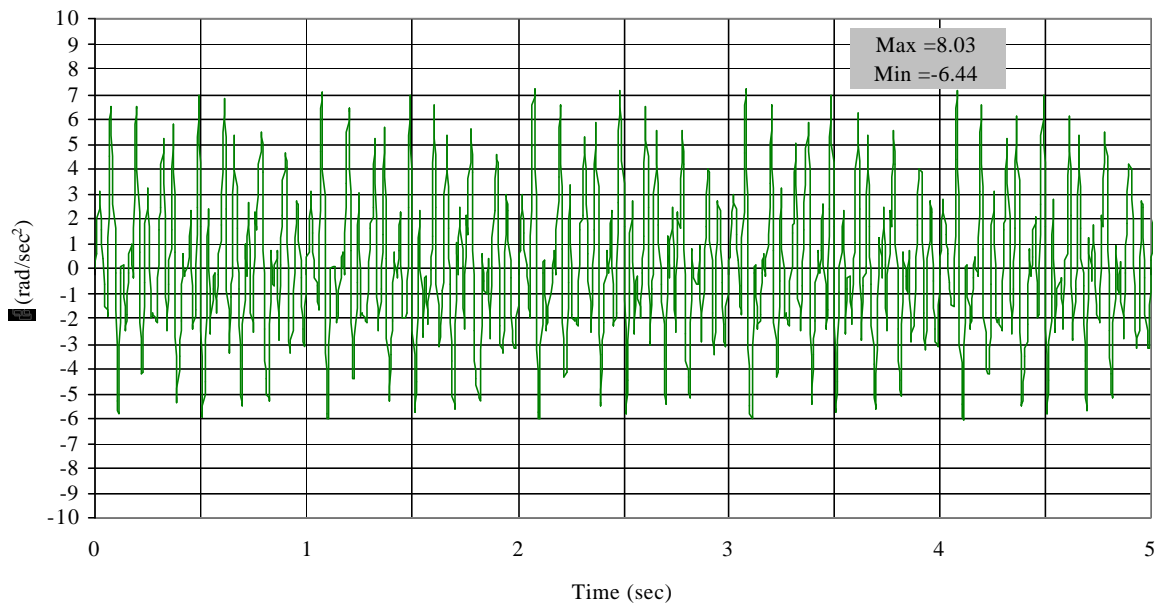


Figure 9.35 (SPS-Zero)-11.0 Hz Sine Wave -  $K_p = 3.5$ .

Figure 9.36 (SPS-Zero)-15.0 Hz Sine Wave –  $K_p = 3.5$ .Figure 9.37 (SPS-Zero)-17.0 Hz Sine Wave –  $K_p = 3.5$

### 9.5.3. COMPARISON IN THE FREQUENCY DOMAIN

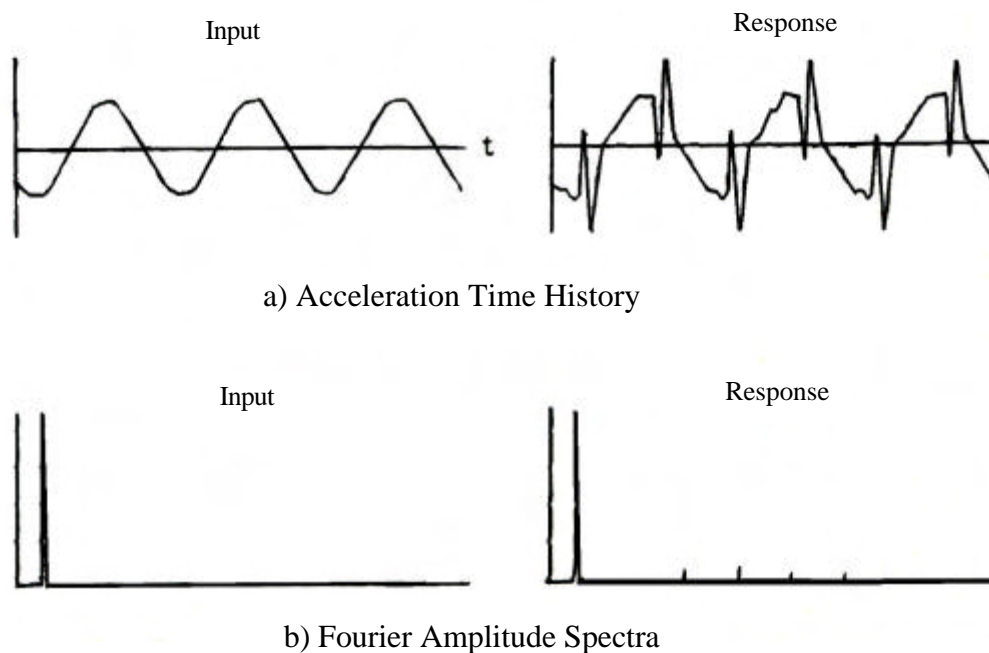
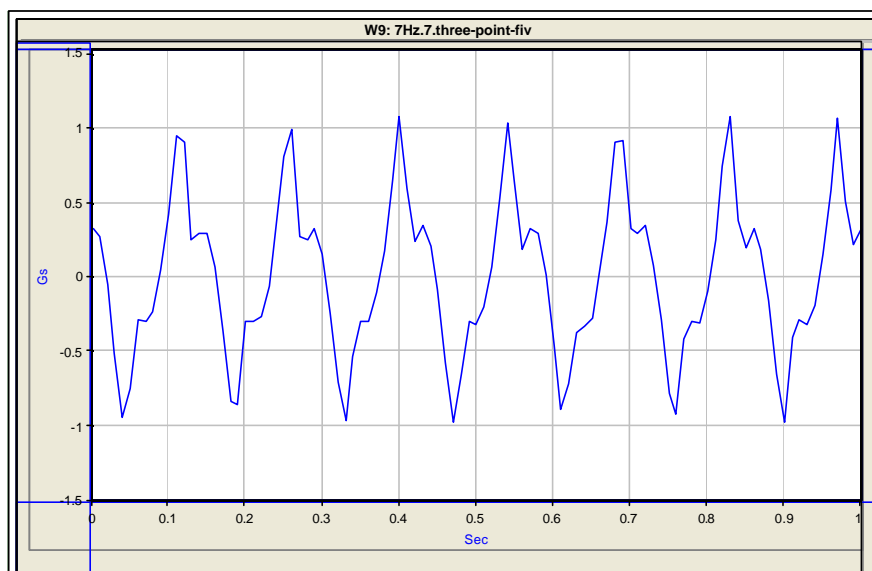


Figure 9.38 Sine Wave Performance [3].

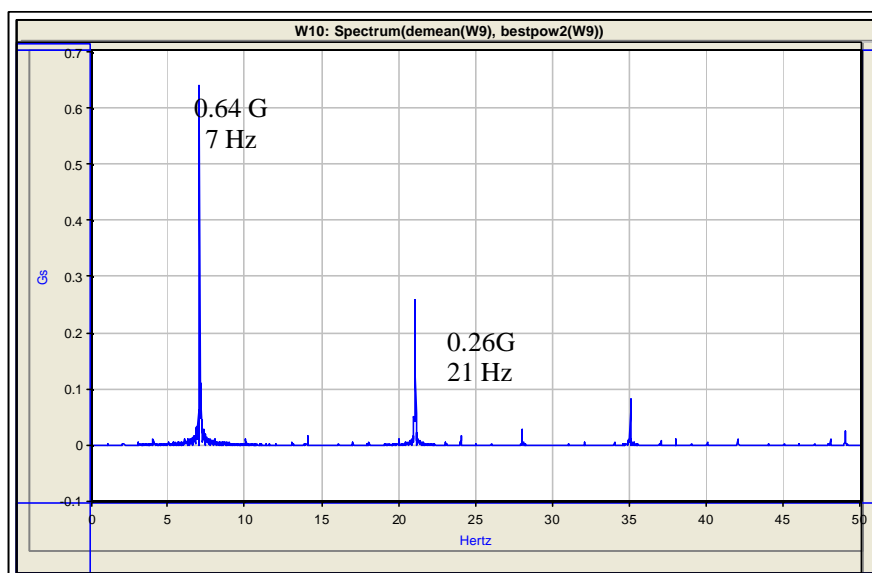
As shown in Figure 9.38, for a single input sine wave the Fourier Spectrum will produce a single frequency impulse. Therefore, any additional frequency components on the Fourier Spectrum of the response signal of the shake table will indicate a distortion of the input signal [3]. The spectrum will also show frequency components that are important to identify, such as the oil column frequency, for further studies using small-scale models on the shaking table.

For this purpose we obtained the Fourier Amplitude Spectrum, of the accelerometer located at Zero- SPW, for all the frequencies studied, from 1 Hz to 18 Hz. For calculating the Fourier Amplitude Spectrum, we used the commercially available program called DADiSP/2002. After studying the results we identified four significant frequency

components: 21 Hz, (24-25) Hz, (27-28) Hz and (30-33) Hz. Figure 9.39 shows the acceleration time history for a 7.0 Hz sine wave and the corresponding Fourier Amplitude Spectrum.



(a) Acceleration Time History of 7.0 Hz Sine Wave –  $K_P = 3.5$ .

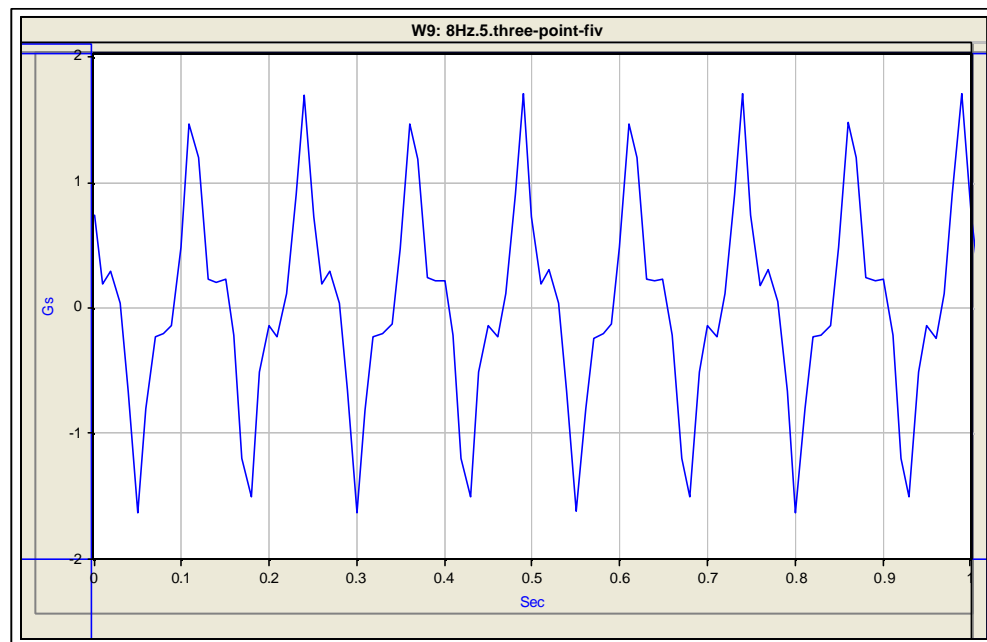


(b) Fourier Amplitude Spectrum for 7.0 Hz Sine Wave –  $K_P = 3.5$ .

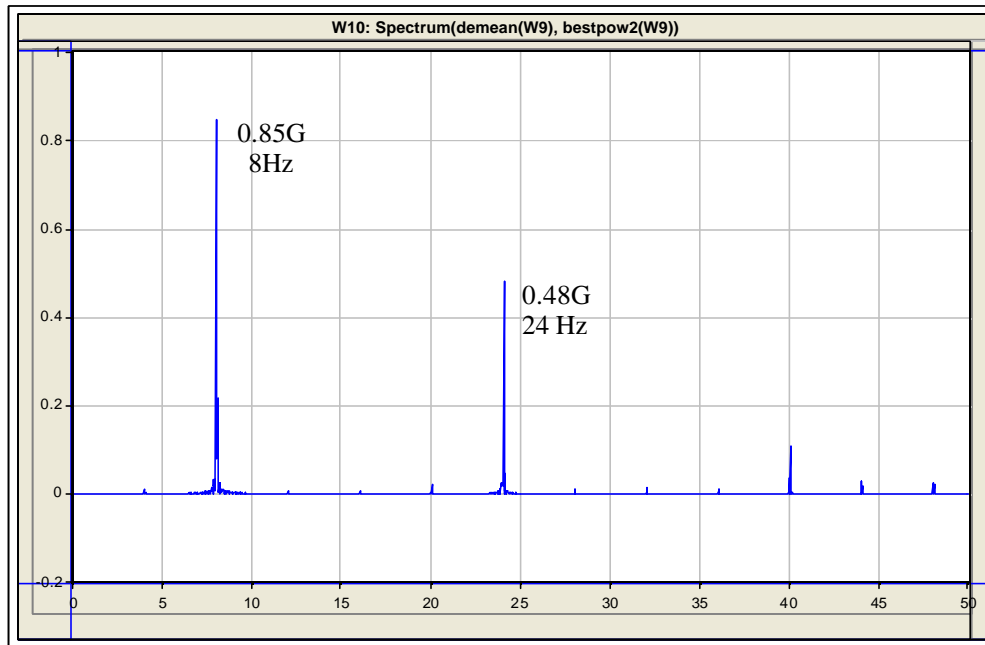
Figure 9.39 7.0 Hz Sine Wave Performance.

Figure 9.39 (a) shows that the response signal has some distortion. The Fourier Spectrum shown in Figure 9.39 (b) shows a frequency component at 7.0 Hz and at 21.0 Hz. The amplitude of the frequency component of 21.0 Hz is almost 40% of the 7.0 Hz component amplitude.

Figure 9.40 shows the acceleration time history for an 8.0 Hz sine wave and the corresponding Fourier Amplitude Spectrum. As before with the 7.0 Hz sine wave, Figure 9.40 (a) shows that the response signal has some distortion. But the distortion seems to be less than the distortion of the 7.0 Hz sine wave. The Fourier Spectrum shown in Figure 9.40 (b) shows a frequency component at 8.0 Hz and at 24.0 Hz. The amplitude of the frequency component of 24.0 Hz is 56% of the 8.0 Hz component amplitude.



(a) Acceleration Time History of 8.0 Hz Sine Wave –  $K_p = 3.5$ .

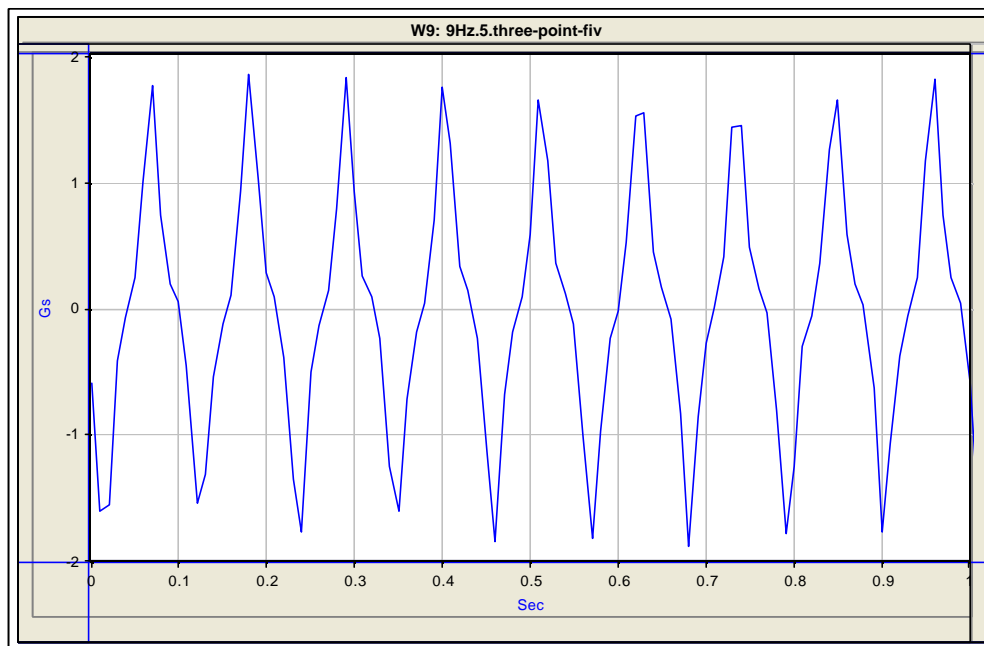


(b) Fourier Amplitude Spectrum for 8.0 Hz Sine Wave –  $K_p = 3.5$ .

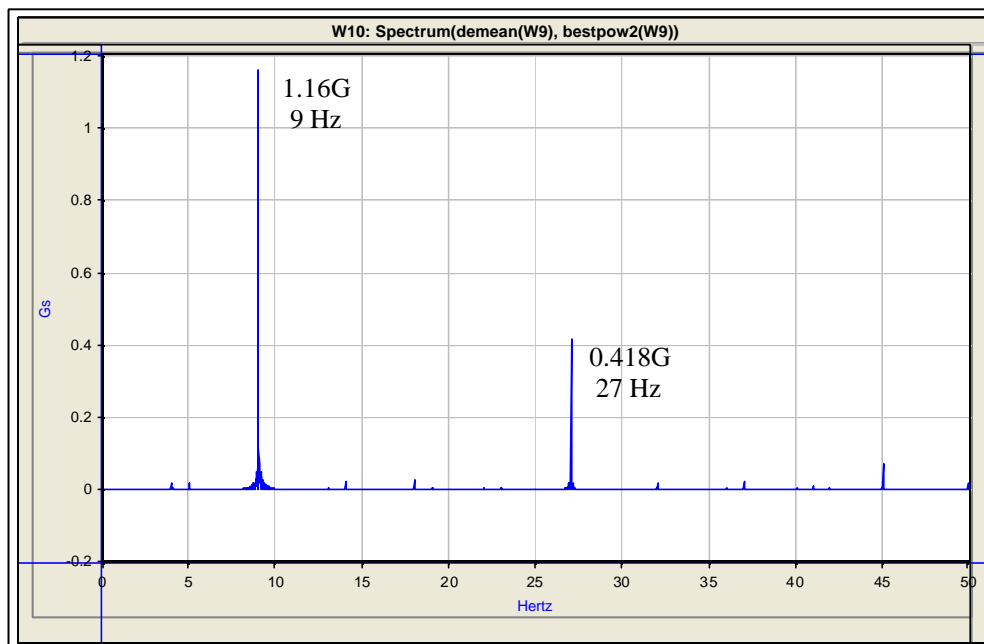
Figure 9.40 8.0 Hz Sine Wave Performance.

Figure 9.41 shows the acceleration time history for a 9.0 Hz sine wave and the corresponding Fourier Amplitude Spectrum. Figure 9.41 (a) also shows that the response signal have some distortion, but it seems to be decreasing with increasing frequency. The Fourier Spectrum shown in Figure 9.41 (b) shows a frequency component at 9.0 Hz and at 27.0 Hz. The amplitude of the frequency component of 27.0 Hz is 36% of the 9.0 Hz component amplitude.

Finally, Figure 9.42 shows the acceleration time history for an 11.0 Hz sine wave and the corresponding Fourier Amplitude Spectrum. Here also Figure 9.42 (a) indicates that the response signal has some distortion. The Fourier Spectrum shown in Figure 9.42 (b) shows a frequency component at 11.0 Hz and at 33.0 Hz. The amplitude of the frequency component of 33.0 Hz is 28% of the 11.0 Hz component amplitude.

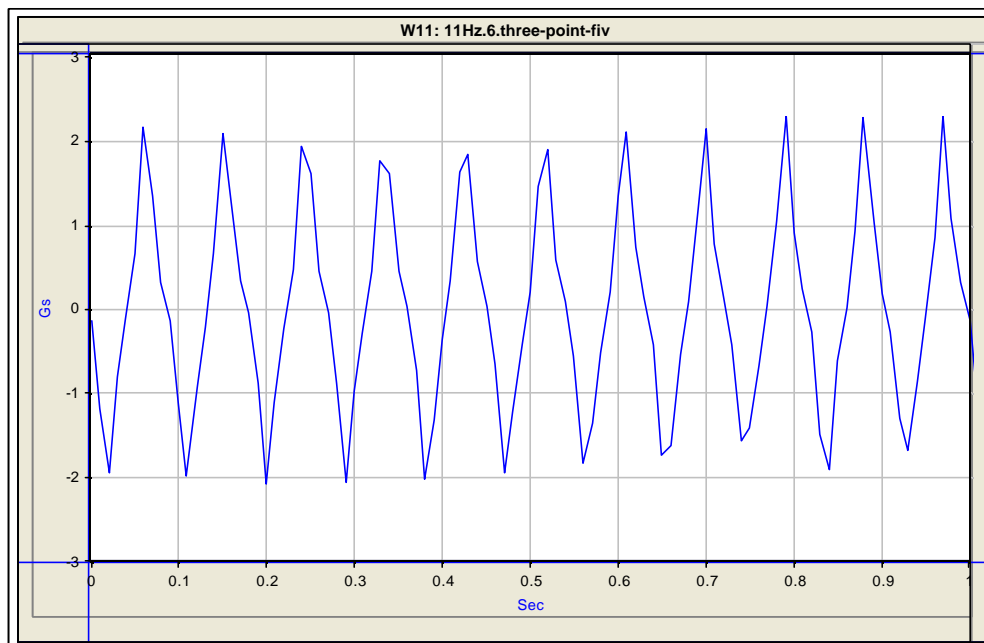


(a) Acceleration Time History of 9.0 Hz Sine Wave –  $K_p = 3.5$ .

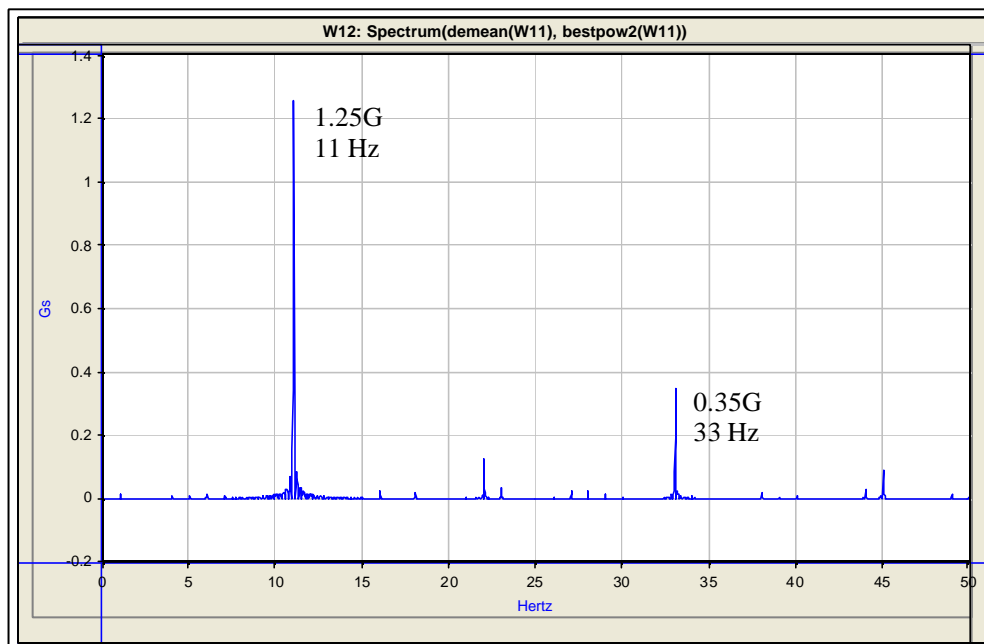


(b) Fourier Amplitude Spectrum for 9.0 Hz Sine Wave –  $K_p = 3.5$ .

Figure 9.41 9.0 Hz Sine Wave Performance.



(a) Acceleration Time History of 11.0 Hz Sine Wave –  $K_p = 3.5$ .

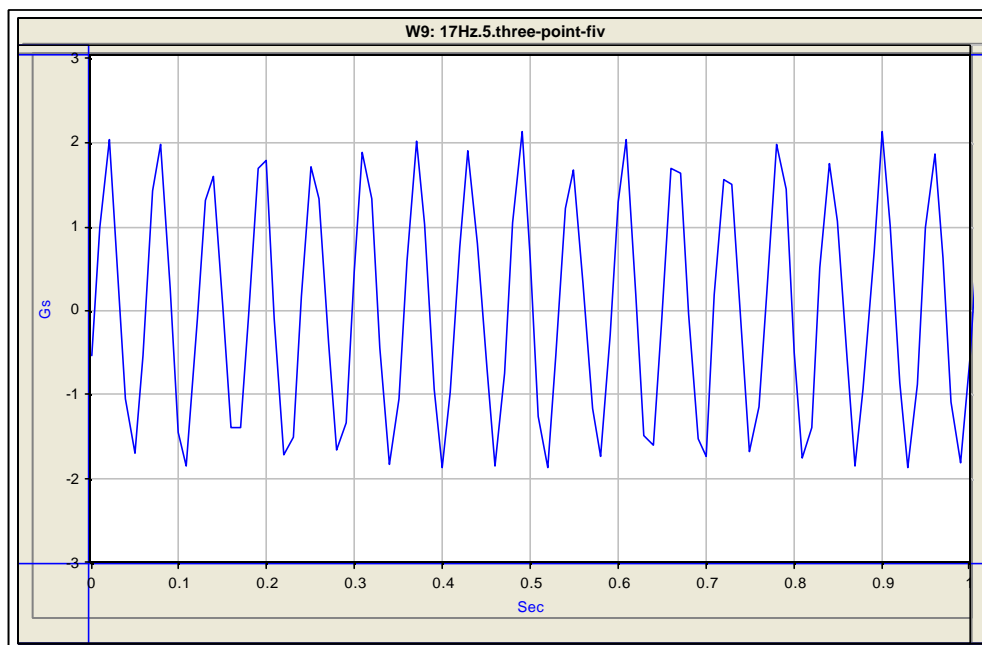


(b) Fourier Amplitude Spectrum for 11.0 Hz Sine Wave –  $K_p = 3.5$ .

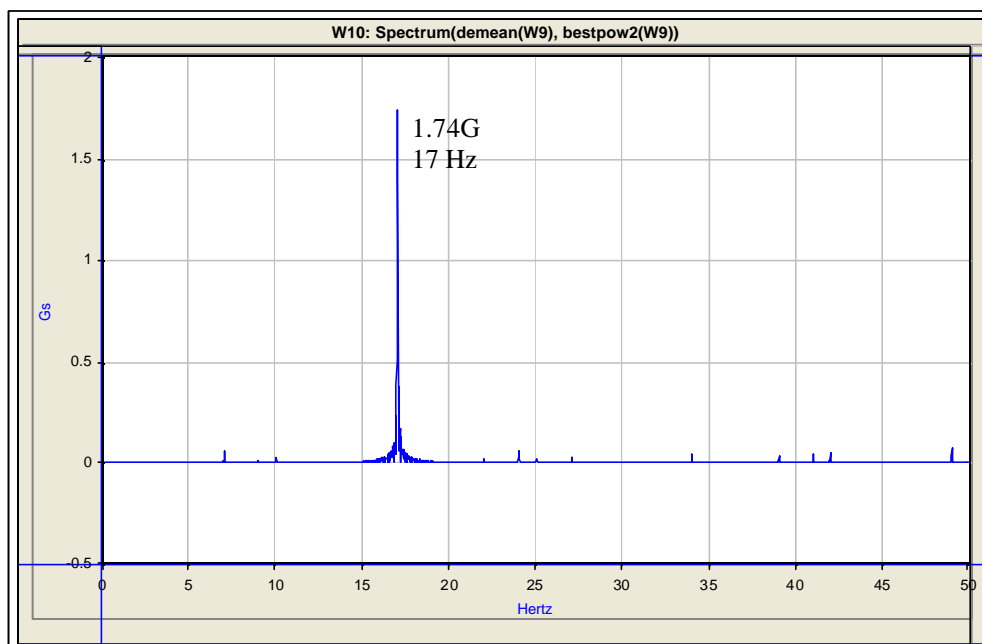
Figure 9.42 11.0 Hz Sine Wave Performance.

Of the four frequency components encountered at the Fourier Amplitude Spectrum of the frequencies studied, we have identified the oil column frequency at a frequency ranging from 30.0 Hz to 33.0 Hz. The oil column frequency changes with the bulk modulus, as discussed in Chapter 7, and the bulk modulus varies the temperature. The operating temperature of the HPS unit is 125°F (51.67°C). However, the temperature ranges from 90°F (32.2°C) when the HPS unit is cool, to 140°F (60°C) where the HPS shuts down. Further studies are needed to identify the other frequency components.

The behavior for the frequencies from 13.0 Hz to 18.0 Hz was different compared to the behavior of the lower frequencies. When we calculated the Fourier Amplitude Spectrum for these frequencies, only the frequency component of the input signal appeared on the spectrum. No other frequency components showed on the Fourier Amplitude Spectrum. The Fourier Amplitude Spectrum in Figure 9.43 (b) confirms this behavior for the acceleration time history for a 17.0 Hz sine wave.



(a) Acceleration Time History of 17.0 Hz Sine Wave –  $K_p = 3.5$ .



b) Fourier Amplitude Spectrum for 17.0 Hz Sine Wave –  $K_p = 3.5$ .

Figure 9.43 17.0 Hz Sine Wave Performance

## **10. CONCLUSIONS**

### **10.1. PROJECT SUMMARY**

This thesis discusses the work performed during the design, calibration and construction of a state-of-the-art small-size uni-directional electro-hydraulic shaking table. It also discusses the variables that govern the development, design and construction of this type of facility. The main objective of this investigation was to provide the UPRM with a shaking table facility for testing of behavior of scaled structural models under dynamic loading, such as earthquakes. In addition, the main objective of this work was to develop a guide for future design of larger shaking tables. Uni-directional earthquake simulators have often been used in the past as stepping-stones towards the development of multi-directional earthquake simulators.

The UPRM earthquake simulator consists of a rigid platform sliding over near frictionless linear bearing system and driven by an actuator attached to a reaction mass. The reaction mass is rigidly connected to the floor.

### **10.2. CONCLUSIONS**

- ◆ The most important variables for the design of the shaking table are:
  - a. Test Model (scale and type of model) - gives the scaling laws that will govern the design.
  - b. Expected type of loading (type of earthquakes) - gives the maximum values of acceleration, velocity and displacement that will give the appropriate hydraulic system.
  - c. Oil Column Frequency – will give the maximum theoretical operating frequency of the system.

- d. Mass ratios ((tests structure/simulator platform) and (simulator platform/foundation mass)) - will give an insight of the table expected dynamics.
- ◆ The maximum theoretical operating frequency, namely the oil column frequency, is 32 Hz. The performance envelopes of the shaking table drop significantly above this frequency.
  - ◆ The simulator platform can be considered rigid, because its natural frequency is almost three times (2.92) the theoretical maximum operating frequency of the table. Therefore, it is not expected any interaction effects between the simulator platform and a test structure at that operating frequency.
  - ◆ The first three natural modes of the reaction frame reflected the flexibility of the top frame, with frequencies in the operational frequency range of the table. Thus, the top frame has to be isolated from the system or stiffen because there could be interaction effects at that operational frequency range.
  - ◆ In the construction phase of the shaking table, it was found that the most important step is the alignment of the linear bearings and the alignment of the actuator. Any misalignment of the linear bearings or the actuator will introduce friction and rotational modes.
  - ◆ The proper location of the transducers is also very important. For example, to measure the rotational modes of the table it is necessary lateral transducers in the simulator platform.

- ◆ The final step of this investigation was the experimental measurement of the shaking table performance. From these tests the following information was obtained:
  - a. The earthquake simulator is capable of producing periodic motion and has been found operational at a range of 0.0 - 20.0 Hz.
  - b. The response of the system improves with increases in the proportional gain until it reaches a value where the system becomes unstable.
  - c. The command error, peak or valley, decreased with increases in proportional gain.
  - d. There is no rotation of the reaction frame.
  - e. There is a small rotation of the simulator platform. This rotation can be due to a mass eccentricity, actuator or linear bearings misalignment.
  - f. There are four significant frequency components interacting at the operational frequency range. The four frequency components are: 21 Hz, (24-25) Hz, (27-28) Hz and (30-33) Hz. Of these frequencies we were able to identify the latter component as the oil column frequency.
- ◆ The constructed UPRM earthquake simulator can now be used either for research or for a teaching aid for professors in many areas of Civil Engineering, as well as other areas of engineering.

### **10.3. FUTURE RESEARCH**

It is recommended that the following tests be carried out:

1. Sine wave tests for the bare table condition with different amplitudes, higher proportional gain, and other calibration parameters.
2. Sine wave tests with different amplitudes and payload conditions (rigid and a flexible - SDOF/MDOF structure).
3. White noise tests to determine the optimal calibration parameters for different payload conditions (rigid and a flexible - SDOF/MDOF structure).
4. Tests with the five earthquake time histories used in the design of the hydraulic system for different model scales and with a flexible - SDOF/MDOF structure payload.

## REFERENCES

1. U.S. Geological Survey, "Information about Past and Historical Earthquakes", <http://earthquake.usgs.gov/activity/past.html>, July 2001.
2. Puerto Rico Seismic Network, "Significant Earthquakes in the Puerto Rico Zone", <http://rmsismo.uprm.edu/ingles/index.html>, July 2001.
3. Mills, R. S., "Model Tests on Earthquake Simulators-Development and Implementation of Experimental Procedures", Ph.D. Thesis, Stanford University, California, June 1979.
4. Moncarz, P. D., "Theory and Application of Experimental Model Analysis in Earthquake Engineering", Ph.D. Thesis, Stanford University, California, May 1981.
5. Muhlenkamp, "Analysis, Design, and Construction of a Shaking Table Facility", M.S. Thesis, Rice University, Houston, Texas, pp. 178, 1997.
6. Rea, D., Abedi-Hayati, S. and Takahashi, Y., "Dynamic Analysis of Electro-Hydraulic Shaking Tables", *EERC Report No. UCB/EERC-91/13*, Earthquake Engineering Research Center, University of California at Berkeley, California, December 1977.
7. Rinawi, A. M. and Clough, R. W., "Shaking Table-Structure Interaction", *EERC Report No. UCB/EERC-91/13*, Earthquake Engineering Research Center, University of California at Berkeley, California, October 1991.
8. Trombetti, T., "Analytical Modeling of a Shaking Table System", M.S. Thesis, Rice University, Houston, Texas, September 1996.
9. Trombetti, T., "Experimental / Analytical Approaches to Modeling, Calibrating and Optimizing Shaking Table Dynamics for Structural Applications", Vol. I, II and III, Ph.D. Thesis, Rice University, Houston, Texas, May 1998.
10. Aristazabal-Ochoa, J.D. and Clark, A. J., "Large-Scale Earthquake Simulation Tables", *Proceedings, Seventh World Conference on Earthquake Engineering*, Vol. 7, Istanbul, Turkey, pp. 157-164, 1980.
11. Stephen, R. M., Bouwkamp, J. G., Clough, R. W. and Penzien J., "Structural Dynamic Testing Facilities at the University of California, Berkeley", *EERC Report No. EERC 69-8*, Earthquake Engineering Research Center, University of California at Berkeley, California, August 1969.

12. Clough, R. W. and Tang, D. T., "Earthquake Simulator Study of a Steel Frame Structure", Vol. I and II, *EERC Report No. EERC 75-6*, Earthquake Engineering Research Center, University of California at Berkeley, California, April 1975.
13. Blondet, J. M., "Studies on Evaluation of Shaking Table Response Analysis Procedures", *EERC Report No. UCB/EERC-81/18*, Earthquake Engineering Research Center, University of California at Berkeley, California, November 1981.
14. Hwang, J. S., Chang, K. C. and Lee, G. C., "The System Characteristics and Performance of a Shaking Table", *Report No. NCEER-87-0004*, National Center for Earthquake Engineering Research, State University of New York at Buffalo, New York, June 1987.
15. Chang, K. C., Yao, G.C., Lee, G. C., Hao, D.S. and Yeh, Y.C. "Dynamic Characteristics of a Full-Size Five-Story Steel Structure and a 2/5 Scale Model", *Report No. NCEER-91-0011*, National Center for Earthquake Engineering Research, State University of New York at Buffalo, New York, July 1991.
16. Constantinou, M.C. and Symans, M.D., "Experimental and Analytical Investigation of Seismic Response of Structures with Supplemental Fluid Viscous Dampers", *Report No. NCEER-92-0032*, National Center for Earthquake Engineering Research, State University of New York at Buffalo, New York, December 1992.
17. Clark, A. and Cross, D., "The Effect of Specimen Resonances on Accurate Control of Multiple Degree-of-Freedom Servo-Hydraulic Shaking Tables", *Proceedings, Eight World Conference on Earthquake Engineering*, San Francisco, California, U.S.A., pp. 47-54, 1984.
18. Kusner, D. A., Rood, J. D. and Burton, G.W., "Signal Reproduction Fidelity of Servohydraulic Testing equipment", *Proceedings, U.S./P.R.C. Workshop on Experimental Methods in Earthquake Engineering*, Report No. 106, The John A. Blume Earthquake Engineering Center, Shanghai, People's Republic of China, pp. 29-39, 1993.
19. Twitchell, B. S., "Analytical Modeling and Experimental Identification of a Uniaxial Seismic Simulator", M.S. Thesis, Washington State University, Pullman, Washington, May 1998.
20. MTS Product Information Manual, "Series 244 Actuators", November 1998.
21. MTS Product Information Manual, "Controller Installation & Calibration for TestStar™ IIs", August 1999.

22. Deltron, "Crossed Roller Slide Tables (Steel),  
[http://www.deltron.com/catalog/general\\_info/?cat\\_id=185#model](http://www.deltron.com/catalog/general_info/?cat_id=185#model).
23. MTS Product Information Manual, "Series 252 Servovalves", November 1999.
24. MTS Product Information Manual, "Model 506.41/.51/.61 Hydraulic Power Supplies", 1978.
25. MTS Product Information Manual, "Series 293.1x Hydraulic Service Manifolds", January 2001.
26. MTS Product Information Manual, "Model 793.00 System Software", November 2000.
27. MTS Product Information Manual, "Model 793.00 Multipurpose Test Ware for TestStar™ IIs, September 1999.
28. Merritt, Herbert E., Hydraulic Control Systems, John Wiley & Sons Publishing Company, New York, 1967.

## **APPENDIX A: CHARACTERISTICS OF THE MODEL TEST STRUCTURE**

It was important to define a model test structure from a prototype structure. Most of the design of the shaking table components are based on the characteristics of this model structure. The laws that govern how to define this model from a prototype structure are illustrated in the following table, previously discussed in Chapter 4.

Table 1. Similitude Relationships for Artificial Mass Simulation Method.<sup>1</sup>

Parameter	Units <sup>2</sup>	Any Material	Same Material as Prototype
Length	L	$I_L$	$I_L$
Time	T	$I_L^{1/2}$	$I_L^{1/2}$
Frequency	$\frac{1}{T}$	$I_L^{-1/2}$	$I_L^{-1/2}$
Velocity	$\frac{L}{T}$	$I_L^{1/2}$	$I_L^{1/2}$
Displacement	L	$I_L$	$I_L$
Gravitational Acceleration	$\frac{L}{T^2}$	1	1
Acceleration	$\frac{L}{T^2}$	1	1
Force	F	$I_E I_L^2$	$I_L^2$
Mass	$\frac{F \cdot T^2}{L}$	$I_E I_L^2$	$I_L^2$
Modulus of Elasticity	$\frac{F}{L^2}$	$I_E$	1

Notes:

3. From [19].
4. L = Length, T = Time, F = Force and E = Modulus of Elasticity.

The design process starts by defining  $N$  scale factor from the table shown above. In seismic testing you can take as basic dimensions force, length and time thus  $N = 3$ . In the case of artificial mass simulation, where you use the same material in the model test structure as in the prototype structure,  $\lambda_g = \lambda_E = 1$  and the designer chooses  $\lambda_L$  [19]. In our case we have decided that the model structure was going to be  $1/4^{\text{th}}$  of the prototype structure thus  $\lambda_L = 4$ . Figure 1 show how the prototype structure was scaled using similitude laws to define the model test structure.

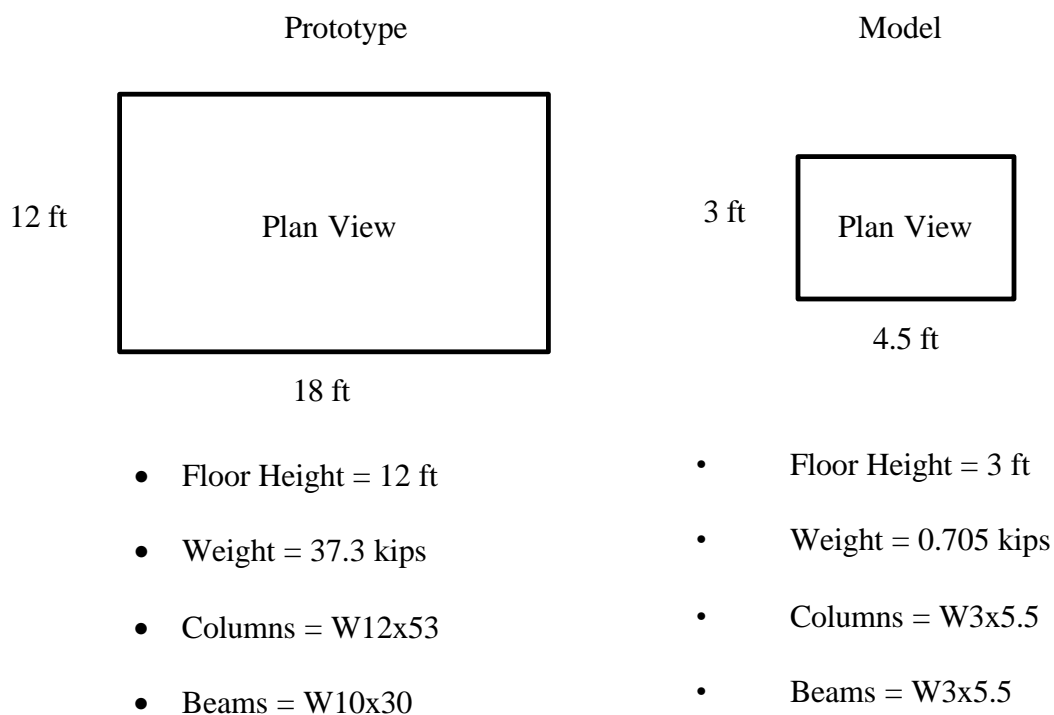


Figure 1 Scaling of Prototype Structure.

For both structures to behave similarly we had to use “Artificial Mass Simulation”. This method involves the addition of structurally uncoupled mass to augment the specific weight of the model structure [19]. The scale factor of mass in our case is:

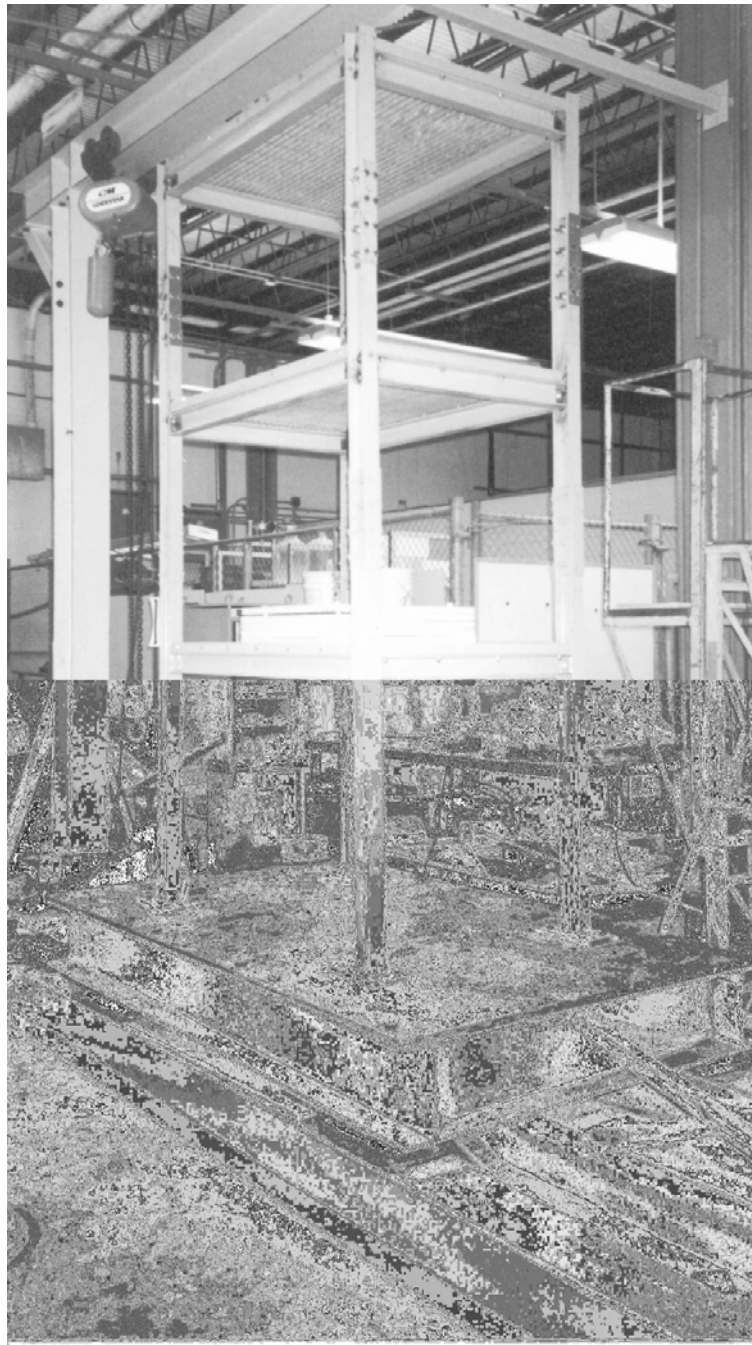
$$\frac{1}{I_L^2} = \frac{1}{4^2} = 0.0625$$

To obtain the additional material per floor for “AMS”, one just simply multiply the prototype structure floor weight by 0.0625 to obtain the required model weight and then subtract the actual model weight from this value. Table 2 illustrates this concept.

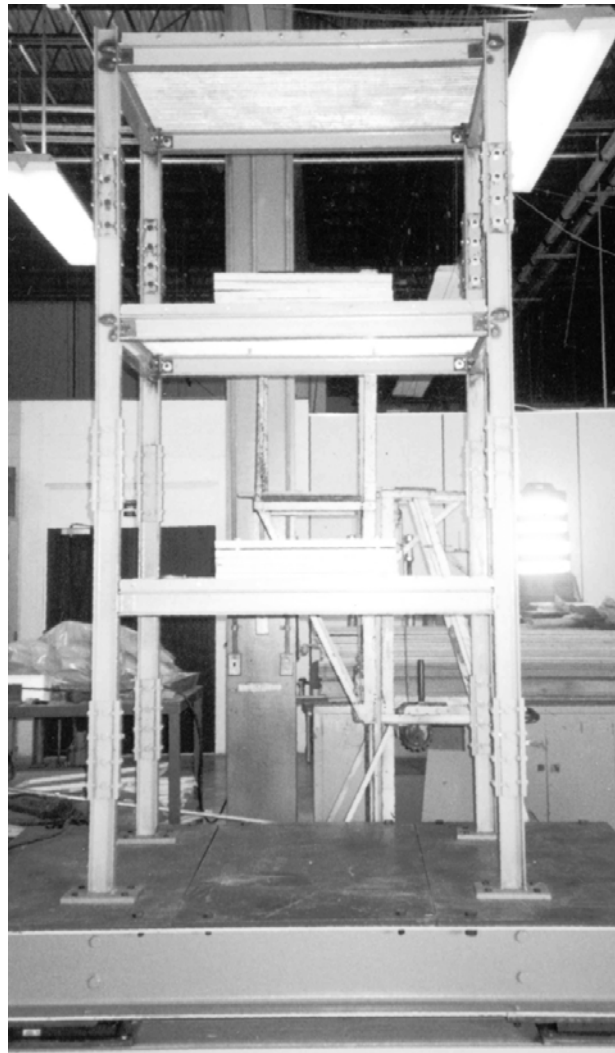
Table 2 Artificial Mass Simulation for our Model Test Structure

Floor	Prototype Weight (kips)	Actual Model Weight (kips)	Required Model Weight (kips)	Additional Weight (kips)
Roof	11.584	0.2134	0.724	0.5106
2	12.858	0.2458	0.804	0.5578
1	12.858	0.2458	0.804	0.5578
Total =	37.2995	0.7051	2.3312	1.6261

Figure 2 shows photos of the 1/4<sup>th</sup> Model Test Structure mounted on the simulator platform.



(a) South- East View of Model Test Structure.



(b) South – View of Model Test Structure.

Figure 2 1/4<sup>th</sup> Model Test Structure.